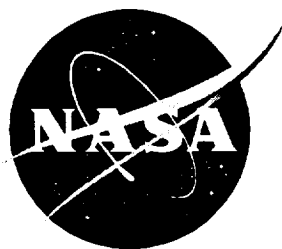NASA Contractor Report 4667

Optimal Guidance Law Development for an Advanced Launch System

Anthony J. Calise and Martin S. K. Leung
Georgia Institute of Technology • Atlanta, Georgia

April 1995

Printed copies available from the following:

NASA Center for AeroSpace Information
800 Elkridge Landing Road
Linthicum Heights, MD 21090-2934
(301) 621-0390

National Technical Information Service (NTIS)
5285 Port Royal Road
Springfield, VA 22161-2171
(703) 487-4650

TABLE OF CONTENTS

Table of Contents (cont.)

<u>Section</u>

LIST OF ILLUSTRATIONS

v

List of Illustrations (cont.)

<u>Figure</u>

List of Illustrations (cont.)

LIST OF TABLES

OPTIMAL GUIDANCE LAW DEVELOPMENT
FOR AN ADVANCED LAUNCH SYSTEM

Anthony J. Calise* and Martin S. K. Leung**

Georgia Institute of Technology, GA 30332

SUMMARY

The objective of this research effort was to develop a real-time guidance approach for launch vehicles ascent to orbit injection. Various analytical approaches combined with a variety of model order and model complexity reduction have been investigated. Singular perturbation methods were first attempted, and found to be unsatisfactory. The second approach based on regular perturbation analysis was subsequently investigated. It also fails because the aerodynamic effects (ignored in the zero order solution) are too large to be treated as perturbations. Therefore, the study demonstrates that perturbation methods alone (both regular and singular perturbations) are inadequate for use in developing a guidance algorithm for the atmospheric flight phase of a launch vehicle.

During a second phase of the research effort, a hybrid analytic/numerical approach was developed and evaluated. The approach combines the numerical method of collocation and the analytical method of regular perturbations. The concept of choosing intelligent interpolating functions is also introduced. Regular perturbation analysis allows the use of a crude representation for the collocation solution, and intelligent interpolating functions further reduce the number of elements without sacrificing the approximation accuracy. As a result, the combined method forms a powerful tool for solving real-time optimal control problems. Details of the approach are illustrated in a fourth order nonlinear example. The hybrid approach is then applied to the launch vehicle problem. The collocation solution is derived from a bilinear tangent steering law, and results in a guidance solution for the entire flight regime, that includes both atmospheric and exoatmospheric flight phases. Assessment of performance and reliability are demonstrated through closed loop simulations. The hybrid guidance approach delivers over 99.9% of optimal performance and orbit injection accuracy while the control computation is completed in tenths of a second on a SPARCstation 1. Wind shear effects and a control constraint are also addressed.

---

* Professor, School of Aerospace Engineering.
** Graduate Research Assistant.

A second effort that paralleled this work under the same grant number was lead by Dr. Dewey Hodges, of the School of Aerospace Engineering at Georgia Tech. This work has been documented under a separate contractor report.

SECTION I

INTRODUCTION

The objective of the Advanced Launch System (ALS) program is to develop an unmanned, all-weather launch system for placing large payloads (100,000lb - 150,000lb) into a low Earth orbit at a fraction of present cost. Part of the guidance requirement is to realize an efficient algorithm for solving the launch vehicle ascent trajectory problem.

1.1 Background

To date, first stage guidance has been realized in open loop form. The vehicle is typically guided by using a pre-stored steering program. The steering program is calculated as a part of pre-launched preparation to account for structural loads from aerodynamic forces and from atmospheric disturbances such as wind shear. Typically it involves flying with nearly zero angle of attack, and performing a gravity turn [1]. Near zero angle of attack is employed to avoid creating excessive aerodynamic bending moments, which is proportional to the product of angle of attack and dynamic pressure. Guidance for the second stage and any subsequent stages is closed loop, employing various approaches. The Saturn V vehicle uses an Iterative Guidance Mode (IGM) [2], and the Space Shuttle employs Powered Explicit Guidance (PEG) [3]. These are retargeting schemes because the guidance commands are recalculated at each update cycle using the current vehicle's position and velocity vectors as the initial conditions for the optimization process.

Traditional Guidance Solution Methods

Traditional launch vehicle guidance may involve either two or three different phases [1 - 3]. The first is an open loop guidance phase for the atmospheric portion of flight which typically flies with a non-optimal piecewise linear attitude program. The second is a closed loop guidance phase for the exoatmospheric portion of flight. This has an analytic solution under certain assumptions. Then a third closed loop phase is possibly required when the vehicle is approaching orbital conditions for final precision orbit injection.

Numerical approaches to optimal guidance typically employ either nonlinear programming [4 - 9] or multiple shooting [10]. In a direct method formulation such as nonlinear programming, the optimization problem is transformed into a parametric optimization problem. The unknown control profile is parameterized with undetermined coefficients of typically piecewise linear polynomials. The states are considered as functions of the control through the differential equations of dynamics. Constraints, if any, are enforced discretely along the trajectory, typically at a finite number of nodal points of the parameterized control. So the original infinite dimensional problem is approximated by

a finite dimensional problem in the reduced space of the control parameters, and gradient techniques are used to search for a solution that optimizes the performance index. In [8], Hargraves and Paris have combined the nonlinear programming method with collocation by approximating all the state and control histories with piecewise smooth functions, thus avoiding any integration process. Similar to the collocation method, Pamadi [9] has used splines as function of velocity to approximate the altitude profile and applied an optimization algorithm to determine the unknown coefficients of the splines. To be useful as a feedback guidance solution, it is essential that these approaches converge quickly and reliably at each instant the solution is updated during the flight.

On the other hand, multiple shooting is a technique used in indirect methods. Instead of evaluating the performance index directly, optimization is achieved by satisfying a set of necessary conditions which are expressed in the form of a Two-Point Boundary Value Problem (TPBVP). For a constrained case, this may lead to a Multi-Point Boundary Value Problem (MPBVP), for which a guess of the switching structure is required. To reduce the sensitivity to an initial guess of the solution, piecewise integration or multiple shooting is used. Instead of integrating for the complete trajectory starting from one set of initial conditions, the trajectory is divided into intervals and integration is performed separately from different sets of initial conditions for each interval. Then the boundary conditions and continuity conditions (or jump conditions in the case of state constraints or discontinuous dynamics) between intervals are enforced. A relaxed Newton's method [11] is typically used to iterate for a solution. Though the indirect method produces extremely accurate results, it involves complicated programming in formulating the costates differential equations and the control structure. The process is also complicated by the requirement to provide an initial guess for both costate and state variables. On the contrary, nonlinear programming is relatively simple to formulate. The method does not require the use of costate variables or a knowledge of switching structure. In practice, it is favored over indirect methods for solving optimization problems in general purpose programs.

Due to the intensive computation requirements, direct and indirect methods are used only to generate off-line solutions for analysis purposes or to provide a first stage open loop guidance program. To compensate for using an open loop approach during the first stage flight, a feedback guidance scheme is introduced for the subsequent exoatmospheric stages of flight where a more simplified dynamic model permits a more analytic solution.

Using Simplified Models

In [2], Chandler and Smith have developed an IGM for the Saturn V vehicle. It is based on a flat Earth no-atmosphere model, and is further simplified with linear angle steering guidance. The guidance solution requires solving only a set of linear equations.

2

Ten years later, the Boeing Aerospace Company [3] adopted the linear tangent steering guidance as the baseline program for the Space Shuttle's PEG. Using an approximate gravity model, the program is extended to handle the spherical Earth case, and the solution is solved by an iterative algorithm.

Perturbation Methods of Analysis

Perturbation methods of analysis have been shown to be powerful approaches to spacecraft guidance design. Breakwell and Rauch [12] have used regular perturbation to solve a low thrust space flight problem. It is a neighboring extremal technique. A linear feedback control is formulated by linearizing about the reference trajectory and the solution is solved with a numerically determined state transition matrix. In [13], Jacobson and Powers have developed an explicit guidance scheme also for low thrust space flight. It is basically a retargeting procedure and uses an analytic solution for the inertially fixed and constant acceleration flight. Recently, Feeley and Speyer [14] have used regular perturbations on the expansion of the Hamilton-Jacobi-Bellman (HJB) equation, and have applied it to the launch vehicle guidance problem for exoatmospheric flight. The approach requires an analytic zero order solution and quadrature evaluation. The analytic solution is again based on a flat Earth, no-atmosphere approximation, and the neglected dynamics are introduced as perturbations. Solution is obtained by expanding the HJB equation. In this method, higher order state histories are not required and higher order corrections for the costates are obtained by partial differentiation of the power series solution to the HJB equation. An alternative approach based on regular expansion of state and costates was also developed by Leung and Calise [15]. This approach has the advantage that on-line quadrature can be avoided. However, both the solution approaches of [14, 15] were later found to be inadequate when aerodynamic effects are included.

1.2 Research Contributions

The major contributions of this research are: (1) an exhaustive study and simulation effort which demonstrates conclusively that perturbation methods alone (both regular and/or singular perturbations) are inadequate for use in developing a guidance algorithm for the atmospheric phase of a launch vehicle trajectory, and (2) the development of a hybrid approach, that combines the numerical method of collocation and the analytic method of regular perturbation to make it suitable for real-time guidance, and superior to either method alone. The hybrid approach retains the desirable and complimentary features of the individual methods. The collocation method is further improved by providing more intelligent choices of the interpolation functions, which are derived from the analytically tractable portion of the necessary conditions for optimality. When applied to the launch

3

vehicle guidance problem, the main result is a bilinear tangent steering law for the thrust vector angle that can be employed for all flight phases, including the atmospheric phase of the trajectory. The progress reports and papers that are related to this research effort can be found in [15 - 25].

A second effort that paralleled this work under the same grant number was lead by Dr. Dewey Hodges, of the School of Aerospace Engineering at Georgia Tech. This work has been documented under a separate contractor report [26].

1.3   Report Organization

Sec. 2 presents the formulation of the launch vehicle trajectory optimization problem, which includes the equations of motion and the vehicle aerodynamic and propulsion models that are based on a generic model of the ALS. The results for two purely analytical approaches are documented in Sec. 3. The first is a singular perturbation approach using an energy state approximation and a 2-state model. The second is a regular perturbation approach based on the zero order solution for a flat Earth no-atmosphere assumption. Sec. 4 details the development of a hybrid approach that employs both regular perturbation analysis and the method of collocation. A fourth order nonlinear system is treated in depth to demonstrate its application, and to compare it to solutions obtained by both regular perturbation analysis and purely numerical collocation methods. In Sec. 5, the launch vehicle guidance problem is presented using the hybrid approach. It includes the zero and the first order correction formulations and their solutions, and compares the resulting guided solution with the optimal solution obtained by the method of multiple shooting. Sec. 6 is the conclusions of this research and the recommendations for future research .

4

SYMBOLS AND ABBREVIATIONS

<u>Symbol</u>

V	- airspeed
W_{ijk}	- wind speed components in the Cijk frame
χ	- heading angle
γ	- flight-path angle
m	- vehicle mass
t_s	- staging time (158.5s for the ALS vehicle)
r	- magnitude of radius vector measured from the Earth's center
r_e	- Earth mean radius (6.378×10^6m)
μ_e	- Earth gravitational constant (3.9906×10^{14}m^{3}s^{-2})
ω_e	- Earth's rotational rate (7.27×10^{-5}rads^{-1})
h	- altitude, $h = r - r_e$
η	- thrust throttle
α	- angle of attack, control variable in the wind frame
β	- sideslip angle, control variable in the wind frame
M	- Mach number
c	- sound speed
c_e	- reference sound speed on Earth's surface (340.3ms^{-1})
C_D	- aerodynamic drag coefficient $C_D = C_D(\alpha, M, \beta)$
C_L	- aerodynamic lift coefficient $C_L = C_L(\alpha, M, \beta)$
ρ	- atmospheric density
ρ_e	- reference atmospheric density on Earth's surface (1.225kgm^{-3})
p	- atmospheric pressure
p_e	- reference atmospheric pressure on Earth's surface (101330Nm^{-2})
q	- dynamic pressure
T_{vac}	- vacuum thrust
A_e	- engine exit nozzle area
S	- aerodynamic reference area
Ω_A	- state transition matrix for the linear system A
v	- local vertical velocity component
u	- local horizontal velocity component
θ	- thrust-vector angle relative to local horizon, the control variable
g_e	- gravitational acceleration on Earth's surface ($g_e = \mu_e/r_e^2$)

Symbols and Abbreviations (cont.)

<u>Symbol</u>

g_i - small nonlinear terms (i = 1, 2)

p_x - interpolated state dynamics in the collocation formulation

q_x - interpolated costate dynamics in the collocation formulation

<u>Abreviations</u>

ALS   - Advanced Launch System

HJB   - Hamilton-Jacobi-Bellman

IGM   - Iterative Guidance Mode

KSC   - Kennedy Space Center

LEO   - Low Earth Orbit

PEG   - Powered Explicit Guidance

TPBVP   - Two-Point Boundary Value Problems

MPBVP   - Multi-Point Boundary Value Problems

SECTION II

PROBLEM FORMULATION

In this section, we first formulate the optimal launch vehicle guidance problem, which includes the equations of motion for a point mass model of a launch vehicle that the subsequent analyses are applied to. The reference aerodynamic, atmospheric and propulsion models are also included.

2.1 Equations of Motion

Referring to Fig. 2.1, the point mass equations of motion for a multi-stage launch vehicle over a spherical, rotating Earth inside a non-stationary atmosphere are:

$$\dot{V} = \frac{T^{(i)} \cos\alpha \cos\beta - D^{(i)}}{m} - \frac{\mu_e}{r^2}\sin\gamma + r\omega_e^2(\sin\gamma\cos^2\lambda - \cos\gamma\sin\lambda\cos\lambda\cos\chi)$$
$$-\dot{W}_i \cos\gamma\sin\chi - \dot{W}_j\cos\gamma\cos\chi - \dot{W}_k\sin\gamma + 2\omega_e[W_i(\sin\gamma\cos\lambda -$$
$$\cos\gamma\sin\lambda\cos\chi) + \cos\gamma(W_j\sin\lambda - W_k\cos\lambda)\sin\chi] \qquad ; V(t_0) = V_0$$

$$\dot{\chi} = \{-\frac{T^{(i)} \cos\alpha\sin\beta + Y^{(i)}}{m} + \frac{V^2}{r}\cos^2\gamma\tan\lambda\sin\chi + r\omega_e^2\sin\lambda\cos\lambda\sin\chi$$
$$+2\omega_e V(\cos\gamma\sin\lambda - \sin\gamma\cos\lambda\cos\chi) - \dot{W}_i\cos\chi + \dot{W}_j\sin\chi +$$
$$2\omega_e[W_i\sin\lambda\sin\chi + (W_j\sin\lambda - W_k\cos\lambda)\cos\chi]\}/(V\cos\gamma) \; ; \chi(t_0) = \chi_0$$

$$\dot{\gamma} = \{\frac{T^{(i)}\sin\alpha + L^{(i)}}{m} - (\frac{\mu_e}{r^2} - \frac{V^2}{r})\cos\gamma + r\omega_e^2(\cos^2\lambda\cos\gamma + \sin\lambda\cos\lambda\sin\gamma\cos\chi)$$
$$+2\omega_e V\sin\chi\cos\lambda + \dot{W}_i\sin\gamma\sin\chi + \dot{W}_j\sin\gamma\cos\chi - \dot{W}_k\cos\gamma$$
$$+2\omega_e[W_i(\cos\gamma\cos\lambda + \sin\gamma\sin\lambda\cos\chi) - \sin\gamma(W_j\sin\lambda -$$
$$W_k\cos\lambda)\sin\chi]\}/V \qquad ; \gamma(t_0) = \gamma_0$$

$$\dot{\phi} = \frac{V\cos\gamma\sin\chi + W_i}{r\cos\lambda} \qquad ; \phi(t_0) = \phi_0$$

$$\dot{\lambda} = \frac{V\cos\gamma\cos\chi + W_j}{r} \qquad ; \lambda(t_0) = \lambda_0$$

$$\dot{r} = V\sin\gamma + W_k \qquad ; r(t_0) = r_0$$

$$\dot{m} = f(\eta, r, t) \qquad ; m(t_0) = m_0 \qquad ; m(t_{s+}^{(i)}) = m_s^{(i)} \qquad (2.1)$$

where
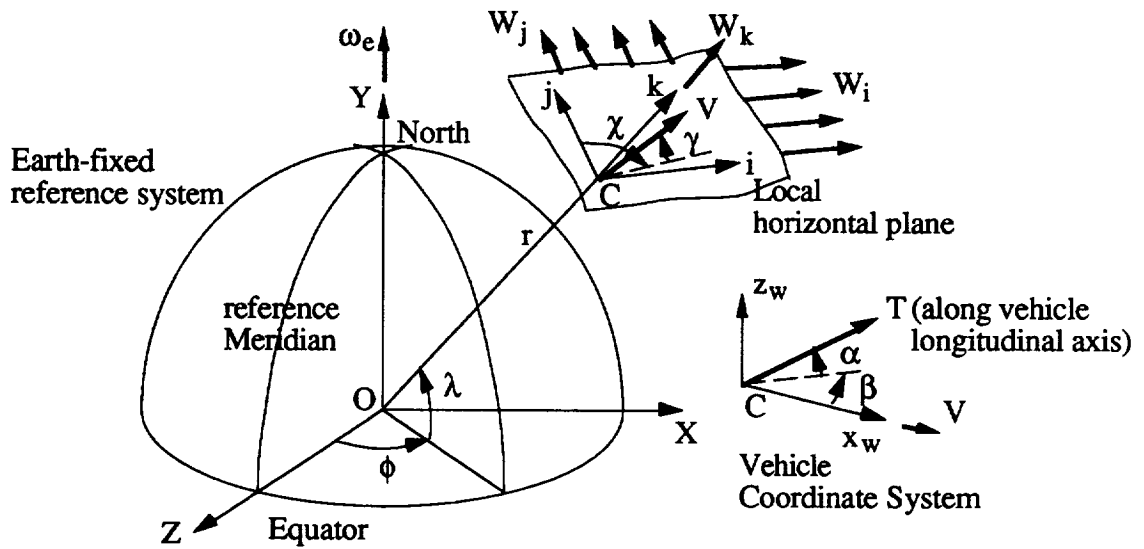
Figure 2.1.   Coordinate Systems: Earth-fixed Frame OXYZ, Local Horizontal Cijk, and Wind Frame*.

---

* Here y_w and z_w are defined in the opposite from their usual convention.

$$\dot{W}_x = \frac{\partial W_x}{\partial \phi}\dot{\phi} + \frac{\partial W_x}{\partial \lambda}\dot{\lambda} + \frac{\partial W_x}{\partial h}\dot{h} \qquad\qquad ; x = \{i, j, k\}$$

$$D^{(i)} = qS^{(i)}C_D^{(i)} \qquad ; Y^{(i)} = qS^{(i)}C_Y^{(i)} \qquad ; L^{(i)} = qS^{(i)}C_L^{(i)}$$

$$q = \rho V^2 / 2 \qquad ; T^{(i)} = \eta T_{max}^{(i)} \qquad ; \eta \in [0, 1] \qquad\qquad (2.2)$$

Here, an inverse-square gravitational field is assumed and μ_e is the Earth's gravitational constant $(3.9906 \times 10^{14} m^3 s^{-2})$. A higher order harmonic model to account for the Earth's oblateness can be used by replacing μ_e/r^2 with the harmonic expression. The superscript (i) = {1, 2, ... , n} indicates different stage values. The above complex model provides sufficient details for most trajectory analysis purposes.

The state variables in this model are airspeed V, heading angle χ, flight-path angle γ, longitude ϕ, latitude λ, radius vector from the Earth's center r, and vehicle mass m. The variables V, γ, χ are relative to the moving air. The wind velocity components W_i, W_j, W_k are assumed to be given as functions of $\{\phi, \lambda, h\}$, where $h = r - r_e$ is the altitude and r_e is the mean Earth radius $(6.378 \times 10^6 m)$. The control variables are throttle η, angle of attack α and sideslip angle β. The coefficients of drag C_D, side force C_Y and lift C_L are functions of α, β and Mach number $M = V/c$. The fuel rate f is a function of throttle setting, altitude and time. The after-jettison stage mass $m(t_{s+})$, staging time t_s, are vehicle parameters, and are both assumed fixed here. Standard atmospheric properties such as density ρ, pressure p, and sound speed c are given functions of h. The coefficients and properties are given in tabular forms which are interpolated as smooth functions of the independent variables.

2.2 Assumptions and Simplifications

To simplify the analysis, the following assumptions are exercised:

<u>Analytic thrust expression</u> - As mentioned in the previous section, a typical launch vehicle employs maximum throttle $\eta = 1.0$ during the ascent phase. For most trajectory analysis purposes, thrust can be adequately modeled as

$$T_{max}^{(i)} = T_{vac}^{(i)} - A_e^{(i)} p \qquad\qquad (2.3)$$

where T_{vac} is the vacuum thrust value and A_e is the engine nozzle exit area. The term $A_e p$ represents the back-pressure effect that causes a drop of thrust level as the engine is operated inside the atmosphere.

Constant fuel rate - For a purely rocket propulsion system the rate of fuel consumption is proportional to the vacuum thrust

$$\dot{m} = -T_{vac}^{(i)} / (g_e I_{sp}^{(i)})$$

(2.4)

where $g_e = \mu_e/r_e^2$, and I_{sp} is the specific impulse, a measure of the fuel efficiency. Modern rocket engines have values ranging from 300s to 450s*.

Non-rotating Earth - The Earth's rotation, ω_e is small (7.27 x 10^{-5}rads^{-1}) and the term $r\omega_e^2$ which represents the transport acceleration, was neglected. The term $2\omega_e V$ which represents the Coriolis acceleration may reach $0.1g_e$ at orbital speed. Here g_e is the gravitational acceleration at the Earth's surface. However, the vehicle reaches orbital speed sharply near the end of its flight phase. Therefore, the dominant effect of this term is only apparent for a short period of time, and setting $\omega_e = 0$ does not produce any significant error.

Planar motion - In actual flight, the lateral maneuver is short. This magnitude is dependent on the launch site which is selected as close to the equator as possible so that a wide range of orbit inclination can be achieved. A large amount of lateral maneuver is typically not required and the desired flight azimuth can be achieved very early in the flight. Hence for simplicity, it is assumed that there is no out-of-plane motion by setting $\beta = W_j = 0$ and considering $C_Y(\beta = 0) = 0$. These assumptions allow us to decouple the dynamics of airspeed, flight-path angle and altitude from those of heading angle, longitude and latitude, and the dynamics are reduced to those associated with motion in the vertical plane. For convenience, the vehicle is assumed to be launched due east on the equator, i.e. $\chi_o = 90^o$ and $\lambda_o = 0$, and ϕ_o is arbitrarily set to zero. The resultant system is a 4-state model:

$$\dot{V} = \frac{T^{(i)}\cos\alpha - D^{(i)}}{m(t)} - \frac{\mu_e}{r^2}\sin\gamma - \dot{W}_i\cos\gamma - \dot{W}_k\sin\gamma \qquad ; V(t_o) = V_o$$

$$\dot{\gamma} = \{\frac{T^{(i)}\sin\alpha + L^{(i)}}{m(t)} - (\frac{\mu_e}{r^2} - \frac{V^2}{r})\cos\gamma + \dot{W}_i\sin\gamma - \dot{W}_k\cos\gamma\}\frac{1}{V} \; ; \gamma(t_o) = \gamma_o$$

$$\dot{\phi} = \frac{V\cos\gamma + W_i}{r} \qquad ; \phi(t_o) = 0$$

$$\dot{r} = V\sin\gamma + W_k \qquad ; r(t_o) = h_o + r_e$$

(2.5)

where

---

* For comparison, specific impulse of turbojet engine is over 5000s.

10

$$m(t) = \begin{cases} m_0 - k^{(1)}(t - t_0) & ; t_0 \le t \le t_s^{(1)} \\ m_s^{(j)} - k^{(j)}(t - t_s^{(j)}) & ; t_s^{(j)} \le t \le t_s^{(j+1)} \end{cases} ; t_s^{(n)} = t_f ; j = 1, ..., n-1$$

$$k^{(i)} = T_{vac}^{(i)} / (g_e I_{sp}^{(i)}) \tag{2.6}$$

The initial conditions chosen for this problem represent the vehicle states following a vertical launch and clearing of the launch tower. The terminal constraints represent direct injection at the perigee of an 80nm x 150nm elliptical transfer orbit.

$$V_0 = 64.49 m/s \qquad ; \gamma_0 = 89.5^o \quad ; h_0 = 400m \qquad ; t_0 = 15s$$

$$V_f = 7858.2 m/s \qquad ; \gamma_f = 0^o \qquad ; h_f = 148160m \tag{2.7}$$

The objective is to minimize the final time, which is equivalent to minimizing the fuel consumption for this formulation. Since there is no constraint on ϕ_f, the ϕ dynamics in Eq. 2.5 are ignorable and can be deleted from the analysis. Also, the optimization must be performed subject to the constraints $q \le q_{max}$ and $|\alpha q| \le (\alpha q)_{max}$.

2.3 Aerodynamic Model and Launch Vehicle Configuration

The aerodynamic model (cf. Figs. 2.3 - 2.8) is obtained from [27]. It corresponds to a generic model of a heavy-lift capacity 2-stage launch vehicle based on a CFD analysis. The vehicle has an asymmetric configuration as shown in Fig. 2.2 with the booster mounted atop the main body. The booster produces a shadowing effect above supersonic speeds during the first stage flight. This shadow effect reduces the C_D at positive angle of attack and the C_D exhibits a nonconvex behavior (cf. Fig. 2.6) in α above Mach 1.3. Other than this behavior, $C_D(\alpha)$ and $C_L(\alpha)$ are nearly parabolic and linear respectively at all Mach numbers.
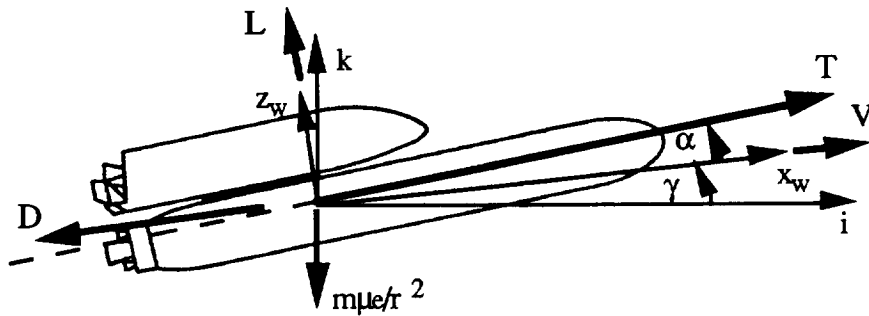
Figure 2.2. Generic Advanced Launch System (ALS) Model in the Cik Plane.
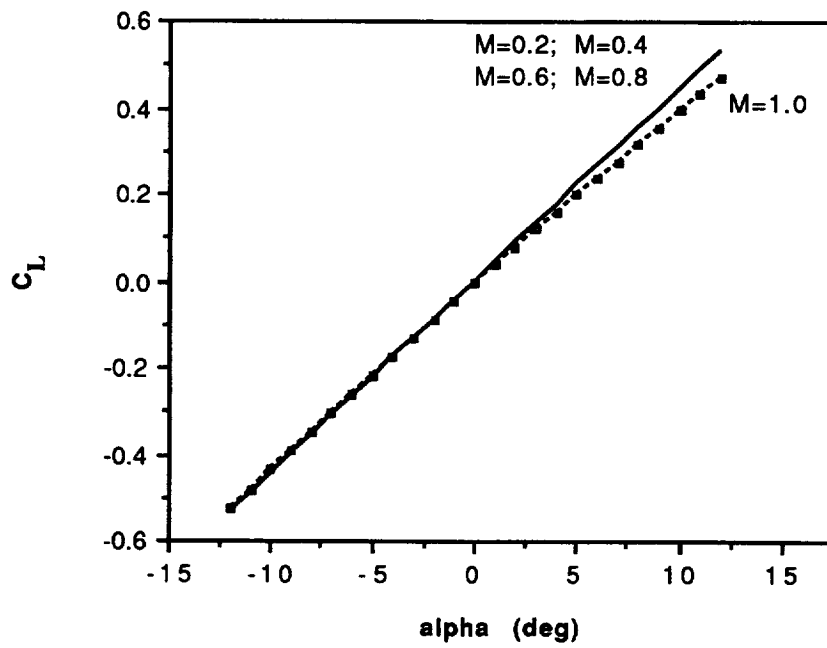
Figure 2.3. ALS First Stage C_L Profile.
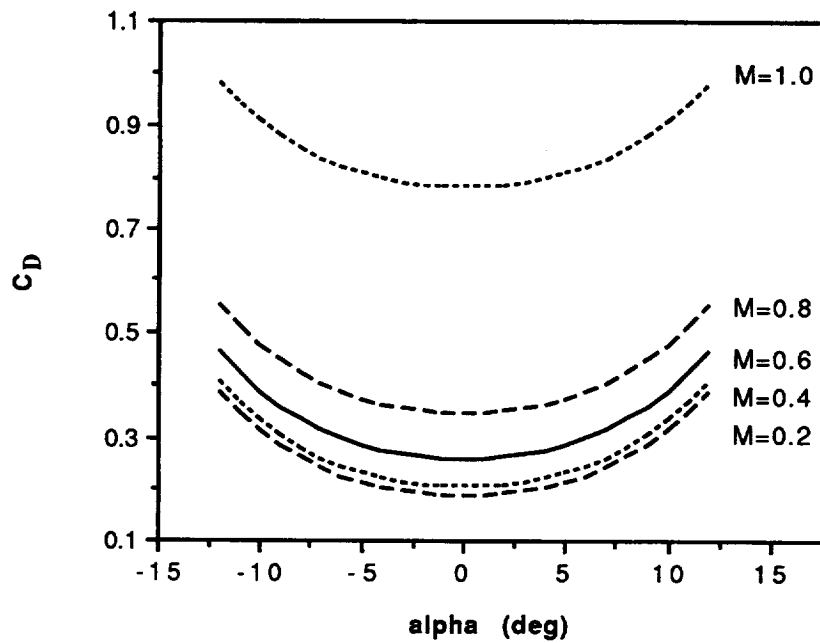
Figure 2.4. ALS First Stage C_D Profile.

12
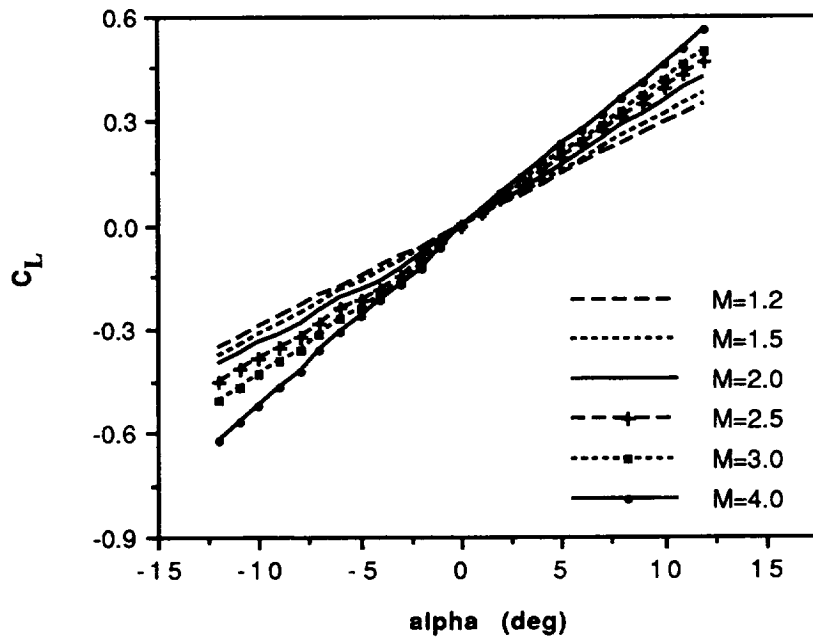
Figure 2.5. ALS First Stage C_L Profile (continued).
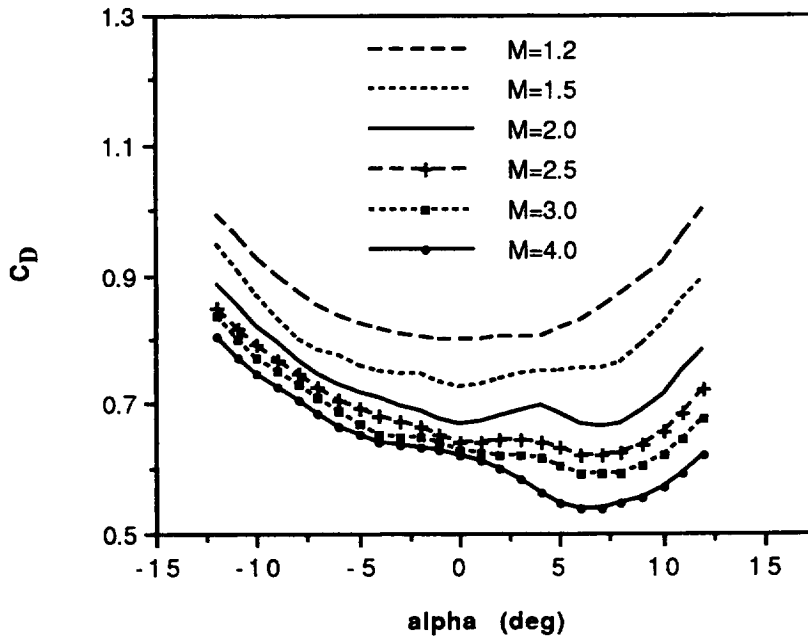
Figure 2.6. ALS First Stage C_D Profile (continued).
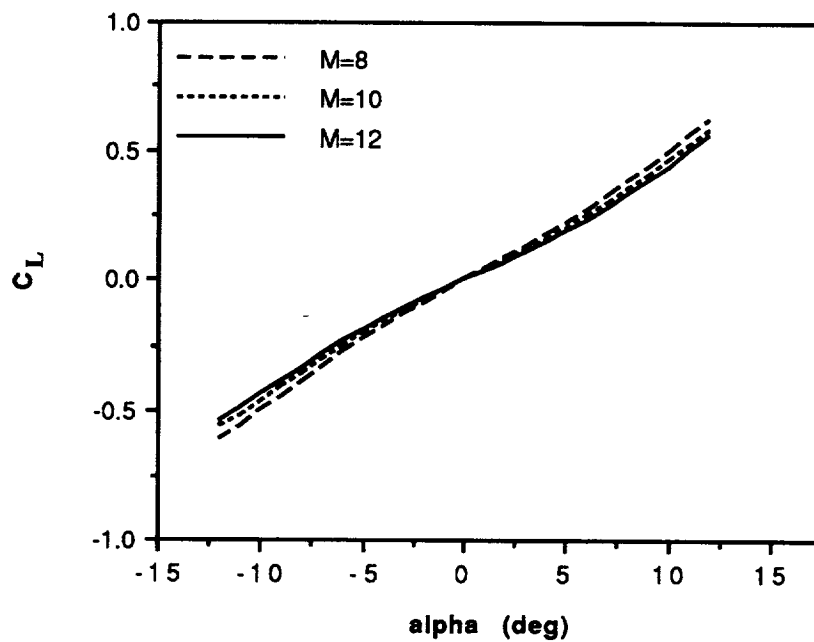
Figure 2.7. ALS Second Stage C_L Profile.
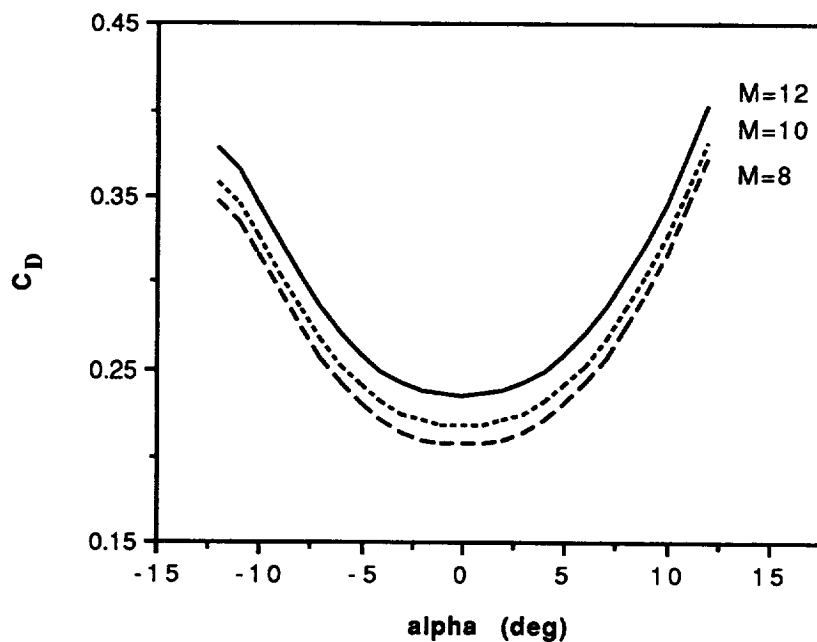
Figure 2.8. ALS Second Stage C_D Profile.

14

Due to the nonconvexity in C_D, the Hamiltonian also becomes nonconvex. The control is expected to jump as α switches from a lower value to higher value when the two peaks (using Maximum Principle) of the Hamiltonian become equal as time progresses. The phenomenon is displayed in Fig. 2.9. The study documented in [22] has shown that the hodograph can be convexized when bank angle is used as a second control variable, and the angle simply switches from 0 to π to make use of the lower C_D at small positive α. It has also shown that the effect of a chattering control of the first kind [27], if exists, will be small and that a chattering arc is not expected. This hypothesis is consolidated by the numerical analysis here, where no high frequency control activity is observed within the nonconvex region.
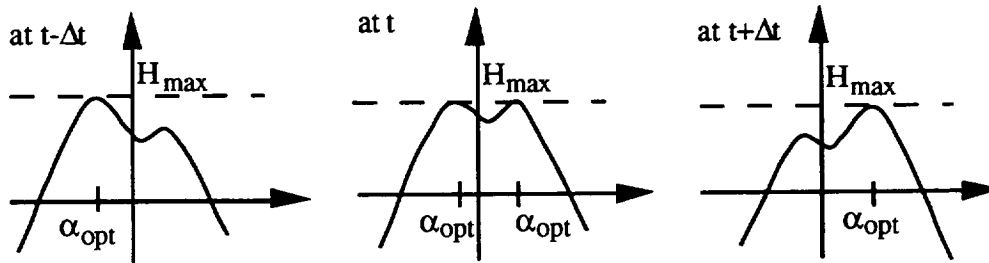
Figure 2.9. Jump in Control due to Nonconvex Hamiltonian.

Table 2.1. ALS Vehicle Physical Data

	1st-stage	2nd-stage
$m_0(t_0)$; $m_s(t_{s+})$	1,523,400kg (15s)	546,600kg (158.5s)
T_{vac}	25,813,000N	7,744,000N
I_{sp}	430s	430s
S	131.34m^2	65.67m^2
A	37.51m^2	11.25m^2
q_{max}	40698.2Nm^{-2}	nil
$(\alpha q)_{max}$	167,580degNm^{-2}	nil

Since sideslip is not considered, the aerodynamic coefficients can be interpolated as bicubic splines [28] in α and M. The interpolation scheme provides up to second order continuous derivatives. Other physical parameters of the ALS vehicle are given in Table 2.1.

2.4 Atmospheric Model

The atmospheric model is based on the 1975 U. S. Standard Atmosphere [29]. Profiles of normalized density, pressure and sound speed with respect to their reference values at the Earth's surface ($\rho_e = 1.225$kgm^{-3}, $p_e = 101330$Nm^{-2}, $c_e = 340.3$ms^{-1}) are

given in Fig. 2.10. To investigate the effect of wind shear, a mean winter wind profile over Kennedy Space Center (KSC) is used to model the non-stationary atmosphere. The profile is shown in Fig. 2.11. It indicates a head-on wind for vehicle launched due east, and the vertical and horizontal (north) wind speed components are assumed to be zero.
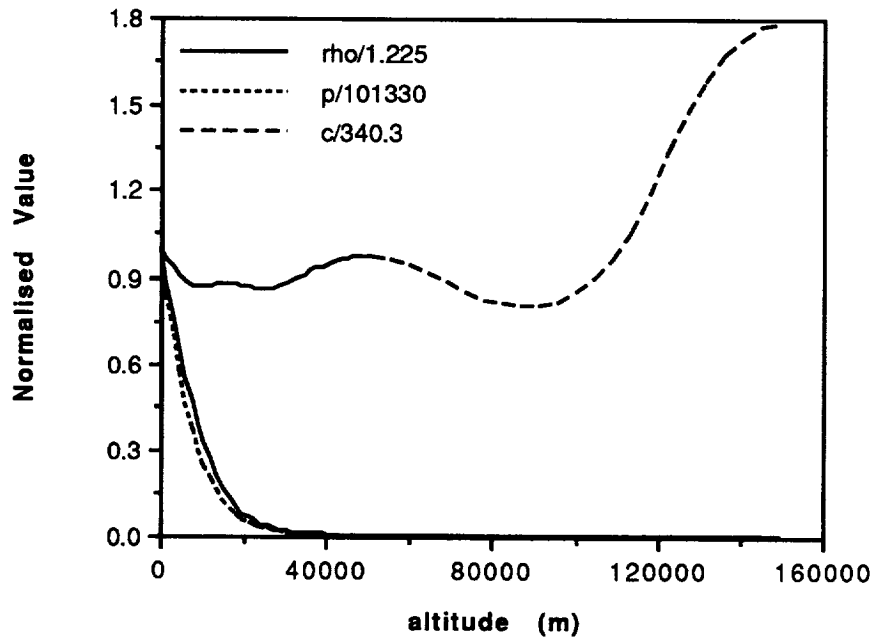
Figure 2.10. Standard Atmospheric Model.
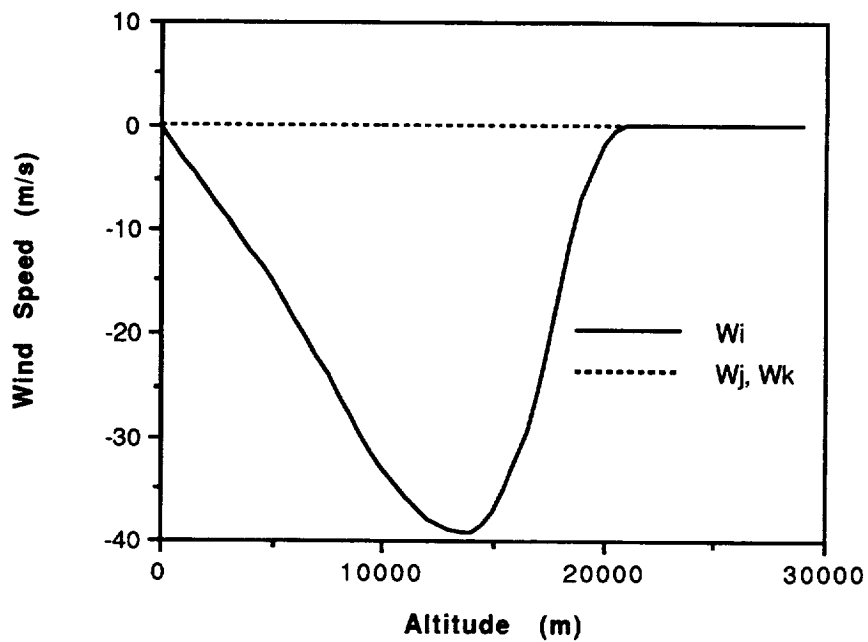
Figure 2.11. KSC Mean Wind Profile.

SECTION III

ANALYTICAL APPROACHES

Two analytical approaches are presented with the objective of simplifying the optimal guidance problem described in Sec. 2. The analytical and numerical results are summarized in this chapter. The analysis results are for: (1) a singular perturbation formulation, and (2) a regular perturbation formulation.

3.1 Singular Perturbations

Singular Perturbation theory is related to the study of a reduced solution of singularly perturbed systems of O. D. E's and the construction of a matched asymptotic series representation of the exact solution. For example, consider the following initial value problem

$$\frac{dx}{dt} = f(x,y,t) \qquad ; x(\varepsilon,0) = x_0$$

$$\varepsilon\frac{dy}{dt} = g(x,y,t) \qquad ; y(\varepsilon,0) = y_0 \qquad (3.1)$$

where x and y are scalar functions and $\varepsilon > 0$ is a scalar parameter. Setting ε to zero, we have the reduced system. Generally the reduced solution will not satisfy initial conditions on y, and the initial behavior of the reduced solution will be quite different from that of the exact one. This loss of boundary conditions on y (meaning that the reduced solution does not provide a uniformly valid approximation for y) is a characteristic of singular perturbation problem formulations. Basically, the system is separated into the slow variables of x and the fast variables of y. The reduction of higher order problems into lower order ones and the separation of numerically stiff parts by using different time scales are the main advantages of the method. Applications of the method are detailed in [30, 31].

a) Energy state approximation

The energy state approximation is the most widely used approximation in aircraft performance optimization, and sometimes referred to as energy management. It has been applied to minimum time-to-climb, minimum fuel-to-climb and minimum time intercept problems. First we replace the velocity with the mass specific energy

---

* A third analytical attempt using matched asymptotic methods is documented in [25].

$$E = V^2 / 2 - \mu_e / r \tag{3.2}$$

as the state variable. Differentiating Eq. 3.2 and using Eqs. 2.5, 2.6 leads to the system

$$\dot{E} = \frac{T^{(i)} \cos\alpha - D^{(i)}}{m(t)} V$$

$$\dot{r} = V \sin\gamma$$

$$\dot{\gamma} = \{\frac{T^{(i)} \sin\alpha + L^{(i)}}{m(t)} - (\frac{\mu_e}{r^2} - \frac{V^2}{r})\cos\gamma\} / V \tag{3.3}$$

where $V = \sqrt{2(E + \mu_e / r)}$. At the moment, the wind shear effects are not considered. In earlier studies on supersonic aircraft [30, 31], specific energy and mass are regarded as slow variables and altitude and flight-path angle are treated as fast variables. So to put Eq. 3.3 into the singular perturbation form, we artificially introduce a bookkeeping parameter ε into Eq. 3.4 as follows:

$$\dot{E} = \frac{T^{(i)} \cos\alpha - D^{(i)}}{m(t)} V$$

$$\varepsilon\dot{r} = V \sin\gamma$$

$$\varepsilon\dot{\gamma} = \{\frac{T^{(i)} \sin\alpha + L^{(i)}}{m(t)} - (\frac{\mu_e}{r^2} - \frac{V^2}{r})\cos\gamma\} / V \tag{3.4}$$

The performance objective is to minimize t_f.

The necessary conditions are formulated by first moving ε to the right hand side of the differential equations, and define the Hamiltonian as

$$H = \tilde{\lambda}_E \frac{T^{(i)} \cos\alpha - D^{(i)}}{m(t)} V + \frac{\tilde{\lambda}_r}{\varepsilon} V \sin\gamma + \frac{\tilde{\lambda}_\gamma}{\varepsilon}\{\frac{T^{(i)} \sin\alpha + L^{(i)}}{m(t)}$$

$$-(\frac{\mu_e}{r^2} - \frac{V^2}{r})\cos\gamma\} / V + constraints \tag{3.5}$$

The costate dynamics satisfy:

$$\dot{\tilde{\lambda}}_E = -\frac{\partial H}{\partial E} \quad ; \dot{\tilde{\lambda}}_r = -\frac{\partial H}{\partial r} \quad ; \dot{\tilde{\lambda}}_\gamma = -\frac{\partial H}{\partial \gamma} \tag{3.6}$$

18

Now introduce the transformations $\lambda_E = \tilde{\lambda}_E$, $\varepsilon\lambda_r = \tilde{\lambda}_r$, $\varepsilon\lambda_\gamma = \tilde{\lambda}_\gamma$ which results in

$$\dot{\lambda}_E = -\frac{\partial H}{\partial E} \quad ; \quad \varepsilon\dot{\lambda}_r = -\frac{\partial H}{\partial r} \quad ; \quad \varepsilon\dot{\lambda}_\gamma = -\frac{\partial H}{\partial \gamma} \tag{3.7}$$

Note that λ_E is a slow variable and that λ_r, λ_γ are fast variables. The optimality condition is given by

$$\partial H / \partial\alpha = 0 \tag{3.8}$$

In the reduced problem ($\varepsilon = 0$) r and γ are treated as control-like variables, which is a consequence of setting $\varepsilon = 0$ in Eq. 3.7. The transformed costates λ_r, λ_γ (when substituted in Eq. 3.6) can be interpreted as Lagrange's multipliers used to enforce the constraints that result from setting $\varepsilon = 0$ in Eq. 3.5.

Reduced (outer) solution

The reduced or outer solution corresponds to the solution of Eqs. 3.4, 3.7 and 3.8 when ε is set to zero. The condition $\partial H/\partial r = 0$ (which results from setting $\varepsilon = 0$ in Eq. 3.7) is a first order necessary condition for a minimum of the Hamiltonian in Eq. 3.5 (we are minimizing the final time). Since the costate λ_E may be interpreted as $\partial t_f/\partial E(t_0)$, it follows that in the reduced problem, $\lambda_E < 0$. Hence a stronger statement for this optimality condition may be written as

$$r^* = \frac{\max}{r} \left\{ \left. \frac{T^{(i)}\cos\alpha - D^{(i)}}{m(t)} V \right\} \right|_{E,m} \tag{3.9}$$

subject to the conditions:

$$\gamma = 0$$

$$0 = \frac{T^{(i)}\sin\alpha + L^{(i)}}{m(t)} - (\frac{\mu_e}{r^2} - \frac{V^2}{r})\cos\gamma$$

$$q \leq 40698.2 \text{Nm}^{-2}$$

$$|\alpha q| \leq 2924.82 \text{radNm}^{-2} \tag{3.10}$$

The last two conditions are the dynamic pressure and aerodynamic load constraints. Starting at an initial energy level and initial mass, a one-dimensional search in altitude is performed. The energy level is then increased and the corresponding change in mass is
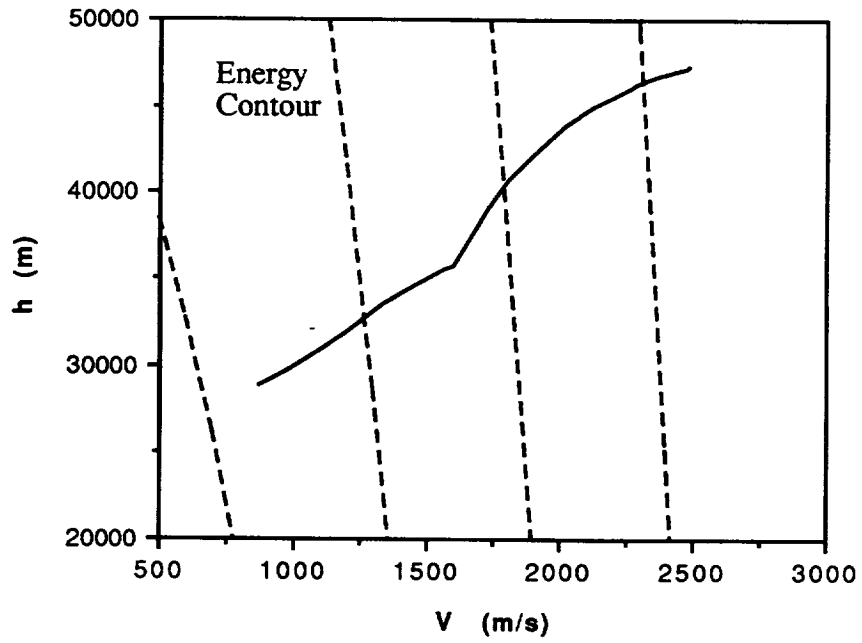
Figure 3.1. Reduced Solution with $\gamma = 0$.
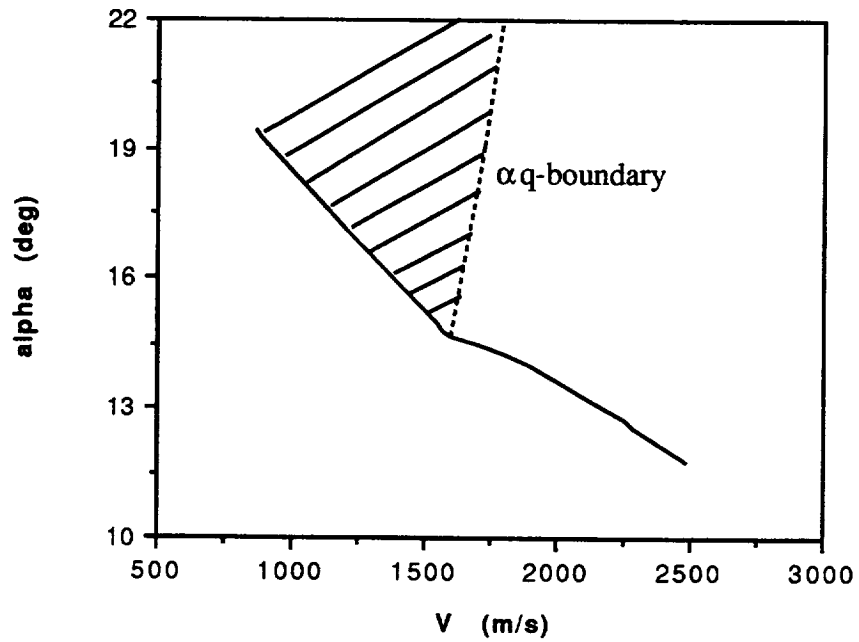
Figure 3.2. Angle of Attack Profile along the Reduced Solution.

20

Since the optimal solution also exhibits a large value of flight-path angle (inconsistent with the reduced solution approximation), another calculation scheme is used to estimated as

$$\Delta m = -k^{(i)}(\Delta E / \dot{E}^*) \tag{3.11}$$

where the superscript '*' denotes evaluation on the reduced solution. Hence by sweeping through all the energy levels of interest, a reduced feedback guidance law that defines the best altitude profile is obtained. Figs. 3.1 and 3.2 show the results for the reduced problem when the optimization in Eq. 3.9 is carried out for the first-stage flight. The initial conditions in E and m are chosen along a reference optimal trajectory. The solutions at low energy levels result in very large values of angle of attack ($> 20^\circ$) that are well beyond the given aerodynamic model range and therefore should not be considered feasible. The reduced solution is unrealistic in that the vehicle stays on the αq constraint up to an energy level of $-6.09 \times 10^7 Jkg^{-1}$.

Since the optimal solution also exhibits a large value of flight-path angle (inconsistent with the reduced solution approximation), another calculation scheme is used to estimate a non-zero flight-path angle and to include the effect of a non-zero flight-path angle in the reduced solution. Assuming the vehicle is already on the reduced solution and is to follow the trajectory, the change in altitude along the reduced solution gives an estimate of the flight-path angle according to

$$\sin \gamma_e = \left\{ \frac{\Delta h}{(\Delta E / \dot{E})V} \right\}^* \tag{3.12}$$

By perturbing the energy level from E to E + ΔE, we have

$$\Delta h^* = h^*(E + \Delta E) - h^*(E) \tag{3.13}$$

and a central difference scheme is used to estimate γ. Then the solution of Eqs. 3.9 and 3.10 is recalculated with $\gamma = 0$ replaced with $\gamma = \gamma_e$. The results are given in Figs. 3.3 and 3.4. The inclusion of γ_e gives a slightly lower value of α, and both angle profiles behave reasonably. However, this calculation scheme becomes numerically unstable once the vehicle left the αq constraint boundary.
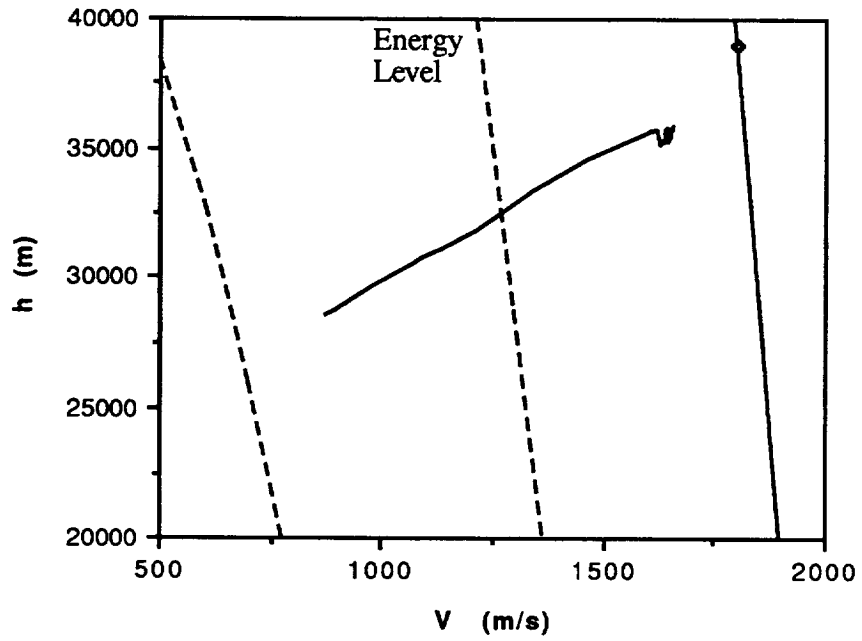
Figure 3.3. Reduced Solution Using Estimated Flight-path Angle.
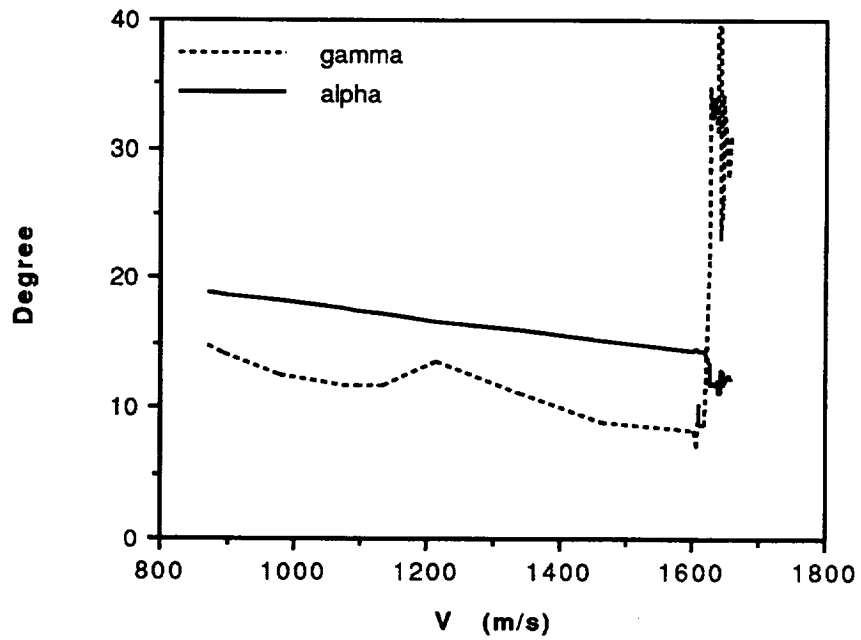
Figure 3.4. Alpha and Gamma Estimate Profiles.

b) Two-state model

Since the energy state approximation does not produce a solution that resembles a reasonable flight trajectory, a more accurate model is employed. The new reduced-order model corresponds to a 2-state approximation:

$$\dot{E} = \frac{T^{(i)} - D^{(i)}}{m(t)} V$$

$$\dot{r} = V \sin \gamma$$

$$\varepsilon \dot{\gamma} = \{ \frac{T^{(i)}\alpha + K_L^{(i)}\alpha}{m(t)} - (\frac{\mu_e}{r^2} - \frac{V^2}{r})\cos\gamma \} / V \tag{3.14}$$

where only the flight-path angle is assumed fast. To make Eq. 2.5 analytically tractable, we adopt the assumptions that the induced drag due to α is negligible and lift is linearly proportional to α ($L^{(i)} = K_L^{(i)}\alpha$). The necessary conditions for optimality of flight-path angle and angle of attack on the reduced solution are:

$$\frac{\partial H}{\partial \gamma} = \lambda_r V \sin\gamma \Rightarrow \quad \gamma = \begin{cases} \pi/2 & ; \lambda_r < 0 \\ singular & ; \lambda_r = 0 \\ -\pi/2 & ; \lambda_r > 0 \end{cases}$$

$$\alpha = \frac{m(t)}{T^{(i)} + K_L^{(i)}} (\frac{\mu_e}{r^2} - \frac{V^2}{r})\cos\gamma \tag{3.15}$$

In [23] it is shown that the velocity hodograph for the 3-state reduced model (including mass) is nonconvex, and that at $\lambda_r = 0$ the optimal solution chatters between $\gamma = \pm\pi/2$. The interpretation here is that when the altitude reaches its optimum value (for the current energy and mass), then a chattering solution is able to maintain the optimum altitude rate while maximizing the ratio of the mass rate to energy rate. Therefore this formulation is totally inappropriate for the analysis of energy climb in that it produces a reduced solution made up of vertical climbs and dives, connected by chattering arcs.

c) Manifold solution and eigenvalue analysis

The fundamental problem inherent in treating launch vehicle dynamics by energy state approximation relates to the constraints on the γ and h dynamics. They are fast in comparison to energy and mass dynamics and without taking into account the dependency on the singular perturbation parameter ε. For instance, the constraint on altitude dynamics implies $\gamma \equiv 0$ along the reduced solution, which is an extremely crude approximation for the
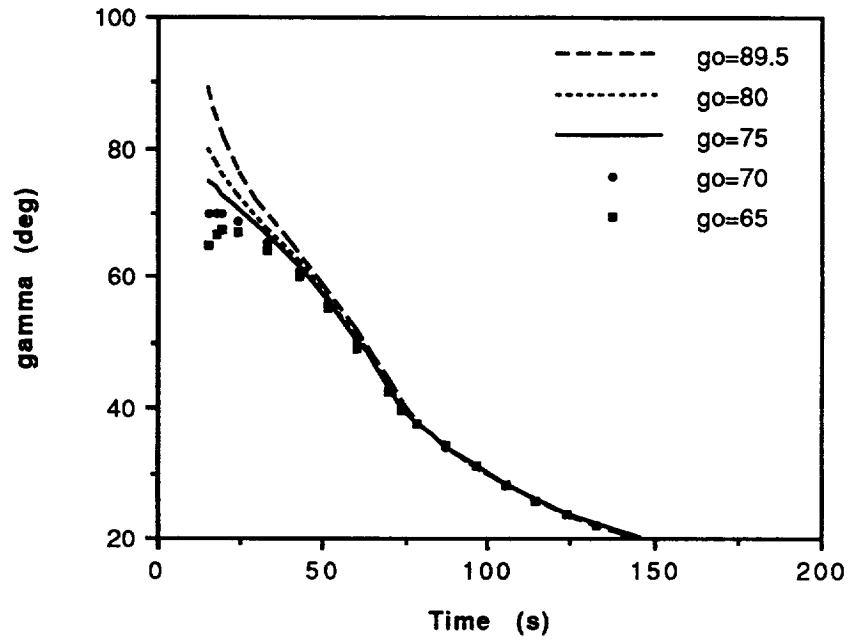
Figure 3.5. Flight-path Angle Profile for Various Reference Trajectories.
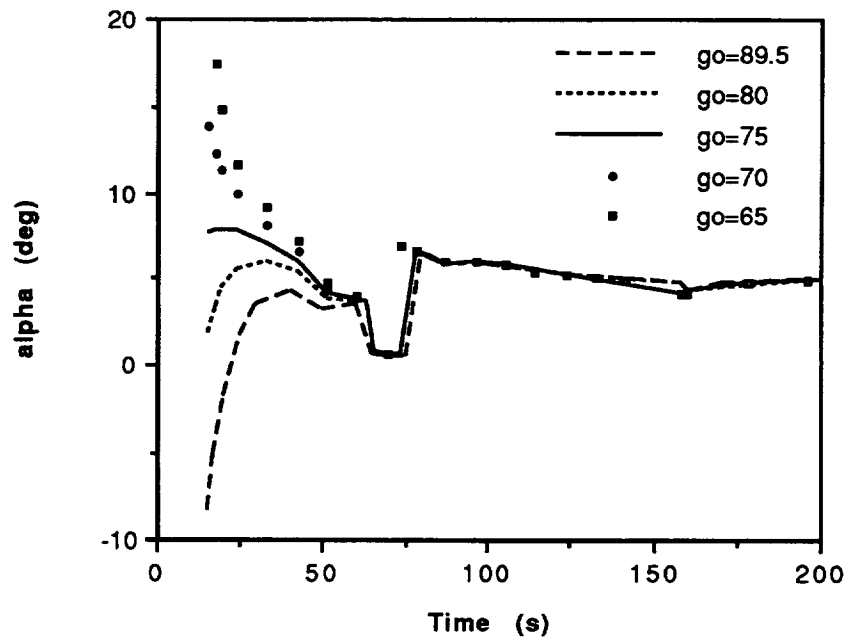
Figure 3.6. Angle of Attack Profile for Various Reference Trajectories.

launch vehicle case. This problem can be alleviated by using a slow manifold solution [32] in place of the reduced solution, which amounts to solving the exact problem with the initial flight-path angle chosen to suppress any fast motion that may be present in the solution. A separate boundary layer analysis could then perform to take into account the actual initial condition on γ (cf. Fig. 3.7). This approach has also been carried out, however it is found that the assumptions regarding the separation of dynamics worsen above supersonic speed, and the reduced-order model approximation deteriorates. This hypothesis is consolidated by the eigenvalues investigation described below.

Computation of the equilibrium manifold corresponds to determining the initial condition on γ so that rapid transients in γ and λ_γ are absent in the exact solution. First a sweep of the initial condition in γ about a nominal value of $\gamma_0 = 89.5^\circ$ is performed, and the exact dynamics of the states and costates (with the control eliminated using the optimality condition) are numerically integrated. This allows us to identify the equilibrium manifold by visual inspection for the absence of fast transients in γ and λ_γ. The closer the actual initial condition for the fast variable lies to the manifold, the more accurate the subsequent boundary layer correction in γ becomes. Figs 3.5 and 3.6 demonstrate that the manifold is estimated to be at $\gamma_0 = 75^\circ$, where it can be seen that there is no apparent boundary-layer-like behavior in the fast variable γ and the control α.
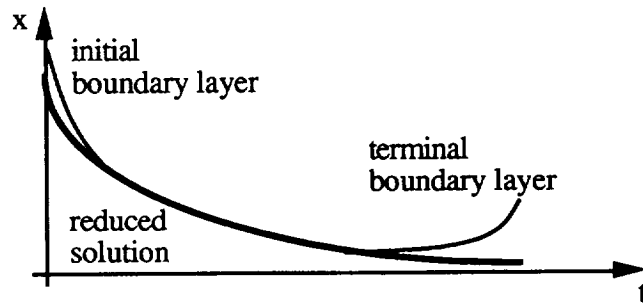
Figure 3.7. Typical Boundary Layer Characteristics.

To shed insight on the separation phenomenon of the fast and slow dynamics of the launch vehicle problem, an eigenvalue test is carried out. By linearizing the dynamics of E, r, γ, λ_E, λ_r, λ_γ about the equilibrium manifold, the eigenvalues of the linearized system are obtained, and the relative magnitudes of the real part of the eigenvalues provide information about the separation possibility of the dynamics. A Hamiltonian matrix appears in the linearized system whose eigenvalues characterize the full order system of dynamics (states and costates) in the vicinity of the equilibrium manifold.

Eigenvalues calculated at discrete points along the trajectory are shown in Figs. 3.8 and 3.9 (only those in the right half s-plane are shown). At the beginning part of the trajec-

25

tory (t < 50s), the results clearly show a separation configuration of 2 slow and 1 fast state (and costate) variables. All the eigenvalues are real. The relative magnitude is separated by a factor of up to 4 in this interval (cf. Fig. 3.9). As the energy level increases, two of the
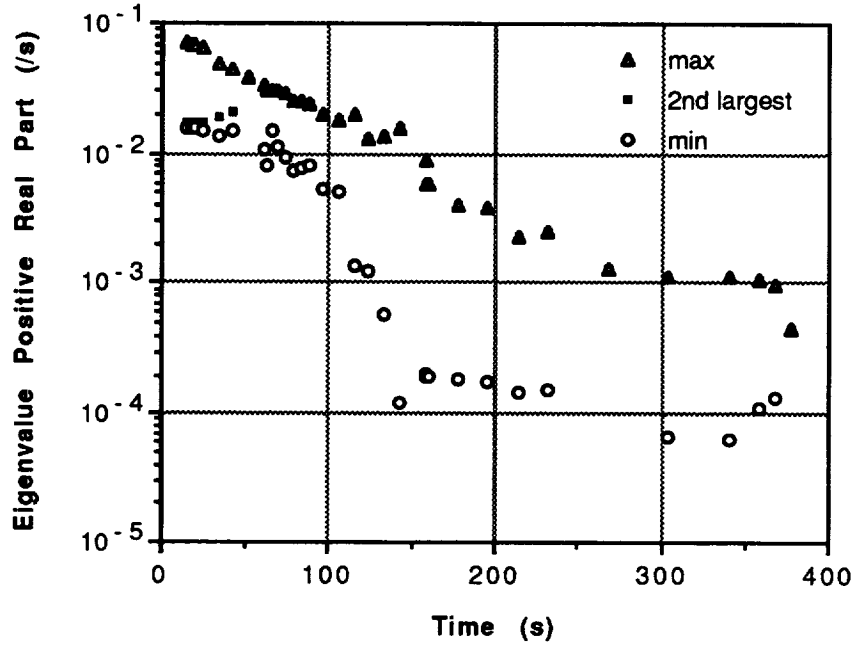
Figure 3.8. Eigenvalue Analysis along the Reference Trajectory of $\gamma_0 = 75^\circ$.
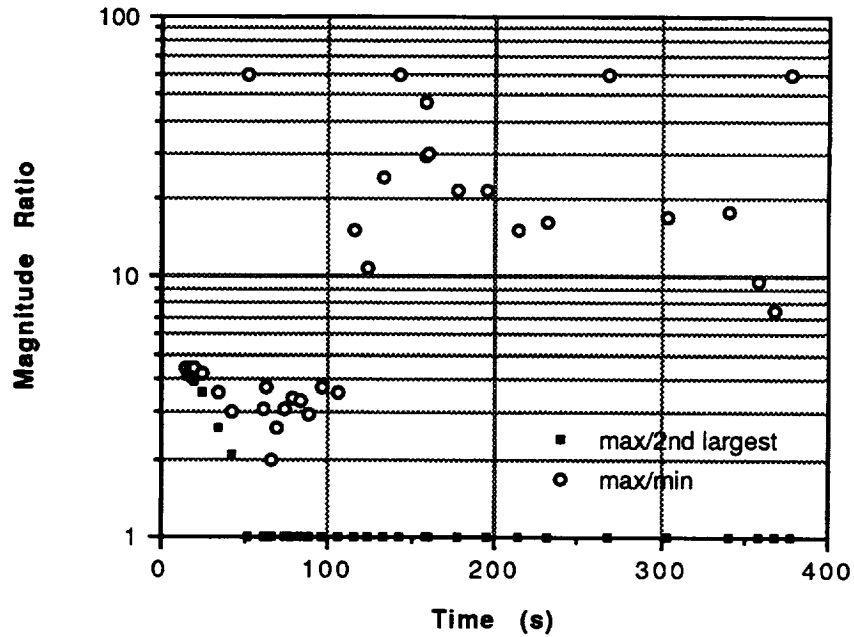
Figure 3.9. Eigenvalue Separation by Relative Magnitude.

26

eigenvalues join to form a complex conjugate pair, the real part of which is an order of magnitude larger than the third (real) root. This suggests a decomposition of 1 slow and 2 fast state variables. An eigenvector analysis indicates that the fast state variable at low energy levels indeed corresponds to the flight-path angle, whereas at high energy levels specific energy is the only slow state variable. Altitude, which was a slow variable at low energy levels, rapidly transitions to being a fast variable at approximately $t = 50s$ as shown in Figs 3.8 and 3.9.

A nonlinear feedback control solution for angle of attack, based on a boundary layer correction for the flight-path angle dynamics, can be formulated as follows:

$$H = -\lambda_{mo}k^{(i)} + \lambda_{Eo}\dot{E}(E_o,h_o,m_o,\alpha) + \lambda_{ro}V_o\sin\gamma + \lambda_\gamma\dot{\gamma}(E_o,h_o,m_o,\alpha) = 0$$

$$H_\alpha = 0 \tag{3.16}$$

where m_o, E_o, h_o, λ_{mo}, λ_{Eo}, λ_{ro} are treated as slow variables* in the manifold solution, and are constant in the boundary layer analysis. The manifold solution is stored as a function of energy, and the boundary layer problem defined in Eq. 3.16 is solved at each control update to form a guided solution. Note that there are two equations for the two unknowns in α and λ_γ. The guided solution using the pre-computed slow manifold (chosen for $\gamma_o = 75^o$ in Fig. 3.6) with an on-line boundary layer correction is plotted in Fig. 3.10. The optimal solution approaches the manifold solution. However the guided solution is first attracted to the manifold, and then diverges at about $t = 25s$. This correlates almost exactly with the transition that takes place in the eigenvalue associated with the altitude state in Fig. 3.8. That is, the role of altitude variable has changed, but the boundary layer analysis has treated the altitude variable as slow (constant to zero-order in ε). This explains the failure of the manifold approach for this problem.

Recalling the previous energy state approximation formulation, even though eigenvalues analysis clearly indicates the existence of a two-time scale behavior, the poor performance of the zero order reduced solution is attributed to the large value of longitudinal load factor inherent in the launch vehicle problem. The value of this non-dimensional variable along the reduced solution is plotted in Fig. 3.10. In comparison with a subsonic transport aircraft with a load factor of 0.1, the launch vehicle averages above 3 in this case and therefore a zero or even a first order solution is not expected to provide any reasonable approximation.

---

* Here we treat m as a state variable, and it is not eliminated by Eq. 2.6.
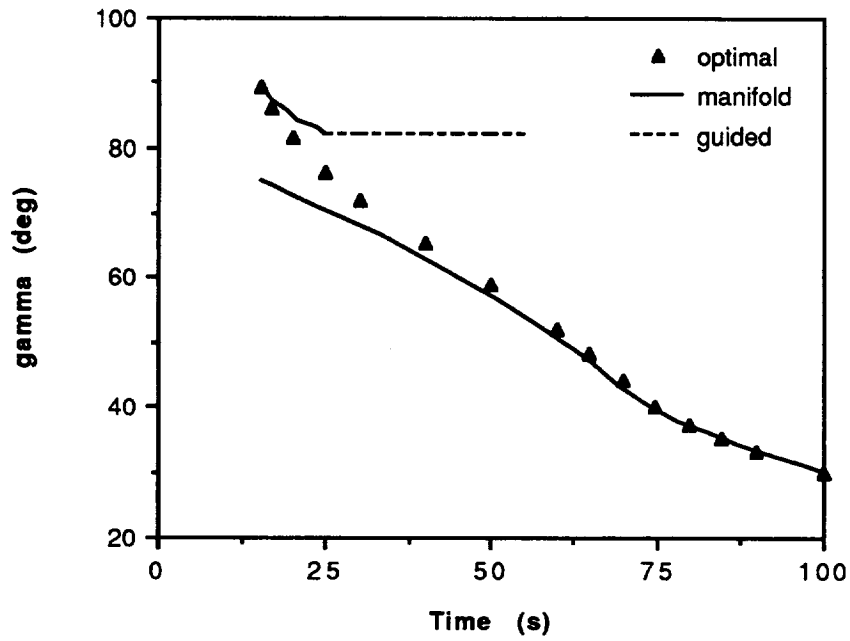
Figure 3.10. Flight-path Angle Profile of the Guided Solution.
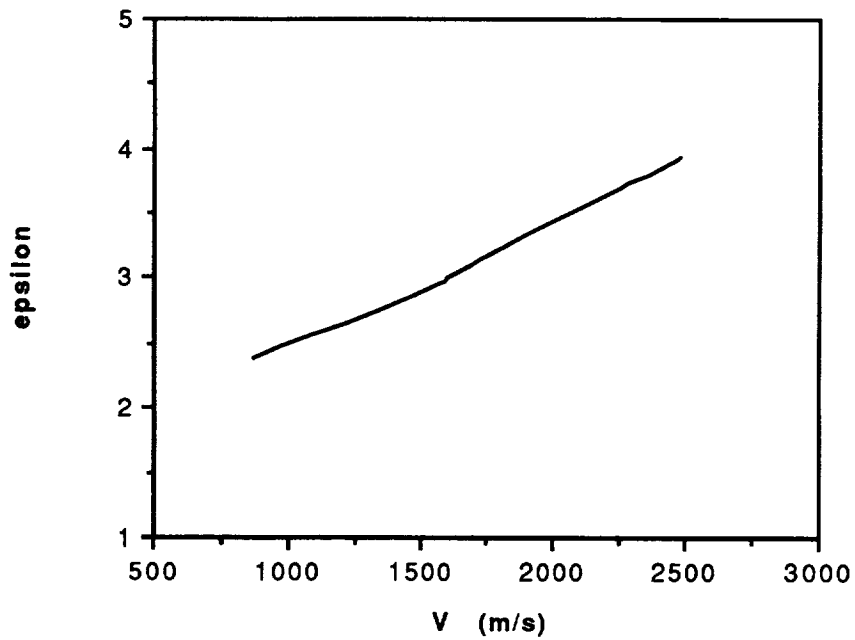
Figure 3.11. Evaluation of the Singular Perturbation
Parameter ε(E) for the ALS Vehicle.

3.2 Regular Perturbations

The unsuccessful attempt by singular perturbation analysis led to consideration of another analytic approach that has been used repeatedly on low thrust spaceflight problems, the regular perturbation analysis. In this section, the general regular perturbation formulation for optimal control problems is discussed. An extension over earlier formulations is that higher order corrections for the free final time are made explicitly in the formulation developed here. Then an analytic zero order solution based on the maximum horizontal speed transfer problem in a constant gravity field and in vacuum [33] is extended to a mass-varying multi-stage rocket. This is then followed by an attempt to compute a first order correction to account for a central gravitational field, spherical Earth and all the atmospheric effects.

a) Regular perturbations in optimal control

The optimal control problem formulation consider here is to maximize a performance index which is a function of the terminal states and time, subject to dynamic constraints:

$$J = \begin{matrix} max \\ u \end{matrix} \{\phi(x,t)\}\bigg|_{t_f} \tag{3.17}$$

$$\dot{x} = f(x,u,t) + \varepsilon g(x,u,t) \qquad ; x(t_0) = x_0 ; t \in [t_0,t_f] \tag{3.18}$$

and the terminal time constraints $\psi_i(x(t_f)) = 0, i = 1, \ldots, p \le n$. In Eq. 3.18, x is an n-dimensional state vector and u is an m-dimensional control vector. In applications, the expansion parameter ε is sometimes artificially inserted to signify the presence of small nonlinear effects, and used as a bookkeeping parameter for the regular expansion analysis. The Hamiltonian and transversality condition are given by:

$$H = \lambda^T \{f + \varepsilon g\} \qquad ; H(t_f) = -\Phi_t\bigg|_{t_f} ; \Phi = \phi + v^T \psi \tag{3.19}$$

The costate equations and associated boundary conditions are:

$$\dot{\lambda} = -H_x \qquad ; \lambda(t_f) = \Phi_x\bigg|_{t_f} \tag{3.20}$$

where the subscript is used to denote partial differentiation. In the absence of control constraints, the optimal control satisfies

$$H_u = \lambda^T \{f_u + \varepsilon g_u\} = 0 \tag{3.21}$$

29

assuming that $H_{uu} > 0$.

In the above final time is free. Thus, we introduce a new independent variable $\tau = (t - t_0)/T$ where $T = t_f - t_0$ and rewrite the necessary conditions of Eqs. 3.18 - 3.20 in the following equivalent form:

$$x' = H_\lambda T \qquad ; x(\tau = 0) = x_0 \ ; \ \psi(x(\tau = 1)) = 0 \qquad\qquad (3.22)$$

$$\lambda' = -H_x T \qquad ; \lambda(\tau = 1) = \Phi_x\Big|_{\tau = 1} \qquad\qquad (3.23)$$

$$T' = 0 \qquad\qquad (3.24)$$

$$H = \lambda^T\{f(x,u,\tau T + t_0) + \varepsilon g(x,u,\tau T + t_0)\} \ ; \ H(\tau = 1) = -\Phi_t\Big|_{\tau = 1} \qquad (3.25)$$

where $(\text{-})'$ denotes $d(\text{-})/d\tau$. In a regular perturbation analysis, the objective is to approximate the solution to Eqs. 3.22 - 3.25 by an asymptotic series in x, λ, u and T as follows:

$$x = x_0 + \varepsilon x_1 + \varepsilon^2 x_2 + \ \dots$$

$$\lambda = x_0 + \varepsilon\lambda_1 + \varepsilon^2\lambda_2 + \ \dots$$

$$u = u_0 + \varepsilon u_1 + \varepsilon^2 u_2 + \ \dots$$

$$T = T_0 + \varepsilon T_1 + \varepsilon^2 T_2 + \ \dots \qquad\qquad (3.26)$$

Assume the functions f, g, ϕ, ψ have piecewise continuous derivatives up to order at least K+1 where K is the order of approximation. Using the Taylor series formula, a finite series approximation is constructed according to

$$F(\sigma_0 + \sum_{k=1}^{K}\sigma_k\varepsilon^k) = F(\sigma_0) + \varepsilon\frac{dF}{d\sigma}\Big|_{\sigma_0}\sigma_1 + \varepsilon^2\{\frac{dF}{d\sigma}\Big|_{\sigma_0}\sigma_2 + \frac{1}{2!}\frac{d^2F}{d\sigma^2}\Big|_{\sigma_0}\sigma_1^2\} + \ \dots \quad (3.27)$$

where $\sigma = \{x, \lambda, v, u, T\}$. Substituting the series representation for each of the variables in Eqs. 3.22 - 3.25 and equating like powers in ε, we obtain the zero order and higher order necessary conditions. To zero order we have:

$$\partial x_0 / \partial\hat{t} = \partial H_0 / \partial\lambda_0 \quad ; x_0(t_0) = x_0 \ ; \ \psi(x_0(t_0 + T_0)) = 0$$

$$\partial\lambda_0 / \partial\hat{t} = -\partial H_0 / \partial x_0 \ ; \ \lambda_0(\hat{t} = t_0 + T_0) = \Phi(x_0,\hat{t}) / \partial x_0\Big|_{\hat{t} = t_0 + T_0}$$

30

$$\partial H_0 / \partial u_0 = 0$$

$$H_0 = \lambda^T f(x_0, u_0, \hat{t}) \quad ; \quad H_0(\hat{t} = t_o + T_0) = -\Phi(x_0, \hat{t}) / \partial \hat{t} \Big|_{\hat{t} = t_o + T_0} \tag{3.28}$$

In Eq. 3.28, the new independent variable $\hat{t} = \tau T_0$ has been introduced, where it should be noted that in the zero order problem $T = T_0$.

For the higher order problems, they are governed by a set of nonhomogeneous linear O. D. E's. with the form of

$$\frac{d}{d\hat{t}}\begin{bmatrix} x_k \\ \lambda_k \end{bmatrix} = \begin{bmatrix} A_{11}(x_0,\lambda_0,T_0) & A_{12}(x_0,\lambda_0,T_0) \\ A_{21}(x_0,\lambda_0,T_0) & A_{22}(x_0,\lambda_0,T_0) \end{bmatrix} \begin{bmatrix} x_k \\ \lambda_k \end{bmatrix} + \frac{T_k}{T_0}\begin{bmatrix} C_1(x_0,\lambda_0,T_0) \\ C_2(x_0,\lambda_0,T_0) \end{bmatrix}$$

$$+ \begin{bmatrix} P_{1k}(x_0,\lambda_0,T_0, ...,x_{k-1},\lambda_{k-1},T_{k-1}) \\ P_{2k}(x_0,\lambda_0,T_0, ...,x_{k-1},\lambda_{k-1},T_{k-1}) \end{bmatrix} \tag{3.29}$$

where

$$A_{11} = f_x - f_u[(f_u^T\lambda)_u]^{-1}(f_u^T\lambda)_x$$

$$A_{12} = -f_u[(f_u^T\lambda)_u]^{-1}f_u^T$$

$$A_{21} = -(f_x^T\lambda)_x + (f_x^T\lambda)_u[(f_u^T\lambda)_u]^{-1}(f_u^T\lambda)_x$$

$$A_{22} = -f_x^T + (f_x^T\lambda)_u[(f_u^T\lambda)_u]^{-1}f_u^T$$

$$C_1 = f + (\hat{t} - t_o)\left\{f_{\hat{t}} - f_u[(f_u^T\lambda)_u]^{-1}(f_u^T\lambda)_{\hat{t}}\right\}$$

$$C_2 = -f_x^T\lambda - (\hat{t} - t_o)\left\{(f_x^T\lambda)_{\hat{t}} - (f_x^T\lambda)_u[(f_u^T\lambda)_u]^{-1}(f_u^T\lambda)_{\hat{t}}\right\} \tag{3.30}$$

and for $k = 1$:

$$P_{11} = g - f_u[(f_u^T\lambda)_u]^{-1}g_u^T\lambda$$

$$P_{21} = -g_x^T\lambda + (f_x^T\lambda)_u[(f_u^T\lambda)_u]^{-1}g_u^T\lambda \tag{3.31}$$

All the matrices in Eq. 3.30 are evaluated at the zero order solution values. To complete the necessary conditions, it is also required to expand the boundary conditions and the transversality condition in Eq. 3.28. Note that Eq. 3.29 explicitly shows the effect of higher order corrections to the final time, T. If the solution process is terminated at say,

k = 1, then a real-time sampled data implementation of the control solution would be constructed as follows. For the original system in Eq. 3.18, an expression for the optimal control is obtained as function of x and λ from the optimality condition in Eq. 3.21. Then, treating the present state as the initial state, a first order approximation is obtained by using $\lambda_0(t_0) + \varepsilon\lambda_1(t_0)$ as an approximation for $\lambda(t_0)$ to compute the control, where $\lambda_0(t_0)$ and $\lambda_1(t_0)$ are obtained from the solutions of the zero and the first order necessary conditions. This process is repeated at the next control update time by regarding the value of the state as the new initial state. Therefore, it is necessary to repeat the zero and first order solutions in updating the estimate of the costate variable.

The non-homogeneous linear ordinary differential equations in Eqs. 3.29 - 3.31 may be expressed in terms of a convolution by first obtaining a state transition matrix. The state transition matrix $\Omega_A(\hat{t}, t_0)$ is merely the partial derivative of the zero order solution at $\hat{t}$ with respect to the initial conditions $x_0(t_0)$ and $\lambda_0(t_0)$, hence it is easily computed given an analytic zero order solution. In Appendix A it is shown that the result can be expressed in the following form

$$\begin{bmatrix} x_k(\hat{t}) \\ \lambda_k(\hat{t}) \end{bmatrix} = \Omega_A(\hat{t}, t_0) \begin{bmatrix} x_k(t_0) \\ \lambda_k(t_0) \end{bmatrix} + \int_{t_0}^{\hat{t}} \Omega_A(\hat{t}, \tau) \left\{ \frac{T_k}{T_0} \begin{bmatrix} C_1(\tau) \\ C_2(\tau) \end{bmatrix} + \begin{bmatrix} P_{1k}(\tau) \\ P_{2k}(\tau) \end{bmatrix} \right\} d\tau$$

$$= \Omega_A(\hat{t}, t_0) \begin{bmatrix} x_k(t_0) \\ \lambda_k(t_0) \end{bmatrix} + T_k \frac{\hat{t} - t_0}{T_0} \begin{bmatrix} \dot{x}_0(\hat{t}) \\ \dot{\lambda}_0(\hat{t}) \end{bmatrix} + \int_{t_0}^{\hat{t}} \Omega_A(\hat{t}, \tau) \begin{bmatrix} P_{1k}(\tau) \\ P_{2k}(\tau) \end{bmatrix} d\tau \quad (3.32)$$

Using the above expression at $\hat{t} = T_0$ along with the expansions of the boundary conditions, we can solve for $\lambda_k(t_0)$, ν_k and T_k from a set of linear algebraic equations. Thus the major part of the computation for the first order term lies in the quadrature that must be performed in Eq. 3.32. In a discrete time implementation, if the current state is regarded as the initial state then $x_k(t_0) = 0$ in Eq. 3.32 since $x_0(t_0)$ satisfies the initial condition on the state variable. Since zero order solution changes at each update of the initial state, it is necessary to repeat the quadrature at each update for the higher order corrections. Alternatively, we can fix the zero order solution and treat $x_k(t_0)$ as the deviation between the current state and the zero order solution computed for the original epoch time, but evaluated at the present time. In this form it would be possible to pre-compute the quadrature and store it as a function of a monotonic variable along the trajectory. Thus the real-time process of solving the zero order problem and the quadrature can be avoided.

The case of discontinuous dynamics, such as might arise in a multi-stage launch vehicle, can be handled by a simple modification of Eq. 3.32. For example, in a two-stage representation we would have

32

$$\begin{bmatrix} x_k(\hat{t}) \\ \lambda_k(\hat{t}) \end{bmatrix} = \Omega_A^{(2)}(\hat{t}, t_s) \left\{ \Omega_A^{(1)}(t_s, t_0) \begin{bmatrix} x_k(t_0) \\ \lambda_k(t_0) \end{bmatrix} + T_k \frac{t_s - t_0}{T_0} \begin{bmatrix} \dot{x}_0^{(1)}(t_s) \\ \dot{\lambda}_0^{(1)}(t_s) \end{bmatrix} + \right.$$

$$\left. \int_{t_0}^{t_s} \Omega_A^{(1)}(\hat{t}, \tau) \begin{bmatrix} P_{1k}^{(1)}(\tau) \\ P_{1k}^{(2)}(\tau) \end{bmatrix} d\tau \right\} + T_k \frac{\hat{t} - t_s}{T_0} \begin{bmatrix} \dot{x}_0^{(2)}(\hat{t}) \\ \dot{\lambda}_0^{(2)}(\hat{t}) \end{bmatrix} +$$

$$\int_{t_s}^{\hat{t}} \Omega_A^{(2)}(\hat{t}, \tau) \begin{bmatrix} P_{1k}^{(2)}(\tau) \\ P_{2k}^{(2)}(\tau) \end{bmatrix} d\tau \quad ; \hat{t} > t_s \tag{3.33}$$

The superscripts (1), (2) denote the expressions for different sets of dynamics and t_s is the interior point where discontinuity occurs.

b) Launch vehicle application

The performance objective is to maximize $-t_f$ (ie. minimize final time) subject to the terminal conditions $V(t_f) = 7858.2 \text{ms}^{-1}$, $\gamma(t_f) = 0$, $h(t_f) = 148160\text{m}$, open $\phi(t_f)$. These conditions correspond to direct injection at the perigee of an 80nm x 150nm elliptical transfer orbit. First, it is necessary to derive a closed form, zero order solution which should be simple, but accurate enough such that the neglected dynamics can be corrected in a first order term.

Assuming that the dominant forces on the launch vehicle are thrust and gravity, an attempt is made to treat the atmospheric effects as a perturbation effect. To further simplify the problem, spherical Earth effects are also considered as perturbations (these effects are only apparent when the vehicle reaches orbital speed near the end of the flight). The result is similar to the maximum horizontal speed transfer problem in [33] for a flat Earth no-atmosphere situation. The differences here are that the mass of the vehicle is varying, the dynamics are discontinuous and the terminal boundary conditions are specified at an unknown final time. We now recast the dynamics of Eq. 2.5 in a regular perturbation format as in Eq. 3.18, in accordance with the above desired approximations:

$$\dot{v} = \frac{T_{vac}^{(i)} \sin\theta}{m^{(i)} - k^{(i)}t} - g_e + \varepsilon \left(\frac{-pA_e^{(i)} \sin\theta - D^{(i)} \sin\gamma + L^{(i)} \cos\gamma}{m^{(i)} - k^{(i)}t} \right.$$

$$\left. + g_e - \frac{\mu_e}{r^2} + \frac{u^2}{r} \right) \quad ; v(t_0) = v_0 ; i = 1, 2$$

$$\dot{u} = \frac{T_{vac}^{(i)} \cos\theta}{m^{(i)} - k^{(i)}t} + \varepsilon \left(\frac{-pA_e^{(i)} \cos\theta - D^{(i)} \cos\gamma - L^{(i)} \sin\gamma}{m^{(i)} - k^{(i)}t} - \frac{uv}{r} \right) \quad ; u(t_0) = u_0$$

$$\dot{r} = v \qquad ; r(t_0) = r_0 \tag{3.34}$$

33

where

$$m^{(1)} = m_0 + k^{(1)}t_0 \quad ; \quad m^{(2)} = m_s + k^{(2)}t_s$$

$$v = V \sin\gamma \qquad ; \quad u = V \cos\gamma \qquad ; \quad \theta = \alpha + \gamma \tag{3.35}$$

Here ε has been artificially introduced as an arbitrary bookkeeping parameter. The dynamics are expressed in a rectangular coordinate system to facilitate the closed form derivation of the zero order solution. The state variables v and u are the local vertical and horizontal velocity components. The control variable is θ, the thrust-vector angle measured from the local horizon.

The necessary conditions of optimality for the above formulation are:

$$\dot{\lambda}_v = -\lambda_r + \varepsilon\left(-\lambda_v \frac{\partial g_1}{\partial v} - \lambda_u \frac{\partial g_2}{\partial v}\right)$$

$$\dot{\lambda}_u = \varepsilon\left(-\lambda_v \frac{\partial g_1}{\partial u} - \lambda_u \frac{\partial g_2}{\partial u}\right)$$

$$\dot{\lambda}_r = \varepsilon\left(-\lambda_v \frac{\partial g_1}{\partial r} - \lambda_u \frac{\partial g_2}{\partial r}\right)$$

$$0 = (\lambda_v \cos\theta - \lambda_u \sin\theta)\frac{T_{vac}^{(i)}}{m^{(i)} - k^{(i)}t} + \varepsilon\left(\lambda_v \frac{\partial g_1}{\partial \theta} + \lambda_u \frac{\partial g_2}{\partial \theta}\right)$$

$$0 = \left\{\lambda_v \dot{v} + \lambda_u \dot{u} + \lambda_r \dot{r}\right\}\Big|_{t_f} - 1 \tag{3.36}$$

where the last two are the optimality and the transversality conditions respectively, and

$$g_1 = \frac{-pA_e^{(i)}\sin\theta - D^{(i)}\sin\gamma + L^{(i)}\cos\gamma}{m^{(i)} - k^{(i)}t} + g_e - \frac{\mu_e}{r^2} + \frac{u^2}{r}$$

$$g_2 = \frac{-pA_e^{(i)}\cos\theta - D^{(i)}\cos\gamma - L^{(i)}\sin\gamma}{m^{(i)} - k^{(i)}t} - \frac{uv}{r} \tag{3.37}$$

Zero order solution

Setting $\varepsilon = 0$, the costate solutions and the optimal control are given as follows (with some license taken with the zero order time notation):

$$\lambda_{v0}(t) = c_{v0} - c_{r0}t \quad ; \quad \lambda_{u0}(t) = c_{u0} \qquad ; \quad \lambda_{r0}(t) = c_{r0}$$

34

$$\tan(\theta_0(t)) = p = qt \quad ; p = c_{v0} / c_{u0} \quad ; q = c_{r0} / c_{u0} \quad (3.38)$$

The control satisfies a linear tangent law. Substituting Eq. 3.38 into Eq. 3.36, the state equations can be integrated in closed form. The solution that relates the states at $t \geq t_s$ to the initial conditions is presented below and for $t < t_s$, the terms involving variables with superscript (1) would simply be deleted.

$$v_0(t) = v_0 - g_e(t - t_0) + \left.\frac{T_{vac}^{(1)}}{k^{(1)}} G(m^{(1)}, k^{(1)}, \tau)\right|_{\tau = t_0}^{\tau = t_s} + \left.\frac{T_{vac}^{(2)}}{k^{(2)}} G(m^{(2)}, k^{(2)}, \tau)\right|_{\tau = t_s}^{\tau = t}$$

$$u_0(t) = u_0 + \left.\frac{T_{vac}^{(1)}}{k^{(1)}} F(m^{(1)}, k^{(1)}, \tau)\right|_{\tau = t_0}^{\tau = t_s} + \left.\frac{T_{vac}^{(2)}}{k^{(2)}} F(m^{(2)}, k^{(2)}, \tau)\right|_{\tau = t_s}^{\tau = t}$$

$$r_0(t) = r_0 + v_0(t - t_0) - \frac{1}{2} g_e(t - t_0)^2 - (t - t_0)\frac{T_{vac}^{(1)}}{k^{(1)}} G(m^{(1)}, k^{(1)}, t_0) -$$

$$(t - t_s)\left\{\frac{T_{vac}^{(2)}}{k^{(2)}} G(m^{(2)}, k^{(2)}, t_s) - \frac{T_{vac}^{(1)}}{k^{(1)}} G(m^{(1)}, k^{(1)}, t_s)\right\} +$$

$$\left.\frac{T_{vac}^{(1)}}{qk^{(1)}} K(m^{(1)}, k^{(1)}, \tau)\right|_{\tau = t_0}^{\tau = t_s} + \left.\frac{T_{vac}^{(2)}}{qk^{(2)}} K(m^{(2)}, k^{(2)}, \tau)\right|_{\tau = t_s}^{\tau = t} \quad ; t \geq t_s \quad (3.39)$$

where

$$F(m^{(i)}, k^{(i)}, \tau) = \frac{-\sinh^{-1}[\tan(\theta_0(\tau) - \eta)]}{\sqrt{1 + \Delta^2}} \quad ; \tan\eta = \frac{1}{\Delta} \quad ; \Delta = \frac{qm^{(i)} - pk^{(i)}}{k^{(i)}}$$

$$G(m^{(i)}, k^{(i)}, \tau) = -\Delta F(m^{(i)}, k^{(i)}, \tau) - \sinh^{-1}[\tan(\theta_0(\tau))]$$

$$K(m^{(i)}, k^{(i)}, \tau) = -\sec(\theta_0(\tau)) - [\tan(\theta_0(\tau)) + \Delta]G(m^{(i)}, k^{(i)}, \tau) \quad (3.40)$$

To solve for the solution, Eqs. 3.38 - 3.40 are evaluated at the zero order final time $t_{f0} = t_0 + t_s + T_0$ where T_0 represents the zero order, second stage, open flight time, and used to enforce the zero order expansion of the terminal boundary conditions and the transversality condition given below:

$$v(t_{f0}) = v_f \quad ; u(t_{f0}) = u_f \quad ; r(t_{f0}) = h_f + r_e$$

$$\left\{\lambda_{v0}\left(\frac{T_{vac}^{(2)} \sin\theta}{m^{(2)} - k^{(2)}t} - g_e\right) + \lambda_{u0}\frac{T_{vac}^{(2)} \cos\theta}{m^{(2)} - k^{(2)}t} + \lambda_{r0}v_0\right\}\bigg|_{t_{f0}} = 1 \quad (3.41)$$

There is a total of four unknowns c_{v0}, c_{u0}, c_{r0}, T_0 to be evaluated by the four conditions in Eq. 3.41.

First order solution

Using Eqs. 3.29 to 3.31, the first order correction dynamics for the launch vehicle problem become

$$\frac{d}{dt}\begin{bmatrix} v_1 \\ u_1 \\ r_1 \\ \lambda_{v1} \\ \lambda_{u1} \\ \lambda_{r1} \end{bmatrix} = \begin{bmatrix} 0 & 0 & 0 & a_{14}^{(i)} & a_{15}^{(i)} & 0 \\ 0 & 0 & 0 & a_{24}^{(i)} & a_{25}^{(i)} & 0 \\ 1 & 0 & 0 & 0 & 0 & 0 \\ 0 & 0 & 0 & 0 & 0 & -1 \\ 0 & 0 & 0 & 0 & 0 & 0 \\ 0 & 0 & 0 & 0 & 0 & 0 \end{bmatrix} \begin{bmatrix} v_1 \\ u_1 \\ r_1 \\ \lambda_{v1} \\ \lambda_{u1} \\ \lambda_{r1} \end{bmatrix} + \frac{T_1}{T_0}\begin{bmatrix} c_1^{(i)}(t) \\ c_2^{(i)}(t) \\ v_0(t) \\ -\lambda_{r0} \\ 0 \\ 0 \end{bmatrix} + \begin{bmatrix} p_1^{(i)}(t) \\ p_2^{(i)}(t) \\ 0 \\ p_4^{(i)}(t) \\ p_5^{(i)}(t) \\ p_6^{(i)}(t) \end{bmatrix} \qquad (3.42)$$

with $v_1(t_0) = u_1(t_0) = r_1(t_0) = v_1(t_{f0}) = u_1(t_{f0}) = r_1(t_{f0}) = 0$, where

$$a_{14} = \frac{T_{vac}^{(i)}}{m^{(i)} - k^{(i)}t}\left(\frac{\cos^2\theta}{\lambda_{v0}\sin\theta_0 + \lambda_{u0}\cos\theta_0}\right)$$

$$a_{15} = \frac{T_{vac}^{(i)}}{m^{(i)} - k^{(i)}t}\left(\frac{-\cos\theta_0\sin\theta_0}{\lambda_{v0}\sin\theta_0 + \lambda_{u0}\cos\theta_0}\right)$$

$$a_{24} = a_{15} \qquad ; \quad a_{25} = \frac{T_{vac}^{(i)}}{m^{(i)} - k^{(i)}t}\left(\frac{\sin^2\theta}{\lambda_{v0}\sin\theta_0 + \lambda_{u0}\cos\theta_0}\right)$$

$$c_1 = \frac{T_{vac}^{(2)}\sin\theta_0}{m^{(2)} - k^{(2)}t}\left[1 + \frac{k^{(2)}(t - t_s)}{m^{(2)} - k^{(2)}t}\right] - g_e \; ; \; c_2 = \frac{T_{vac}^{(2)}\cos\theta_0}{m^{(2)} - k^{(2)}t}\left[1 + \frac{k^{(2)}(t - t_s)}{m^{(2)} - k^{(2)}t}\right]$$

$$p_1 = g_1 - \frac{T_{vac}^{(i)}\cos\theta}{(m^{(i)} - k^{(i)}t)(\lambda_v\sin\theta + \lambda_u\cos\theta)}\left\{\lambda_v\frac{\partial g_1}{\partial\theta} + \lambda_u\frac{\partial g_2}{\partial\theta}\right\}$$

$$p_2 = g_2 + \frac{T_{vac}^{(i)}\sin\theta}{(m^{(i)} - k^{(i)}t)(\lambda_v\sin\theta + \lambda_u\cos\theta)}\left\{\lambda_v\frac{\partial g_1}{\partial\theta} + \lambda_u\frac{\partial g_2}{\partial\theta}\right\}$$

$$p_4 = -\lambda_v\frac{\partial g_1}{\partial v} - \lambda_u\frac{\partial g_2}{\partial v} \qquad ; \; p_5 = -\lambda_v\frac{\partial g_1}{\partial u} - \lambda_u\frac{\partial g_2}{\partial u}$$

$$p_6 = -\lambda_v\frac{\partial g_1}{\partial r} - \lambda_u\frac{\partial g_2}{\partial r} \qquad (3.43)$$

36

All the variables are evaluated along the zero order solution. Since the first stage flight time is assumed to be fixed, $T = t_f - t_s$. Consequently, $T_1 = 0$ for the dynamics describing $t < t_s$, and the second term in Eq. 3.42 is discarded for the correction dynamics corresponding to this time interval. In this example, the state transition matrix has a structure of

$$\Omega_A^{(i)}(t_2, t_1) = \begin{bmatrix} 1 & 0 & 0 & \omega_{14}^{(i)} & \omega_{15}^{(i)} & \omega_{16}^{(i)} \\ 0 & 1 & 0 & \omega_{24}^{(i)} & \omega_{25}^{(i)} & \omega_{26}^{(i)} \\ t_2 - t_1 & 0 & 1 & \omega_{34}^{(i)} & \omega_{35}^{(i)} & \omega_{36}^{(i)} \\ 0 & 0 & 0 & 1 & 0 & t_1 - t_2 \\ 0 & 0 & 0 & 0 & 1 & 0 \\ 0 & 0 & 0 & 0 & 0 & 1 \end{bmatrix} \tag{3.44}$$

Complete expression of the ω's are given in Appendix B, and the expansion of the transversality condition for the first order case is

$$0 = \left\{ \lambda_{v1} \left(\frac{T_{vac}^{(2)} \sin\theta_0}{m^{(2)} - k^{(2)} t} - g_e + g_{10} \right) + \lambda_{u1} \left(\frac{T_{vac}^{(2)} \cos\theta_0}{m^{(2)} - k^{(2)} t} + g_{20} \right) + \right.$$
$$\left. T_1 \frac{T_{vac}^{(2)} k^{(2)}}{(m^{(2)} - k^{(2)} t)^2} (\lambda_{v0} \sin\theta_0 + \lambda_{u0} \cos\theta_0) \right\} \Bigg|_{t = t_{f0}} \tag{3.45}$$

From Eq. 3.33, the first order variables at t_{f0} are related to their initial values at t_0 by

$$\begin{bmatrix} x_1(t_{f0}) \\ \lambda_1(t_{f0}) \end{bmatrix} = \Omega_A^{(2)}(t_{f0}, t_s) \left\{ \Omega_A^{(1)}(t_{f0}, t_s) \begin{bmatrix} x_1(t_0) \\ \lambda_1(t_0) \end{bmatrix} + \int_{t_0}^{t_s} \Omega_A^{(1)}(t_s, \tau) \begin{bmatrix} P_{11}^{(1)} \\ P_{21}^{(1)} \end{bmatrix} d\tau \right\} +$$
$$T_1 \begin{bmatrix} \dot{x}_1^{(2)}(t_{f0}) \\ \dot{\lambda}_1^{(2)}(t_{f0}) \end{bmatrix} + \int_{t_s}^{t_{f0}} \Omega_A^{(2)}(t_{f0}, \tau) \begin{bmatrix} P_{11}^{(2)} \\ P_{21}^{(2)} \end{bmatrix} d\tau \tag{3.46}$$

where $x_1 = \{v_1, u_1, r_1\}$, $\lambda_1 = \{\lambda_{v1}, \lambda_{u1}, \lambda_{r1}\}$, $P_{11} = \{p_1, p_2, 0\}$ and $P_{21} = \{p_4, p_5, p_6\}$. Substituting Eq. 3.46 into Eq. 3.45 and using the boundary conditions defined in Eq. 3.42, the unknown costate and final time corrections $\lambda_{v1}(t_0)$, $\lambda_{u1}(t_0)$, $\lambda_{r1}(t_0)$, T_1 can be found from a set of linear algebraic equations.

Figures 3.12 to 3.18 give the zero and first order results for a no-aerodynamic force case (obtained by setting the reference area $S = 0$). The optimal solution obtained from a multiple shooting code [10] is also included for comparison. As far as spherical Earth and back-pressure effects are concerned, the regular perturbation approach produces very accurate results, especially in the state histories. Next the aerodynamic effect is included,

the resulting angle of attack profile is shown in Fig. 3.19. No reasonable first order solution is found at low altitudes in the region of high dynamic pressure and aerodynamic forces. The first order solution over-corrects the zero order result and gives a very large value of angle of attack that is not considered feasible. The conclusion that is drawn from these results has been that the aerodynamic forces are simply too large to be ignored in the zero order solution. Figure 3.20 show the ratios of the aerodynamic forces to the thrust components along the optimal solution. The magnitude of lift to thrust ratio reaches almost 40% over some time interval during the first stage flight and indicates that a significant amount of aerodynamics effects exist in the ALS vehicle.

Figure 3.12. Regular Perturbation Results in v with
Spherical Earth and Back-pressure Effects.

Figure 3.13. Regular Perturbation Results in u with
Spherical Earth and Back-pressure Effects.

Figure 3.14. Regular Perturbation Results in h with
Spherical Earth and Back-pressure Effects.

Figure 3.15. Regular Perturbation Results in λ_v with
Spherical Earth and Back-pressure Effects.

Figure 3.16. Regular Perturbation Results in λ_u with
Spherical Earth and Back-pressure Effects.

40

Figure 3.17. Regular Perturbation Results in λ_r with
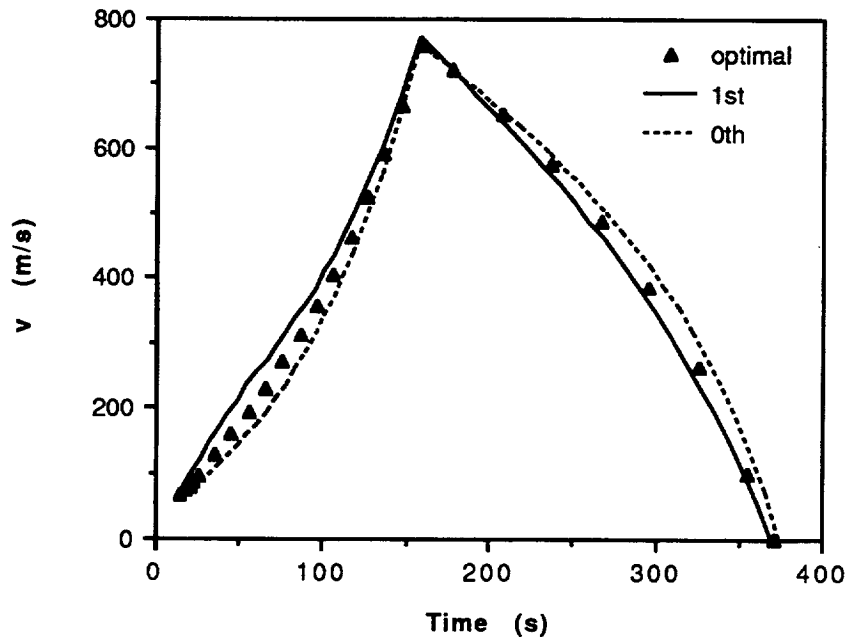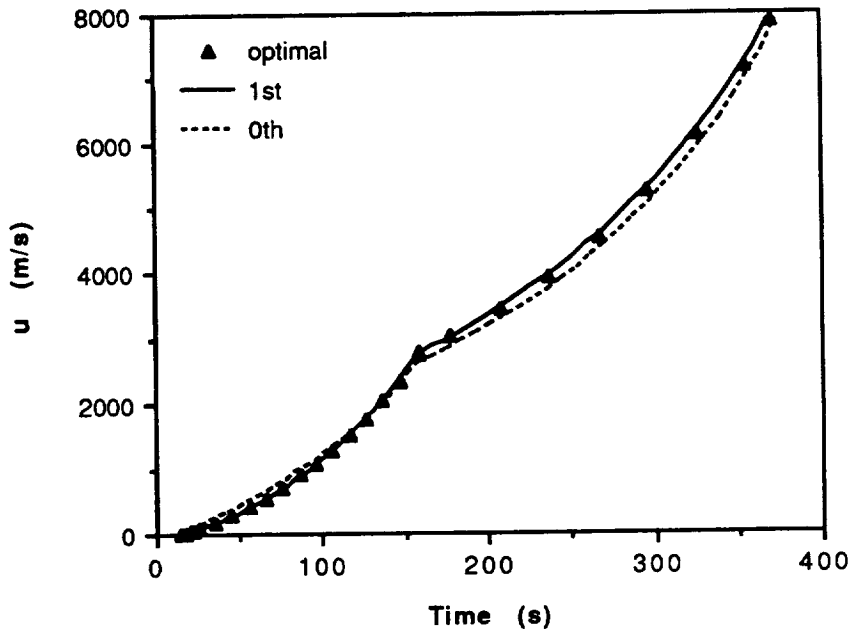Spherical Earth and Back-pressure Effects.

Figure 3.18. Regular Perturbation Results in α with
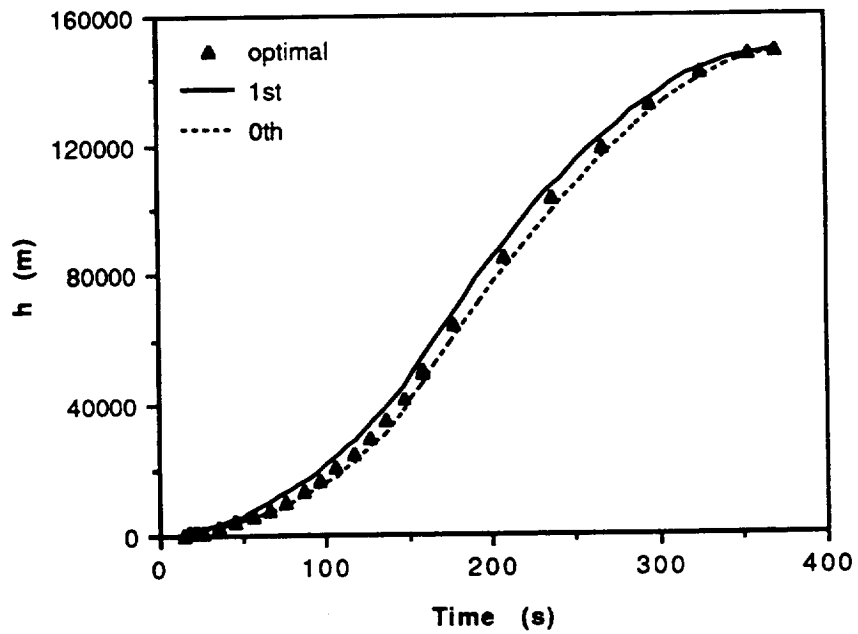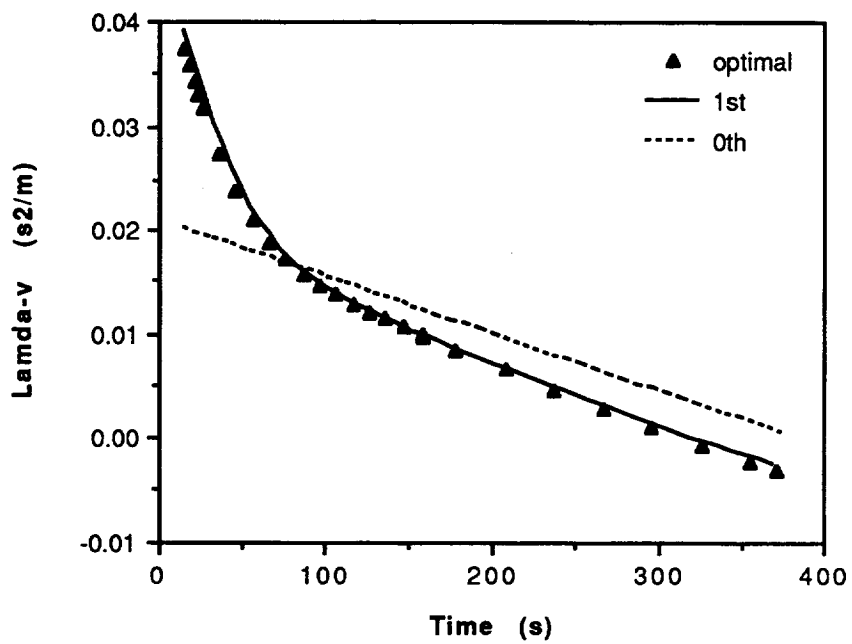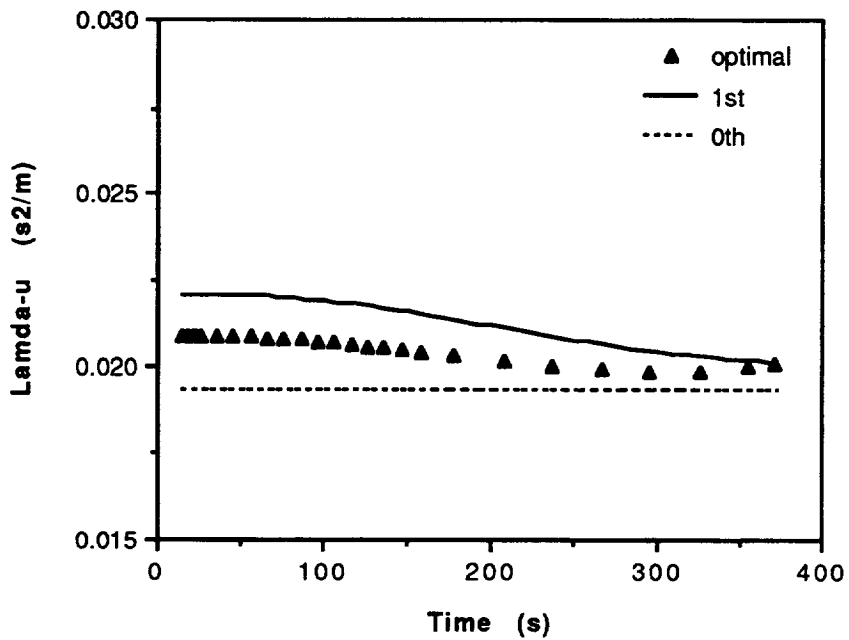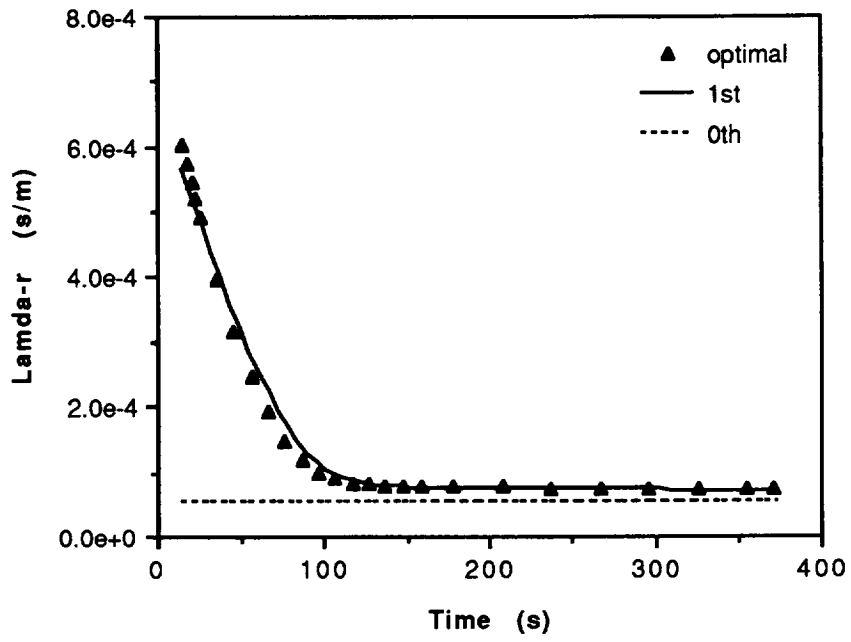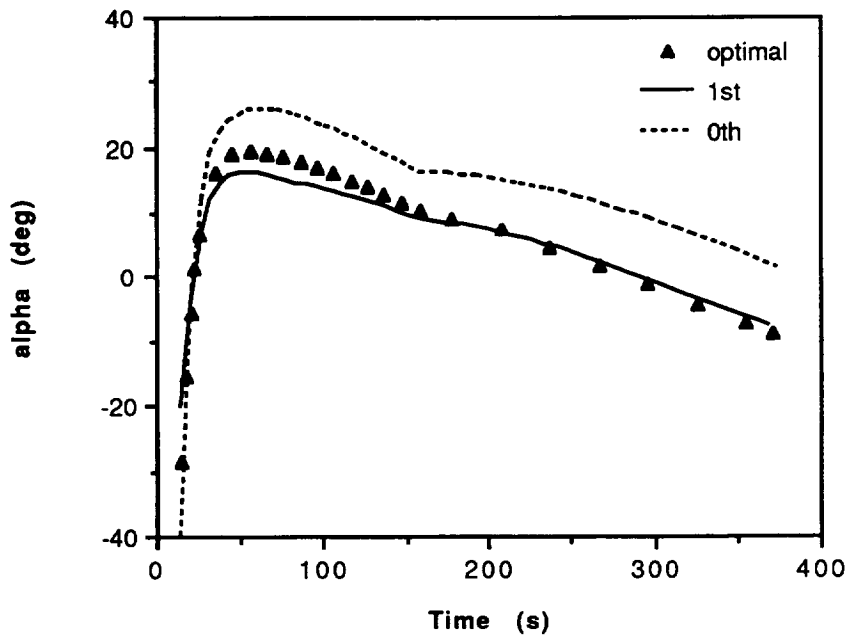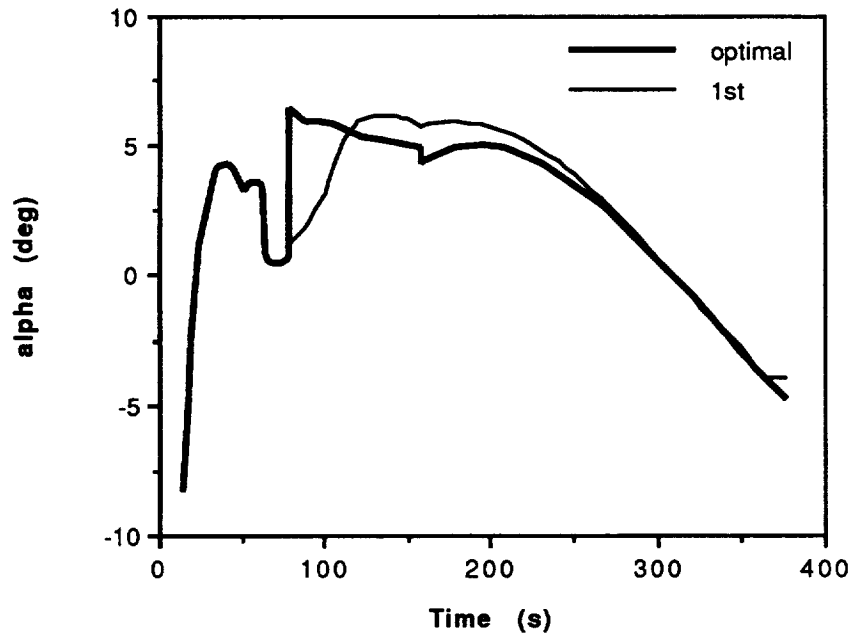Spherical Earth and Back-pressure Effects.

Figure 3.19. Regular Perturbation Results in α Including
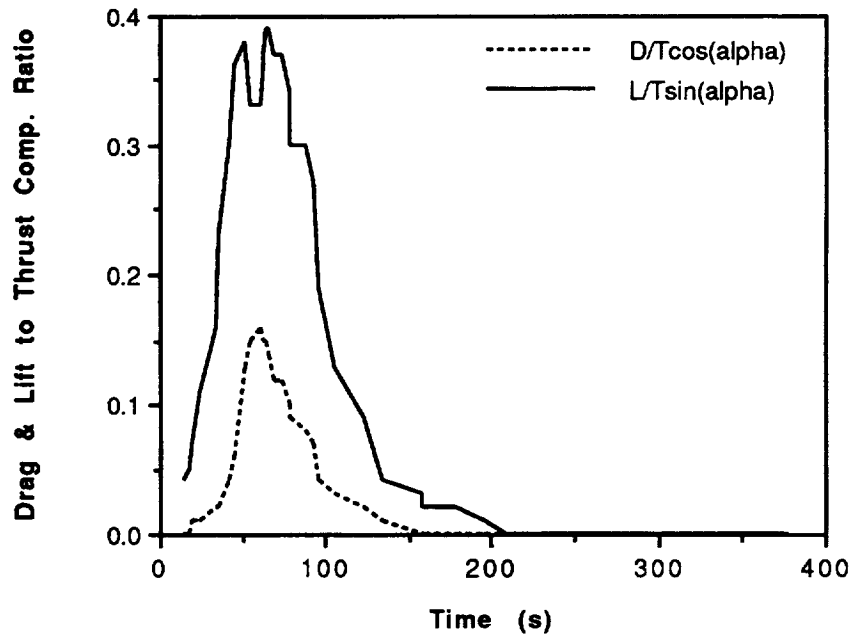Aerodynamic Effects.

Figure 3.20. Aerodynamic to Propulsive Force Ratios
Along the Optimal Trajectory.

42

SECTION IV

A HYBRID COLLOCATION/REGULAR
PERTURBATION ANALYSIS

This chapter develops a solution approach for nonlinear optimization problems that seeks to combine the desirable features of analytical methods which are based on the use of simplified models, and numerical methods that use elementary interpolation functions and finite elements to represent the solution. The approach is developed for a combination of regular perturbation analysis and collocation technique. A simple fourth order nonlinear system is used to illustrate the conceptual approach for several possible levels of approximation.

4.1 Introduction

Among the proposed analytical approaches for real time guidance in Chapter 3, the analysis by regular perturbation expansion of the solution is most appealing. However, crucial to the success of the method is that the optimal solution is reasonably approximated by the zero order solution, so that the addition of first or higher order corrections to the series solution (which usually is not convergent) results in an improvement in accuracy. The approach has had great success when applied to systems with small nonlinear terms [34, 35] so that the zero order problem is linear. Also, in certain applications a state transition matrix may be determined for the first and higher order corrections, further facilitating the solution process. The major limitation in guidance applications appears to be that significant nonlinearities, such as aerodynamic effects must be neglected in the zero order problem in order to obtain an analytic solution for the zero order problem, which is also nonlinear even in the absence of aerodynamic effects. It turns out in this case that the zero order problem is not sufficiently close to the original problem and the solution begins to diverge even when a first order correction is attempted (cf. Sec. 3.2b). A second drawback which is inherent in any attempt of analysis by model simplification is that a significant amount of re-analysis is required when even a minor change in the optimal control problem formulation is made.

Collocation [8, 36] is a general method for obtaining an approximate solution of differential equations. It involves choosing simple interpolating functions and enforcing the interpolatory constraints at specific points within finite elements to evaluate the unknown coefficients. Thus when applied to an optimal control problem, it reduces the associated two point boundary value problem to a set of coupled nonlinear algebraic equat-

ions. Collocation methods have the advantages that they are simple to use for a wide variety of optimization problems, and their accuracy can be improved by increasing the number of elements used in the approximation. The major disadvantages are that there is no general guarantee that the numerical methods employed will successfully solve the nonlinear programming problem under all circumstances, and the dimension of the problem increases proportionately with the number of elements.

It is apparent from the above discussion that the advantages of analytical and numerical methods are in many respects complementary in the sense that if the advantages can be combined in some way, then most of the important disadvantages (from the viewpoint of real time applications) can be reduced. In this chapter, two of possibly many ways to obtain such a hybrid methodology are presented, with the potential for use in the development of real time optimal guidance algorithms. The first approach uses the method of regular expansion to improve upon a collocation solution, thereby reducing the error for a given number of elements. The second approach improves upon the first by using both regular expansion and analytical methods to identify more intelligent interpolating functions in the collocation method, again with the objective of improving the level of accuracy without increasing the number of elements.

4.2 The Method of Collocation

Collocation is a method for constructing an approximate solution to a set of differential equations by using finite elements of polynomials or simple analytic interpolating functions. The unknown coefficients are determined by enforcing continuity at the nodes and that the time derivatives of the interpolating functions satisfy the differential equations at some specified points within each element. We consider an optimization problem with unperturbed (ie. $g(x, u, t) = 0$) dynamics $dx/dt = f(x, u, t)$ and Hamiltonian $H = \lambda^T f$. For simplicity, assume a first order polynomial approximation where the derivative constraints are enforced at the mid point of each element. These constraints can be expressed as:

$$p_j = \frac{x_j - x_{j-1}}{\hat{t}_j - \hat{t}_{j-1}} = \frac{\partial H}{\partial \lambda}\bigg|_{\hat{t}=(\hat{t}_j+\hat{t}_{j-1})/2\ ;\ x=(x_j+x_{j-1})/2\ ;\ \lambda=(\lambda_j+\lambda_{j-1})/2}$$

$$q_j = \frac{\lambda_j - \lambda_{j-1}}{\hat{t}_j - \hat{t}_{j-1}} = -\frac{\partial H}{\partial x}\bigg|_{\hat{t}=(\hat{t}_j+\hat{t}_{j-1})/2\ ;\ x=(x_j+x_{j-1})/2\ ;\ \lambda=(\lambda_j+\lambda_{j-1})/2}$$

$$x(\hat{t}) = x_{j-1} + p_j(\hat{t} - \hat{t}_{j-1}) \qquad ;\ j = 1,\ \dots\ ,\ N$$

$$\lambda(\hat{t}) = \lambda_{j-1} + q_j(\hat{t} - \hat{t}_{j-1}) \qquad ;\ \hat{t} \in [\hat{t}_{j-1}, \hat{t}_j]\ ;\ \hat{t}_0 = t_0\ ;\ \hat{t}_N = t_0 + T_0 \qquad (4.1)$$

44

where N is the number of elements. The control is assumed to have been eliminated using the optimality condition. In practice, it is more convenient to directly evaluate the nodal values $(x_0, \lambda_0, ..., x_N, \lambda_N)$ rather than finding the coefficients of the interpolating functions. Though higher order polynomials such as Hermite's cubic are generally preferred (because of their smoothness properties), we consider a first order representation to simplify the presentation, although the approach applies equally well for higher order representations.

4.3 Regular Perturbation Formulation

A regular perturbation formulation may be introduced by rewriting the actual dynamics in the following form:

$$\dot{x} = p_j + \varepsilon(H_\lambda - p_j)$$

$$\dot{\lambda} = q_j + \varepsilon(-H_x - q_j)$$

$$H_u = 0 \qquad\qquad ; \hat{t} \in [\hat{t}_{j-1}, \hat{t}_j] \qquad\qquad (4.2)$$

Note that ε has again been introduced as a bookkeeping parameter. The justification for this step is that if the collocation solution alone accurately approximates the true solution, then the second terms in Eq. 4.2 may be regarded as having a small perturbing effects on the state and costate derivatives, which is actually zero at the mid points of the elements. If the control cannot be eliminated explicitly in the collocation formulation in Eq. 4.1, then an analytic portion $\Pi(u, x, \lambda)$ of the optimality condition (for which it is possible to eliminate u) can be extracted such that

$$0 = \Pi + \varepsilon(H_u - \Pi) \qquad\qquad (4.3)$$

Note that in the above equations H is the Hamiltonian corresponding to the original system without a perturbation parameter. As presented above, a collocation solution may be viewed as the zero order solution for the regular perturbation problem formulated in Eq. 4.2. Also, as will be shown by example in the next section, more intelligent choices of interpolating functions can be identified from the necessary conditions, by utilizing to the extent possible the analytically tractable portions of the solution. This results in a significant decrease in the computational requirements for a given level of accuracy.

Now we can apply the perturbation technique described in the Section 3.2 to improve the approximate zero order solution from collocation. For the higher order problems defined in Eqs. 3.29 - 3.31, we have:

$$A_{11_j} = \frac{\partial p_j}{\partial x} = \frac{\partial^2 H}{\partial x \partial \lambda}\bigg|_{\hat{t}=(\hat{t}_j+\hat{t}_{j-1})/2 \ ; \ x=(x_j+x_{j-1})/2 \ ; \ \lambda=(\lambda_j+\lambda_{j-1})/2}$$

$$A_{12_j} = \frac{\partial p_j}{\partial \lambda} = \frac{\partial^2 H}{\partial^2 \lambda}\bigg|_{\hat{t}=(\hat{t}_j+\hat{t}_{j-1})/2 \ ; \ x=(x_j+x_{j-1})/2 \ ; \ \lambda=(\lambda_j+\lambda_{j-1})/2}$$

$$A_{21_j} = \frac{\partial q_j}{\partial x} = -\frac{\partial^2 H}{\partial^2 x}\bigg|_{\hat{t}=(\hat{t}_j+\hat{t}_{j-1})/2 \ ; \ x=(x_j+x_{j-1})/2 \ ; \ \lambda=(\lambda_j+\lambda_{j-1})/2}$$

$$A_{22_j} = \frac{\partial q_j}{\partial \lambda} = -\frac{\partial^2 H}{\partial \lambda \partial x}\bigg|_{\hat{t}=(\hat{t}_j+\hat{t}_{j-1})/2 \ ; \ x=(x_j+x_{j-1})/2 \ ; \ \lambda=(\lambda_j+\lambda_{j-1})/2}$$

$$C_{1_j} = p_j + (\hat{t} - \hat{t}_{j-1})p_{t_j}$$

$$= \{\frac{\partial H}{\partial \lambda} + (\hat{t} - \hat{t}_{j-1})\frac{\partial^2 H}{\partial t \partial \lambda}\}\bigg|_{\hat{t}=(\hat{t}_j+\hat{t}_{j-1})/2 \ ; \ x=(x_j+x_{j-1})/2 \ ; \ \lambda=(\lambda_j+\lambda_{j-1})/2}$$

$$C_{2_j} = q_j + (\hat{t} - \hat{t}_{j-1})q_{t_j}$$

$$= \{-\frac{\partial H}{\partial x} - (\hat{t} - \hat{t}_{j-1})\frac{\partial^2 H}{\partial t \partial x}\}\bigg|_{\hat{t}=(\hat{t}_j+\hat{t}_{j-1})/2 \ ; \ x=(x_j+x_{j-1})/2 \ ; \ \lambda=(\lambda_j+\lambda_{j-1})/2} \quad (4.4)$$

and for k = 1,

$$P_{11_j} = \frac{\partial H}{\partial \lambda}\bigg|_{\hat{t} \ ; \ x=x_{j-1}+p_j(\hat{t}-\hat{t}_{j-1}) \ ; \ \lambda=\lambda_{j-1}+q_j(\hat{t}-\hat{t}_{j-1})} - p_j$$

$$P_{21_j} = -\frac{\partial H}{\partial x}\bigg|_{\hat{t} \ ; \ x=x_{j-1}+p_j(\hat{t}-\hat{t}_{j-1}) \ ; \ \lambda=\lambda_{j-1}+q_j(\hat{t}-\hat{t}_{j-1})} - q_j \quad (4.5)$$

where all the terms in Eq. 4.4 are constant* within an element, and are evaluated using the collocation solution. The matrix A_j is simply the perturbation of the original state and costate dynamics evaluated at the constraint point of each element. The expression in Eq. 3.32, which now corresponds to a piecewise constant system matrix A_j, can be written as

$$\begin{bmatrix} x_k(\hat{t}) \\ \lambda_k(\hat{t}) \end{bmatrix} = \Omega_A(\hat{t},t_o)\begin{bmatrix} x_k(t_o) \\ \lambda_k(t_o) \end{bmatrix} + \frac{T_k}{T_0}\int_{t_o}^{\hat{t}} \Omega_A(\hat{t},\tau)\begin{bmatrix} C_1 \\ C_2 \end{bmatrix}d\tau + \int_{t_o}^{\hat{t}} \Omega_A(\hat{t},\tau)\begin{bmatrix} P_{1k} \\ P_{2k} \end{bmatrix}d\tau \quad (4.6)$$

---

* If higher order interpolating polynomials are chosen, the dynamical system will be a time varying matrix polynomial with piecewise constant coefficients.

and for a constant system matrix A_j, it can be written as

$$\begin{bmatrix} x_k(\hat{t}) \\ \lambda_k(\hat{t}) \end{bmatrix} = \Omega_{A_j}(\hat{t},\hat{t}_{j-1}) \begin{bmatrix} x_k(\hat{t}_{j-1}) \\ \lambda_k(\hat{t}_{j-1}) \end{bmatrix} + \frac{T_k}{T_0} \Omega_{A_j}(\hat{t},\hat{t}_{j-1}) A_j^{-1} \left(\begin{bmatrix} p_j \\ q_j \end{bmatrix} + (\hat{t} - \hat{t}_{j-1}) \begin{bmatrix} p_{t_j} \\ q_{t_j} \end{bmatrix} \right.$$

$$\left. + A_j^{-1} \begin{bmatrix} p_{t_j} \\ q_{t_j} \end{bmatrix} \right) + \int_{\hat{t}_{j-1}}^{\hat{t}} \Omega_{A_j}(\hat{t},\tau) \begin{bmatrix} P_{1k}(\tau) \\ P_{2k}(\tau) \end{bmatrix} d\tau \ ; \ \hat{t} \in [\hat{t}_j, \hat{t}_{j-1}] \qquad (4.7)$$

where Ω_{A_j} is the state transition matrix and p_{t_j}, q_{t_j} are defined as in Eq. 4.4. Note that Ω_{A_j} is not the same as in Eqs. 3.32 and 3.33 because A is defined differently. The state transition matrix here may not have an analytic expression because the zero order solution is not necessarily analytic. If this is true, we can solve Eqs. 4.4 and 4.5 using the sensitivity functions and superposition property of linear systems. This is done by assigning a unit vector for the initial conditions, and numerically integrates the system from t_0 to $t_0 + T_0$. Thus by changing the position of the non-zero element in the unit vector, the sensitivity functions are obtained. This process can be done in parallel for different unit vector.

In the zero order solution, ε in Eq. 4.2 is set to zero, which means that the standard collocation constraints in Eq. 4.1 are employed and an approximate solution is obtained by solving the algebraic equations. Then first and higher order corrections may be computed by quadrature as explained in the earlier section on regular perturbation.

4.4 A Duffing's Equation Example

This investigation is carried out to demonstrate the hybrid approach outlined in the preceding section. The example is based on Duffing's equation presented in its first order form:

$$\dot{x} = v \qquad\qquad ; \ x(0) = x_0$$

$$\dot{v} = -x - ax^3 + u \qquad ; \ v(0) = v_0 \qquad\qquad\qquad (4.8)$$

and the objective is to

$$\min_u \left\{ S_x x^2(t_f) + S_v v^2(t_f) + \int_0^{t_f} (1 + \frac{u^2}{2}) dt \right\} \qquad\qquad (4.9)$$

with S_x, S_v being the weights on the terminal values and t_f is free. The problem can be converted to the Mayer's form in Eq. 3.17 (if desired) through the usual method of introdu-

cing an additional state equation whose right hand side is the integrand of Eq. 4.9. We investigate the problem in different levels of complexity according to how the dynamics of the full system are treated.

a) Level 0 formulation

This is the degenerate case in which there is an analytic zero order solution, and therefore collocation is not required (solely a regular perturbation approach as discussed in Sec. 3.2). Let $\varepsilon = a$, thus neglecting the hardening effect ax^3 in the original problem. The necessary conditions are:

$$\dot{x} = v \qquad\qquad ; x(0) = x_0$$

$$\dot{v} = -x + u - \varepsilon x^3 \qquad\qquad ; v(0) = v_0$$

$$\dot{\lambda}_x = \lambda_v + \varepsilon 3\lambda_v x^2 \qquad\qquad ; \lambda_x(t_f) = 2S_x x(t_f)$$

$$\dot{\lambda}_v = -\lambda_x \qquad\qquad ; \lambda_v(t_f) = 2S_v v(t_f)$$

$$H_u = u + \lambda_v = 0$$

$$\left\{ H = \lambda_x v + \lambda_v(-x + u - \varepsilon x^3) + 1 + u^2/2 \right\}\Big|_{t_f} = 0 \qquad\qquad (4.10)$$

The zero order problem ($\varepsilon = 0$) is linear and time invariant, and can easily be solved as

$$\begin{bmatrix} x_0(\hat{t}) \\ v_0(\hat{t}) \\ \lambda_{x0}(\hat{t}) \\ \lambda_{v0}(\hat{t}) \end{bmatrix} = \begin{bmatrix} \cos\bar{t} & \sin\bar{t} & (\sin\bar{t} - \bar{t}\cos\bar{t})/2 & -\bar{t}\sin\bar{t}/2 \\ -\sin\bar{t} & \cos\bar{t} & \bar{t}\sin\bar{t}/2 & -(\sin\bar{t} + \bar{t}\cos\bar{t})/2 \\ 0 & 0 & \cos\bar{t} & \sin\bar{t} \\ 0 & 0 & -\sin\bar{t} & \cos\bar{t} \end{bmatrix} \begin{bmatrix} x_0(\hat{t}_0) \\ v_0(\hat{t}_0) \\ \lambda_{x0}(\hat{t}_0) \\ \lambda_{v0}(\hat{t}_0) \end{bmatrix} \qquad (4.11)$$

where

$$\bar{t} = \hat{t} - \hat{t}_0 \qquad\qquad ; \hat{t}_0, \hat{t} \in [0, T_0] \qquad\qquad (4.12)$$

The above state transition matrix is also the state transition matrix $\Omega_A(\hat{t}, \hat{t}_0)$ for the higher order correction. Given the boundary conditions of $x_0(0) = x_0$, $v_0(0) = v_0$, $\lambda_{x0}(T_0) = 2S_x x_0(T_0)$, $\lambda_{v0}(T_0) = 2S_v v_0(T_0)$, the remaining unknowns $\lambda_{x0}(0)$, $\lambda_{v0}(0)$, $\lambda_{x0}(T_0)$, $\lambda_{v0}(T_0)$, T_0 can be solved with a Newton's method using Eq. 4.11 and the corresponding transversality condition

48

$$\left\{ H_0 = \lambda_{x0}v_0 - \lambda_{v0}x_0 - \lambda_{v0}^2 / 2 + 1 \right\}\Big|_{T_0} = 0 \qquad (4.13)$$

From Eq. 3.29, the differential equations governing the higher order correction dynamics are

$$\frac{d}{d\hat{t}}\begin{bmatrix} x_k \\ v_k \\ \lambda_{xk} \\ \lambda_{vk} \end{bmatrix} = \begin{bmatrix} 0 & 1 & 0 & 0 \\ -1 & 0 & 0 & -1 \\ 0 & 0 & 0 & 1 \\ 0 & 0 & -1 & 0 \end{bmatrix}\begin{bmatrix} x_k \\ v_k \\ \lambda_{xk} \\ \lambda_{vk} \end{bmatrix} + \frac{T_k}{T_0}\begin{bmatrix} v_0(\hat{t}) \\ -x_0(\hat{t}) - \lambda_{v0}(\hat{t}) \\ \lambda_{v0}(\hat{t}) \\ -\lambda_{x0}(\hat{t}) \end{bmatrix} + \begin{bmatrix} P_{1k}(\hat{t}) \\ P_{2k}(\hat{t}) \\ P_{3k}(\hat{t}) \\ P_{4k}(\hat{t}) \end{bmatrix} \qquad (4.14)$$

with the boundary conditions

$$x_k(0) = v_k(0) = 0 \; ; \; \lambda_{xk}(T_0) = 2S_x x_k(T_0) \; ; \; \lambda_{vk}(T_0) = 2S_v v_k(T_0) \qquad (4.15)$$

In this case, we have for k = 1, 2:

$$P_{11} = 0 \qquad\qquad ; P_{21} = -x_0^3 \qquad ; P_{31} = 3\lambda_{v0}x_0^2 \quad ; P_{41} = 0$$

$$P_{12} = v_1 T_1 / T_0 \quad ; P_{22} = -(x_1 + \lambda_{v1} + x_0^3)T_1 / T_0 - 3x_0^2 x_1$$

$$P_{32} = (\lambda_{v1} + 3\lambda_{v0}x_0^2)T_1 / T_0 + 3\lambda_{v1}x_0^2 + 3\lambda_{v0}x_0 x_1 \quad ; P_{42} = -\lambda_{x1}T_1 / T_0 \qquad (4.16)$$

and the transversality conditions:

$$\left\{ H_1 = \lambda_{x1}v_0 - \lambda_{v1}(x_0 + \lambda_{v0}) + \lambda_{x0}v_1 - \lambda_{v0}(x_1 + x_0^3) \right\}\Big|_{T_0} = 0$$

$$\left\{ H_2 = \lambda_{x2}v_0 - \lambda_{v2}(x_0 + \lambda_{v0}) + \lambda_{x0}v_2 + \lambda_{v1}x_1 - 3\lambda_{v0}x_0^2 x_1 \right.$$
$$\left. -\lambda_{v1}(x_1 + \lambda_{v1} + x_0^3) + \lambda_{v1}^2 / 2 \right\}\Big|_{T_0} = 0 \qquad (4.17)$$

which are needed to compute the first and second order corrections by quadrature. The results are shown in Figs. 4.1 - 4.4 for $S_x = S_v = 100$, and a = 0.4. The first order state and costate histories are stored and later retrieved by linear interpolation to construct the second order solution. The optimal solution generated using a multiple shooting technique is also included for comparison. These results clearly show that the series is not convergent, and that the most accurate approximation is obtained using a first order solution. If we regard this level of accuracy as insufficient, then the conclusion must be that the nonlinear term (ax^3) is too large to be neglected in the zero order solution.
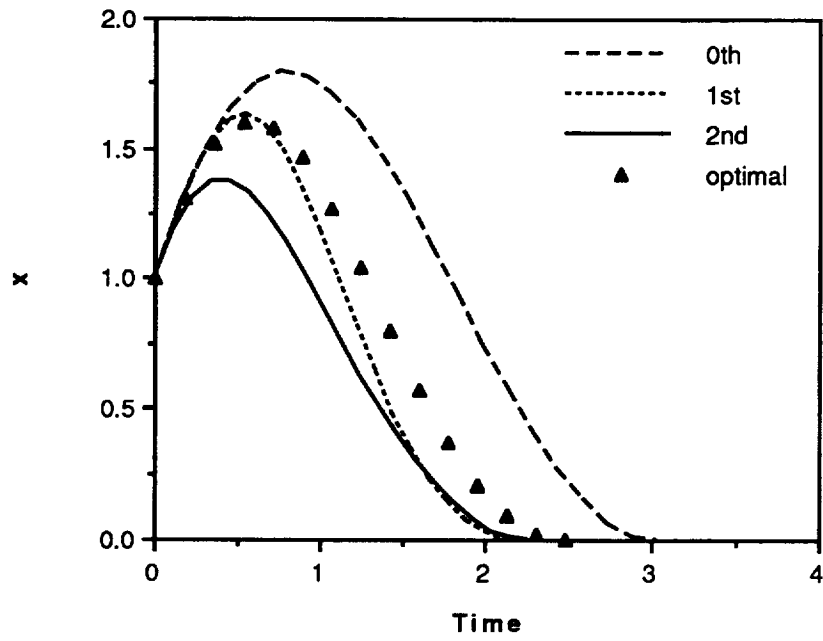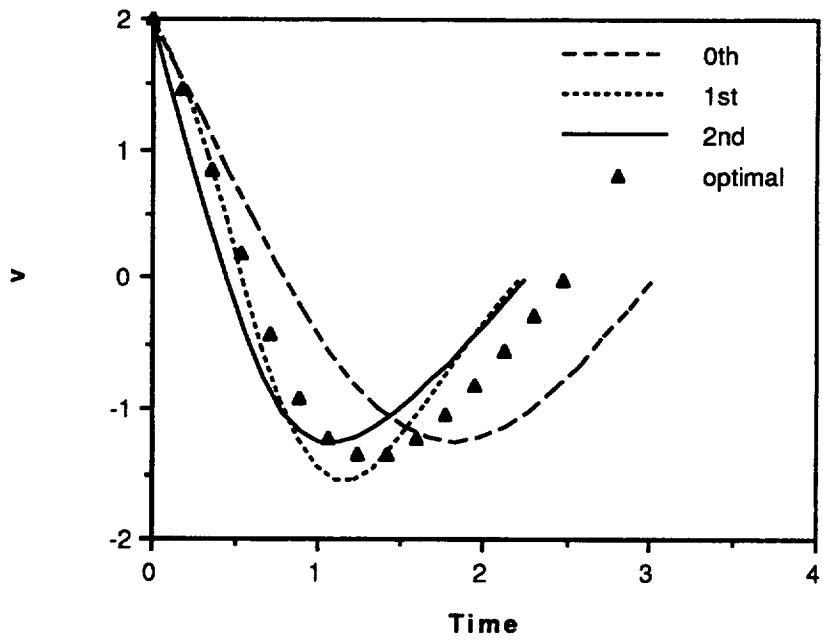
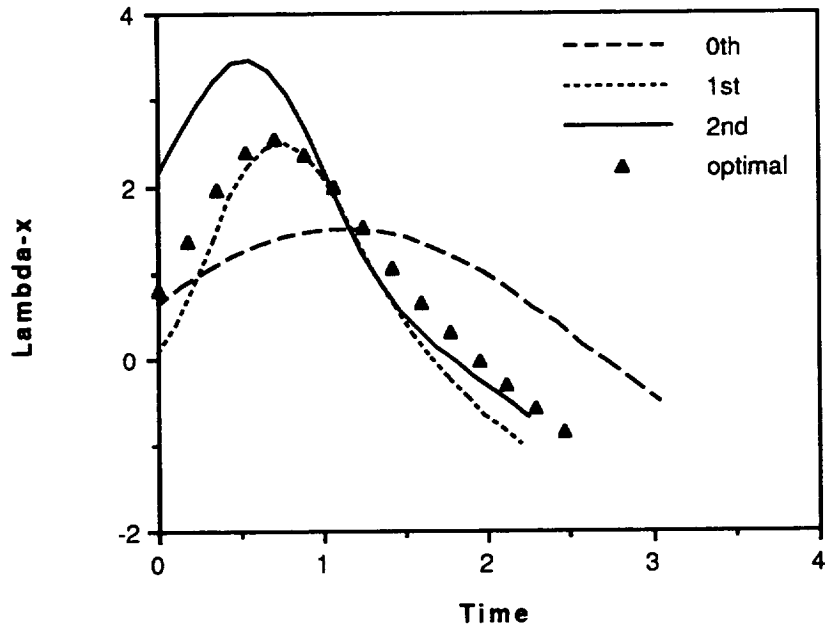Figure 4.1. Level 0 Result in x.

Figure 4.2. Level 0 Result in v.
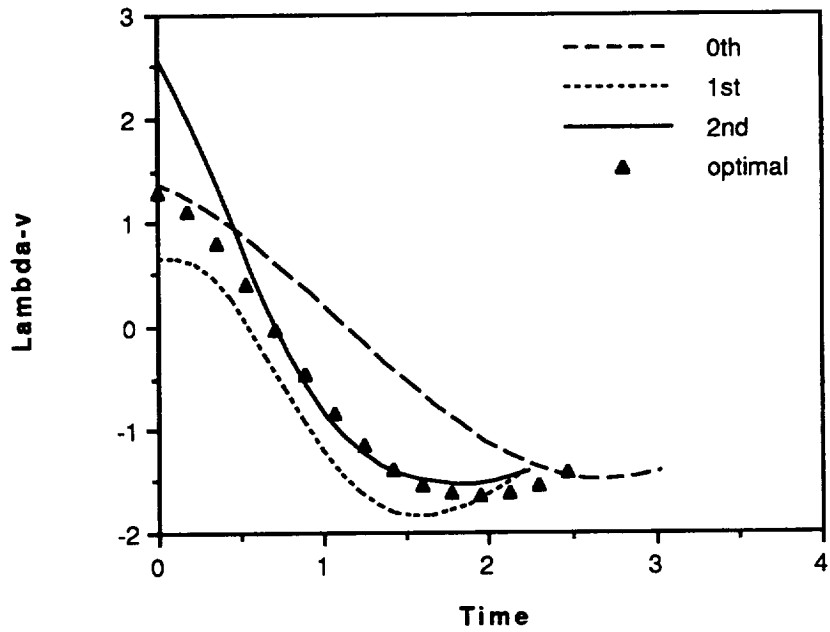
50

Figure 4.3. Level 0 Result in λ_x.

Figure 4.4. Level 0 Result in λ_v.

51

b) Level 1 formulation

This case illustrates the hybrid approach as outlined in the section on collocation, using a piecewise linear representation to approximate the states and the costates for the zero order solution. The interpolatory constraints for an N equally spaced segmentation are:

$$\frac{x_{0j} - x_{0j-1}}{T_0 / N} = \frac{v_{0j} + v_{0j-1}}{2} = p_{xj}$$

$$\frac{v_{0j} - v_{0j-1}}{T_0 / N} = -\frac{x_{0j} + x_{0j-1}}{2} - \frac{\lambda_{v0j} + \lambda_{v0j-1}}{2} - a(\frac{x_{0j} + x_{0j-1}}{2})^3 = p_{vj}$$

$$\frac{\lambda_{x0j} - \lambda_{x0j-1}}{T_0 / N} = \frac{\lambda_{v0j} + \lambda_{v0j-1}}{2}\left[1 + 3a(\frac{x_{0j} + x_{0j-1}}{2})^2\right] = q_{xj}$$

$$\frac{\lambda_{v0j} - \lambda_{v0j-1}}{T_0 / N} = -\frac{\lambda_{x0j} - \lambda_{x0j-1}}{2} = q_{vj} \tag{4.18}$$

with the boundary conditions and transversality condition given by:

$$x_{00} = x_0 \quad ; v_{00} = v_0 \quad ; \lambda_{x0N} = 2S_x x_{0N} \quad ; \lambda_{v0N} = 2S_v v_{0N}$$

$$\lambda_{x0N}v_{0N} + \lambda_{v0N}(-x_{0N} - \lambda_{v0N} - ax_{0N}^3) + \lambda_{v0N}^2 / 2 + 1 = 0 \tag{4.19}$$

There are 4N+5 equations to solve for the 4N+5 unknowns of x_{00}, v_{00}, λ_{x00}, λ_{x00}, ... , x_{0N}, v_{0N}, λ_{x0N}, λ_{v0N}, T_0. Solutions for several values of N are presented in Figs. 4.5 to 4.8. Note that accuracy improves with increasing N, but at the expense of having to solve a large nonlinear system of equations.

The higher order dynamics in this case are

$$\frac{d}{d\hat{t}}\begin{bmatrix} x_k \\ v_k \\ \lambda_{xk} \\ \lambda_{vk} \end{bmatrix} = \begin{bmatrix} 0 & 1 & 0 & 0 \\ -c & 0 & 0 & -1 \\ b & 0 & 0 & c \\ 0 & 0 & -1 & 0 \end{bmatrix}\begin{bmatrix} x_k \\ v_k \\ \lambda_{xk} \\ \lambda_{vk} \end{bmatrix} + \frac{T_k}{T_0}\begin{bmatrix} p_{xj} \\ p_{vj} \\ q_{xj} \\ q_{vj} \end{bmatrix} + \begin{bmatrix} P_{1k}(\hat{t}) \\ P_{2k}(\hat{t}) \\ P_{3k}(\hat{t}) \\ P_{4k}(\hat{t}) \end{bmatrix} ; \hat{t} \in [\hat{t}_j, \hat{t}_{j-1}] \tag{4.20}$$

where

$$c = 1 + 3ax_0^2\Big|_{\bar{t}} \quad ; b = 6a(\lambda_{v0}x_0)\Big|_{\bar{t}} \quad ; \bar{t} = (\hat{t}_j + \hat{t}_{j-1})/2 \tag{4.21}$$

52

The state transition matrix expression for this case is given in Appendix C. For k = 1, 2, the forcing function terms in Eq. 4.20 are:

$$P_{11} = v_0 - p_{xj} \qquad ; P_{21} = -x_0 - \lambda_{v0} - ax_0^3 - p_{vj}$$

$$P_{31} = \lambda_{v0}(1 + 3ax_0^3) - q_{xj} \qquad ; P_{41} = -\lambda_{x0} - q_{vj}$$

$$P_{12} = (v_1 + v_0 - p_{xj})T_1 / T_0$$

$$P_{22} = \{-cx_1 - \lambda_{v1} - x_0 - \lambda_{v0} - ax_0^3 - p_{vj}\}T_1 / T_0 - 3ax_0\Big|_t x_1^2 - (1 + 3ax_0^2 - c)x_1$$

$$P_{32} = \{c\lambda_{v1} + bx_1 + \lambda_{v0}(1 + 3ax_0^2 - q_{xj})\}T_1 / T_0 + 6ax_0\Big|_t \lambda_{v1}x_1 + 3a\lambda_{v0}\Big|_t x_1^2$$
$$+ (1 + 3ax_0^2 - c)\lambda_{v1} + (6a\lambda_{v0}x_0 - b)x_1$$

$$P_{42} = (-\lambda_{x1} - \lambda_{x0} - q_{vj})T_1 / T_0 \tag{4.22}$$

where

$$x_0(\hat{t}) = x_{0j-1} + p_{xj}(\hat{t} - \hat{t}_{j-1}) \qquad ; v_0(\hat{t}) = v_{0j-1} + p_{vj}(\hat{t} - \hat{t}_{j-1})$$

$$\lambda_{x0}(\hat{t}) = \lambda_{x0j-1} + q_{xj}(\hat{t} - \hat{t}_{j-1}) \qquad ; \lambda_{v0}(\hat{t}) = \lambda_{v0j-1} + q_{vj}(\hat{t} - \hat{t}_{j-1}) \tag{4.23}$$

plus the boundary conditions in Eq. 4.14 by replacing $x_k(0)$, $v_k(0)$, $x_k(T_0)$, $v_k(T_0)$, $\lambda_{xk}(T_0)$, $\lambda_{vk}(T_0)$ with x_{k0}, v_{k0}, x_{kN}, v_{kN}, λ_{xkN}, λ_{vkN}. The corresponding expansion of the transversality conditions in this case are defined as

$$0 = \lambda_{x1N}v_{0N} + \lambda_{x0N}v_{1N} - \lambda_{v1N}(x_{0N} + ax_{0N}^3) + \lambda_{v0N}(-x_{1N} - \lambda_{v0N} - ax_{0N}^3)$$

$$0 = \lambda_{x2N}v_{0N} + \lambda_{x0N}v_{2N} + \lambda_{x1N}v_{1N} - \lambda_{v2N}(x_{0N} + ax_{0N}^3) + \lambda_{v0N}(-x_{2N}$$
$$-\lambda_{v2N} - 3ax_{0N}^2x_{2N}) + \lambda_{v1N}(-x_{1N} - 3ax_{0N}^2x_1) - \lambda_{v1N}^2 / 2 \tag{4.24}$$

First and second order corrections are computed for the case where N = 3 is used in the zero order collocation solution (note here ε is 1.0). The results are shown in Figs. 4.9 - 4.12. Comparison with the N = 3 results in Figs. 4.5 - 4.8 show that a significant improvement in accuracy is achievable without requiring a large number of elements. In Figs. 4.9 - 4.12 the second order solution is indistinguishable from the optimal solution. The discontinuity in slope (which is a consequence of using first order interpolation functions for the collocation solution) is also smoothed as the order of the correction

increases. Contrary to Level 0's results, the second order corrections do not diverge due to the fact that the nonlinear term has been accounted for in the zero order solution.
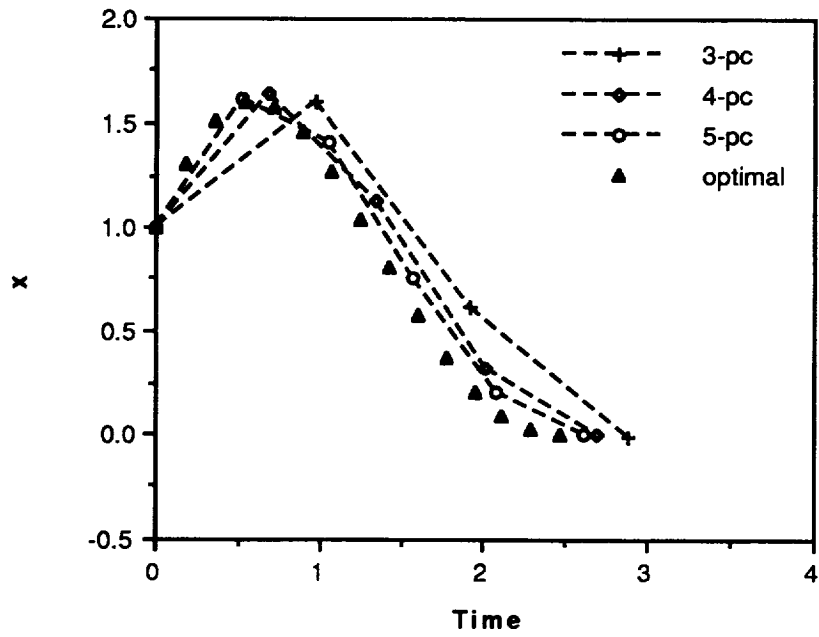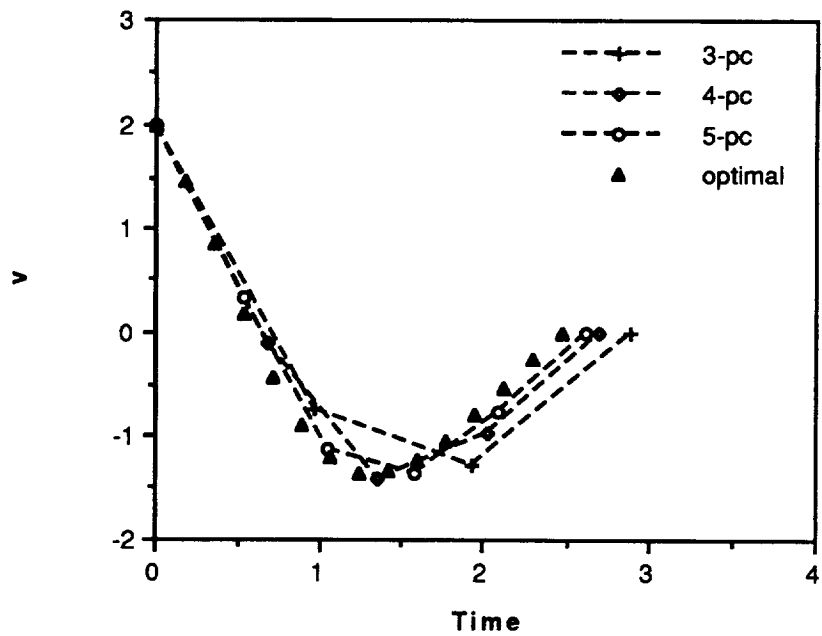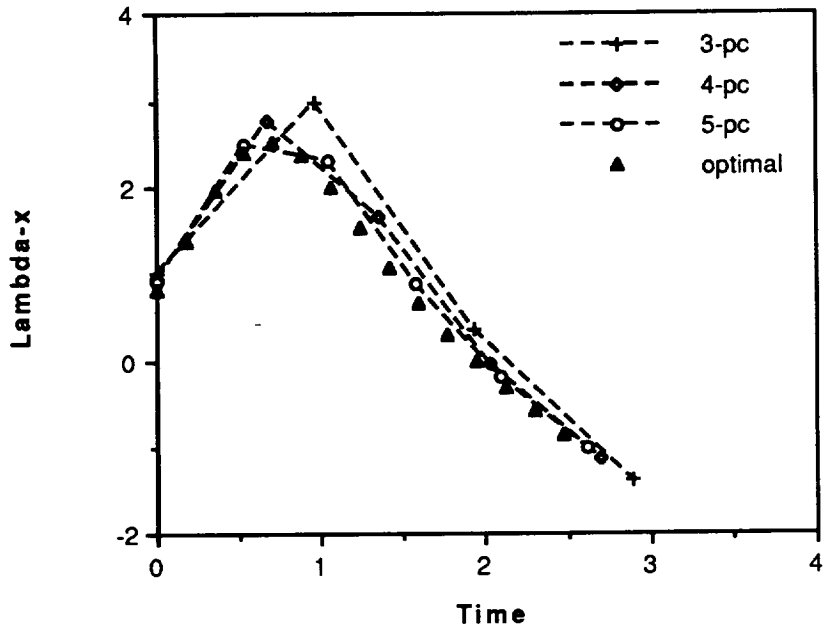

Figure 4.5. Level 1 Zero Order Results in x for Different N.

Figure 4.6. Level 1 Zero Order Results in v for Different N.

Figure 4.7. Level 1 Zero Order Results in λ_x for Different N.
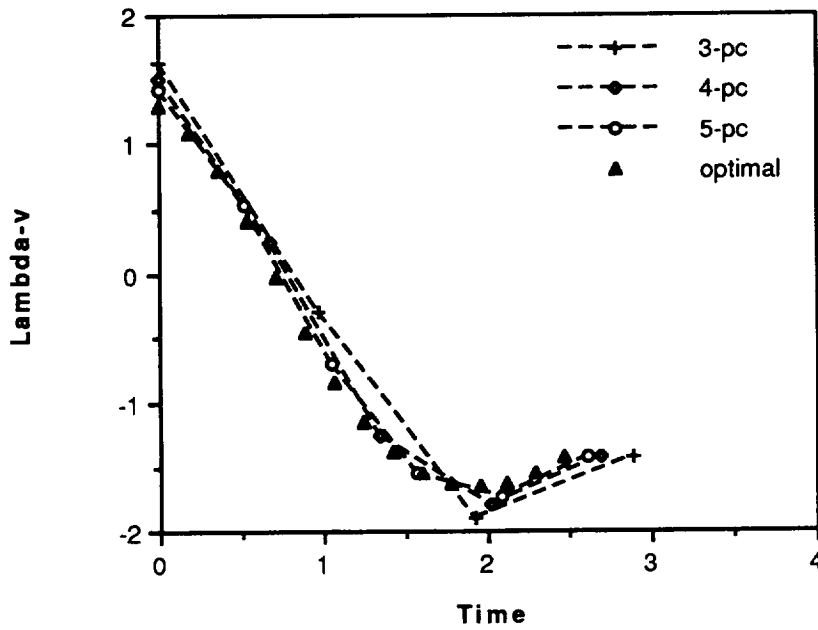
Figure 4.8. Level 1 Zero Order Results in λ_v for Different N.
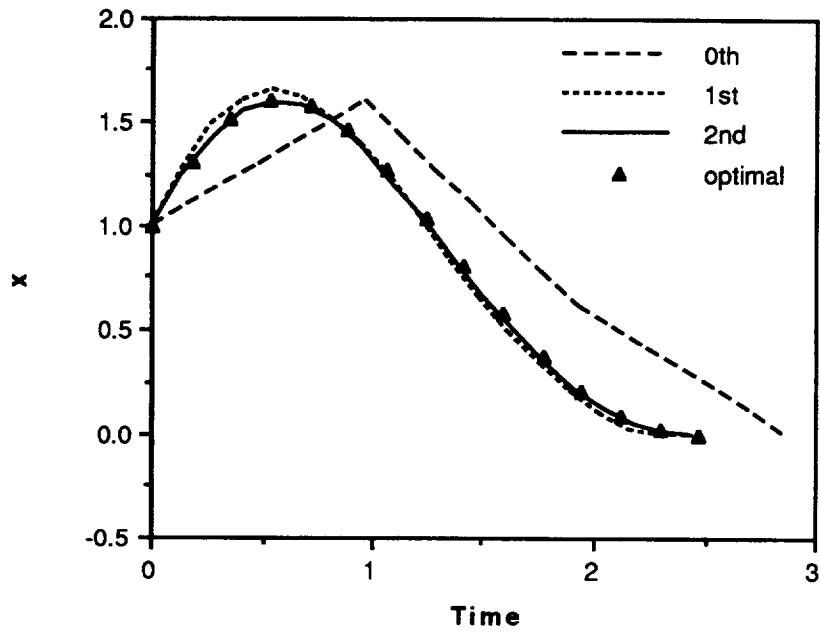
Figure 4.9. Level 1 Higher Order Results in x for N=3.
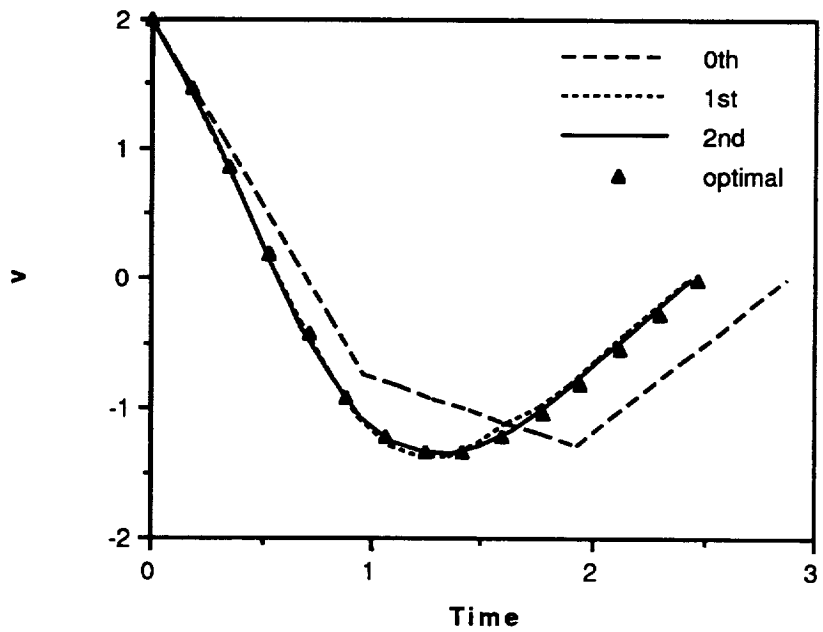
Figure 4.10. Level 1 Higher Order Results in v for N=3.

56
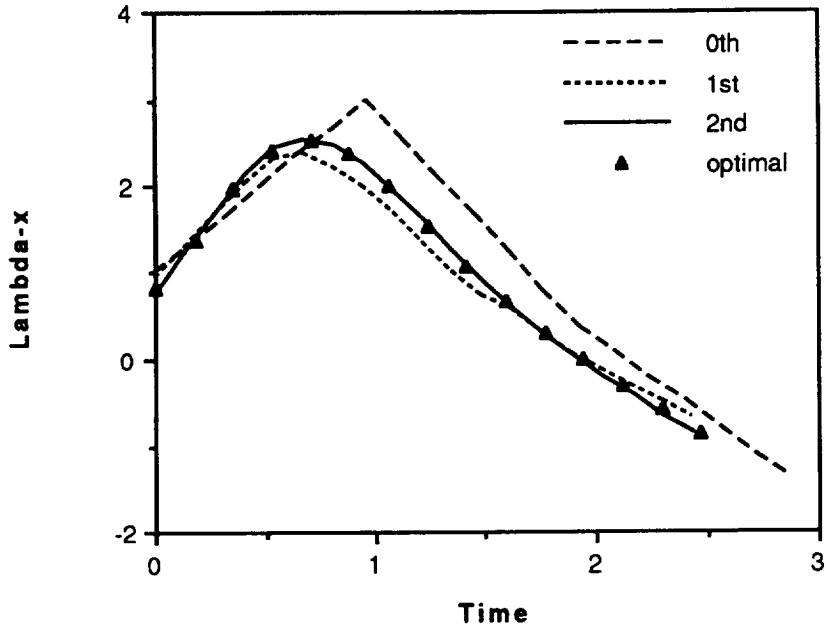
Figure 4.11. Level 1 Higher Order Results in λ_x for N=3.

Figure 4.12. Level 1 Higher Order Results in λ_v for N=3.

c) Level 2 formulation

    As a second illustration of a hybrid solution approach we retain a portion of the dynamics from the necessary conditions to identify a more intelligent interpolating function for the hybrid Level 1 formulation. Consider the following simple modification of the

regular perturbation formulation for this example:

$$\dot{x} = v$$

$$\dot{v} = p_{vj} + \varepsilon\left\{-x - \lambda_v - ax^3 - p_{vj}\right\}$$

$$\dot{\lambda}_x = q_{xj} + \varepsilon\left\{\lambda_v(1 + 3ax^2) - q_{xj}\right\}$$

$$\dot{\lambda}_v = -\lambda_x \tag{4.25}$$

Note that we interpolate only the variables that have nonlinear coupling, and that the resulting interpolation retains more of the dynamics in the original problem than in the Level 1 formulation. The interpolating functions in this case are:

$$x_0(\hat{t}) = x_0(\hat{t}_{j-1}) + \left[v_{0j-1} + \frac{1}{2}p_{vj}(\hat{t} - \hat{t}_{j-1})\right](\hat{t} - \hat{t}_{j-1})$$

$$v_0(\hat{t}) = v_{0j-1} + p_{vj}(\hat{t} - \hat{t}_{j-1})$$

$$\lambda_{x0}(\hat{t}) = \lambda_{x0j-1} + q_{xj}(\hat{t} - \hat{t}_{j-1})$$

$$\lambda_{v0}(\hat{t}) = \lambda_{v0}(\hat{t}_{j-1}) - \left[\lambda_{x0j-1} + \frac{1}{2}q_{xj}(\hat{t} - \hat{t}_{j-1})\right](\hat{t} - \hat{t}_{j-1}) \tag{4.26}$$

Consequently, there are fewer unknowns (2N+5) to be solved and the dynamics retained in the formulation should improve the zero order collocation approximation. This allows even fewer elements to be used. To evaluate the zero order solution, conditions in Eq. 4.19 are enforced by replacing x_{0N}, λ_{v0N} with $x_0(\hat{t}_N)$, $\lambda_{v0}(\hat{t}_N)$ from Eq. 4.26, and similarly for the first order expressions. The forcing terms for this case are:

$$P_{11} = 0 \qquad\qquad ; P_{21} = -x_0 - \lambda_{v0} - ax_0^3 - p_{vj}$$

$$P_{31} = \lambda_{v0}(1 + 3ax_0^2) - q_{xj} \qquad ; P_{41} = 0 \tag{4.27}$$

and the state transition matrix is same as that in Level 1.

Figures 4.13 - 4.16 show the zero and first order state solutions for the case $N = 2$. The results show that the zero order solution is dramatically improved especially in the state variables in comparison to the zero order solution for $N = 3$ of the Level 1 formulation in Figs. 4.9 and 4.10. The accuracy of the first order solutions in Figs. 4.13 to 4.16 are very good and are almost riding on the exact solutions, even though a cruder segmentation has

58

been used. A similar trend is also prevailed on the costates histories.
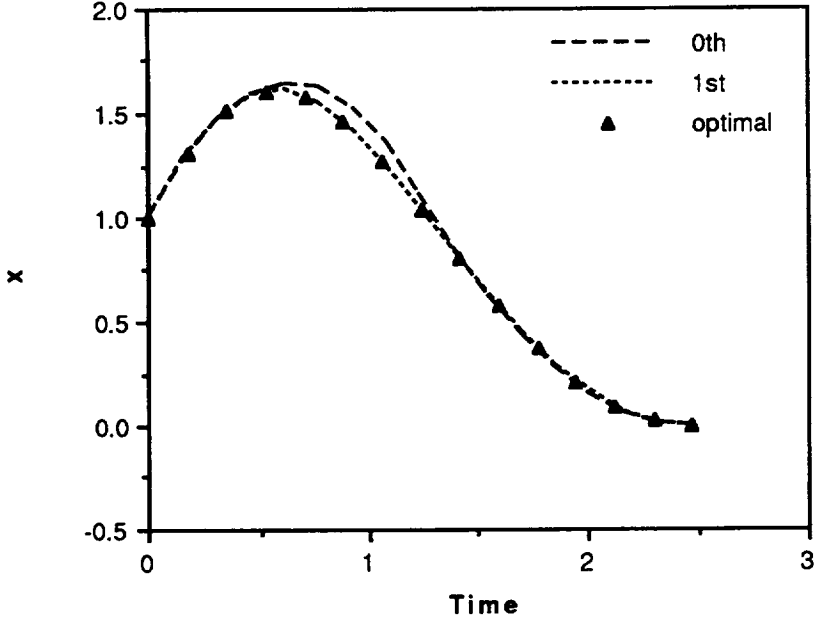
Figure 4.13. Level 2 Higher Order Results in x for N=2.
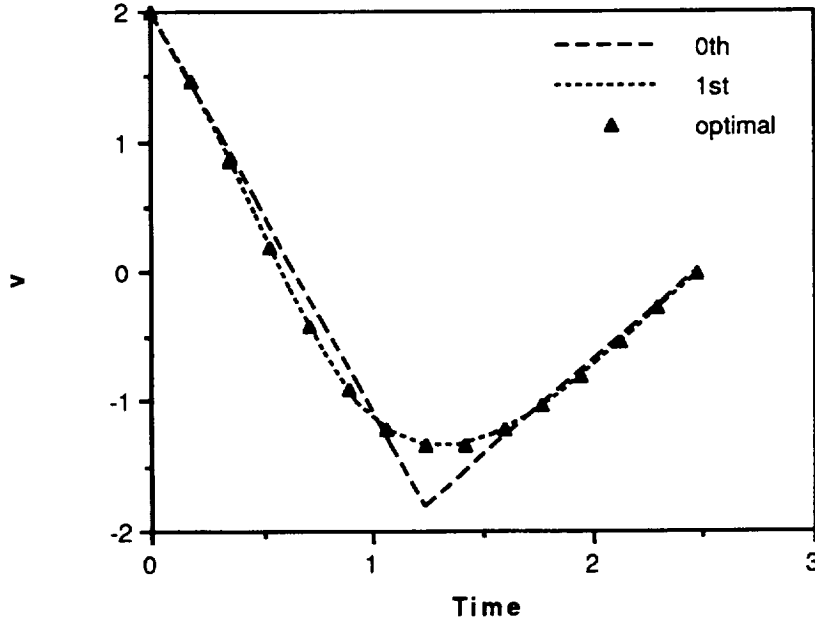
Figure 4.14. Level 2 Higher Order Results in v for N=2.
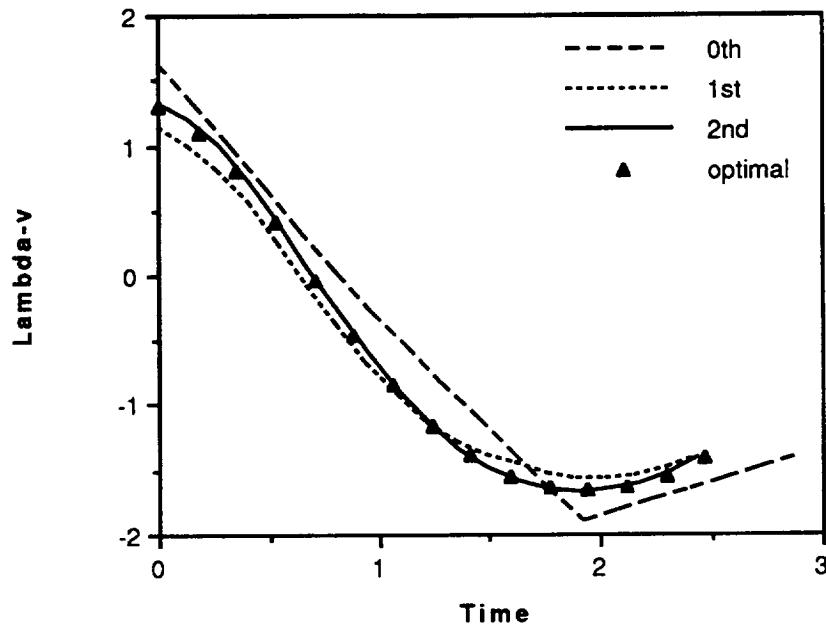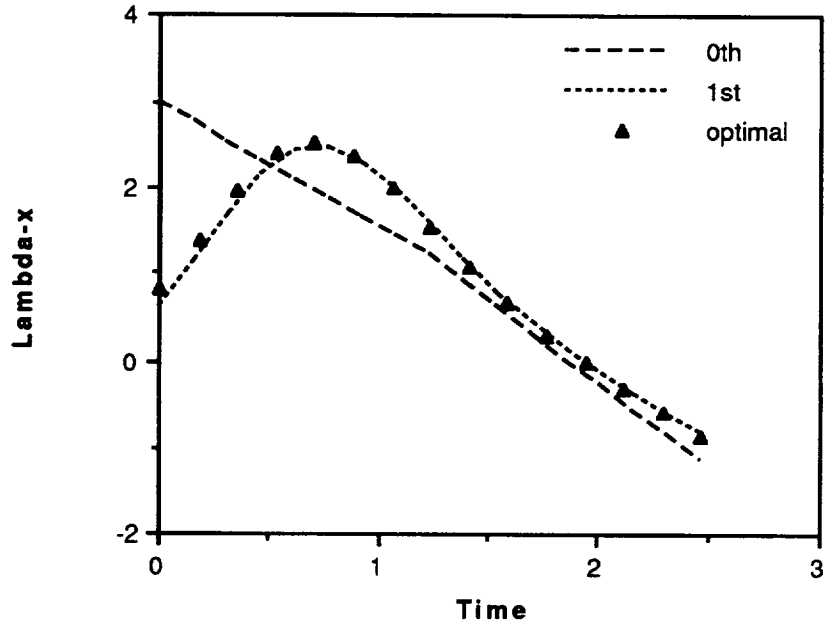
Figure 4.15. Level 2 Higher Order Results in λ_x for N=2.

Figure 4.16. Level 2 Higher Order Results in λ_v for N=2.

d) Level 3 formulation

In this last demonstration, the Level 2 formulation is further enhanced. All the linear terms are retained in the zero order problem, and the nonlinear terms in the v and λ_v dynamics are approximated by piecewise constants. The resultant expressions become:

60

$$\dot{x} = v$$

$$\dot{v} = -x - \lambda_v + p_{vj} + \varepsilon\left\{-ax^3 - p_{vj}\right\}$$

$$\dot{\lambda}_x = \lambda_v + q_{xj} + \varepsilon\left\{3a\lambda_v x^2 - q_{xj}\right\}$$

$$\dot{\lambda}_v = -\lambda_x \tag{4.28}$$

This is equivalent to the Level 0 problem except for the presence of two additional unknown constants. This formulation represents an attempt to make maximum utilization of the analytically tractable portion of the solution in selecting the interpolating function for the collocation solution in the zero order problem. The zero order solutions in this case are also similar to that for the Level 0 case:

$$x_0(\hat{t}) = (x_0(\hat{t}_{j-1}) - p_{vj} - q_{xj})\cos\bar{t} + v_0(\hat{t}_{j-1})\sin\bar{t} + \lambda_{x0}(\hat{t}_{j-1})[\sin\bar{t} - \bar{t}\cos\bar{t}]/2$$
$$- (\lambda_{v0}(\hat{t}_{j-1}) + q_{xj})\bar{t}\sin\bar{t}/2 + p_{vj} + q_{xj}$$

$$v_0(\hat{t}) = -(x_0(\hat{t}_{j-1}) - p_{vj} - q_{xj})\sin\bar{t} + v_0(\hat{t}_{j-1})\cos\bar{t} + \lambda_{x0}(\hat{t}_{j-1})\bar{t}\sin\bar{t}/2$$
$$- (\lambda_{v0}(\hat{t}_{j-1}) + q_{xj})[\sin\bar{t} + \bar{t}\cos\bar{t}]/2$$

$$\lambda_{x0}(\hat{t}) = \lambda_{x0}(\hat{t}_{j-1})\cos\bar{t} + (\lambda_{v0}(\hat{t}_{j-1}) + q_{xj})\sin\bar{t}$$

$$\lambda_{v0}(\hat{t}) = -\lambda_{x0}(\hat{t}_{j-1})\sin\bar{t} + (\lambda_{v0}(\hat{t}_{j-1}) + q_{xj})\cos\bar{t} - q_{xj} \tag{4.29}$$

where

$$p_{vj} = -ax^3\Big|_{x((\hat{t}_j + \hat{t}_{j-1})/2)} \quad ; \quad q_{xj} = 3a\left(\lambda_v x^2\right)\Big|_{\lambda_v((\hat{t}_j + \hat{t}_{j-1})/2);\ x((\hat{t}_j + \hat{t}_{j-1})/2)}$$

$$\bar{t} = \hat{t} - \hat{t}_{j-1} \quad\quad ; \quad \hat{t} \in [t_{j-1}, t_j] \tag{4.30}$$

In this formulation, an efficient way to find the collocation solution is to solve for the 2N+5 unknowns of $x_0(0)$, $v_0(0)$, $\lambda_{x0}(0)$, $\lambda_{v0}(0)$, p_{v1}, q_{x1}, ..., p_{vN}, q_{xN}, t_{f0} using Eq. 4.29 in Eqs. 4.30 and 4.19. The high order formulations are obtained in the same manner as the previous levels and are not repeated here. The zero and first order results using only one element are shown in Figs. 4.17 - 4.20. Though the first order results are not as accurate as those in Level 2 (because only one element is used), both zero and first order solutions are far superior than the Level 0 results (Figs. 4.1 - 4.4) which correspond to the degenerate case of only one element.

61
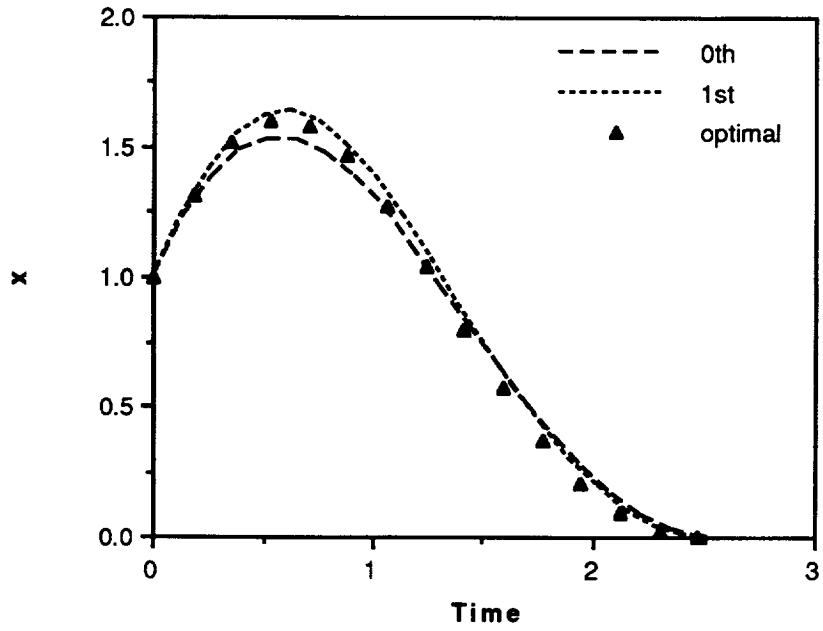
Figure 4.17. Level 3 Higher Order Results in x for N=1.
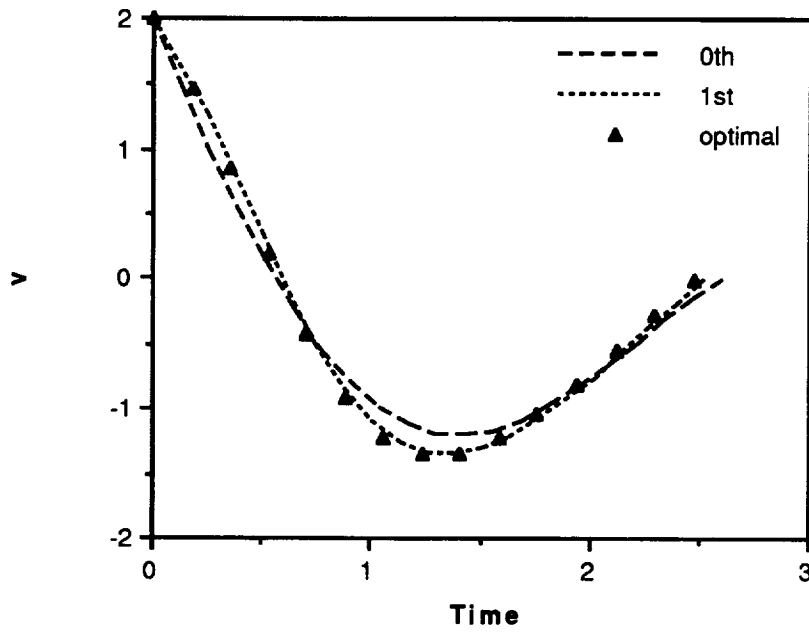
Figure 4.18. Level 3 Higher Order Results in v for N=1.

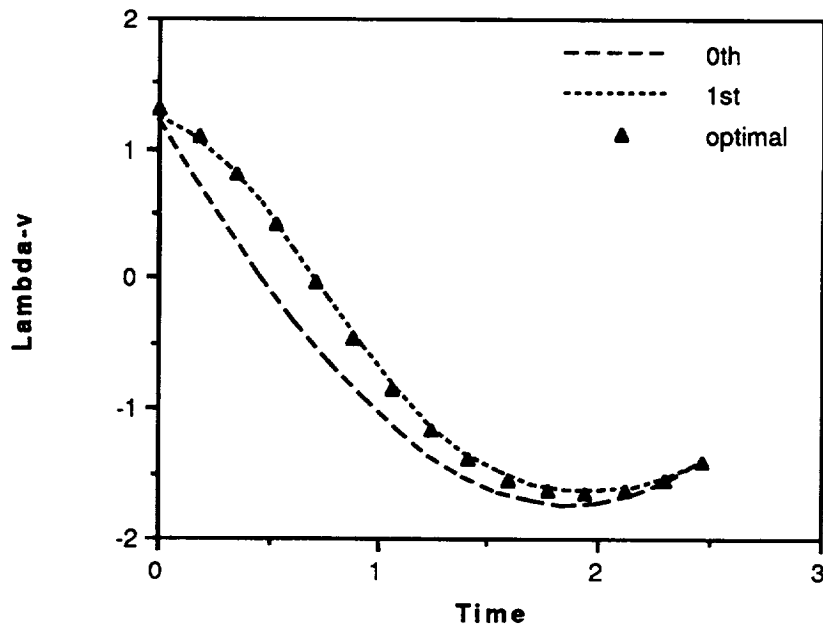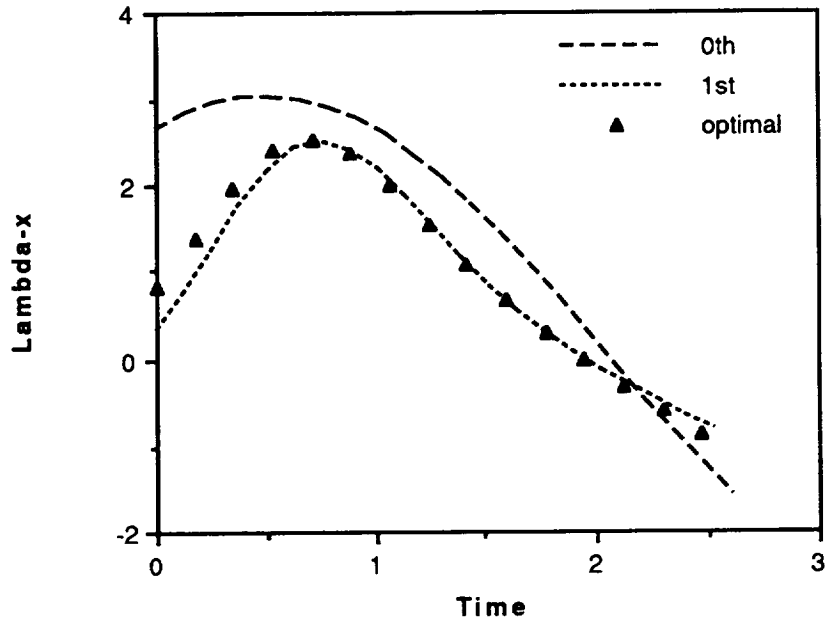Figure 4.19. Level 3 Higher Order Results in λ_x for N=1.
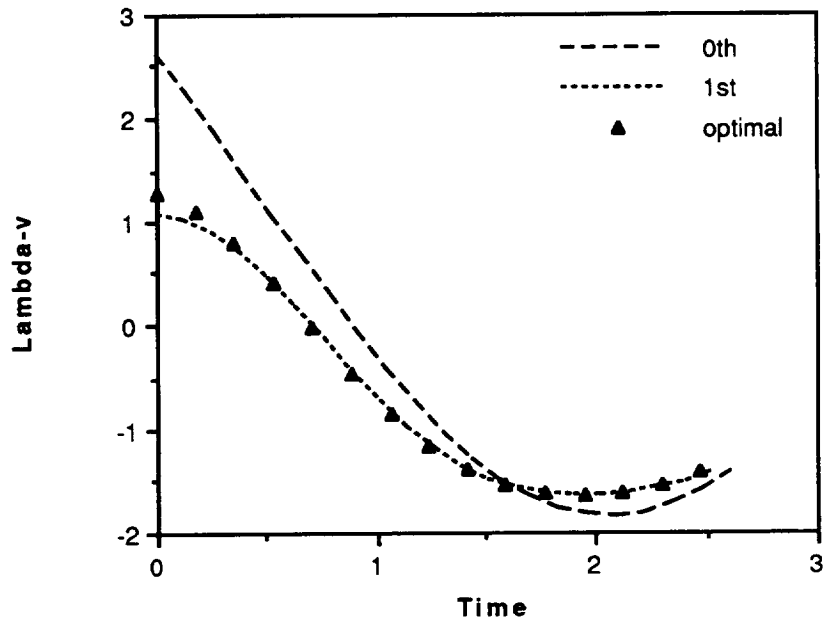
Figure 4.20. Level 3 Higher Order Results in λ_v for N=1.

4.5 Conclusions

A hybrid analytical/numerical approach for solving optimization problems using regular perturbation and collocation methods has been developed. The hybrid approach shows that it is possible to significantly improve a collocation solution without increasing the number of finite elements. The loss in accuracy that results from using a smaller number of finite elements is compensated by the addition of higher order corrections to the solution based on regular perturbation theory. Viewed a second way, using collocation to solve the zero order problem in a regular perturbation expansion allows more of the dynamics to be retained in the zero order solution. It has also shown that further dramatic improvements can be achieved by selecting more intelligent interpolating functions which are derived from the analytically tractable portions of the necessary conditions. The results show important implications in real-time guidance applications which will be demonstrated in Chapter 5 on the launch vehicle problem.

SECTION V

THE HYBRID APPROACH TO NEAR-OPTIMAL
LAUNCH VEHICLES GUIDANCE

This section applies the hybrid analytical/numerical approach of Section 4 to the problem defined in Section 2. The feedback guidance approach is based on a piecewise nearly analytic zero order solution evaluated using the collocation method. Each piecewise representation of the collocation solution obeys a bilinear tangent law for the thrust vector angle, which serves as an intelligent interpolating function for the collocation method. The zero order solution is then improved through a regular perturbation analysis, wherein the neglected dynamics are corrected in the first order term. Wind shear effects and constraints are also investigated.

5.1 Zero Order Solution

As discussed in Section 4, it is possible to improve a collocation solution by using more intelligent interpolating functions than the first order representations in Eq. 4.1. The interpolating functions can be derived from analysis of the analytically tractable portions in the necessary conditions. In this case if spherical Earth and atmospheric effects are neglected then the previous linear tangent law guidance solution results (Sec. 3.2b). However, the costate dynamics are poorly represented as either constant or zero. Hence, the strategy is to keep the approximation for the state dynamics and use the collocation method to improve the representation of the costates (cf. Level 2 and 3 formulation in Sec. 4.3). This also reduces the number of unknowns by half. Thus instead of using Eq. 4.1 to interpolate both the states and costates, only the latter are chosen for interpolation. The perturbed collocation formulation in Eq. 4.2 becomes:

$$
\dot{v} = \frac{T_{vac}^{(i)} - \bar{p}^{(i)} A_e^{(i)}}{m(t)} \sin\theta - \bar{g}_v^{(i)} + \varepsilon \left(\frac{(\bar{p}^{(i)} - p) A_e^{(i)} \sin\theta - D^{(i)} \sin\gamma + L^{(i)} \cos\gamma}{m(t)} \right.
$$

$$
\left. + \bar{g}_v^{(i)} - \frac{\mu_e}{r^2} + \frac{u^2}{r} \right)
$$

$$
\dot{u} = \frac{T_{vac}^{(i)} - \bar{p}^{(i)} A_e^{(i)}}{m(t)} \cos\theta - \bar{g}_u^{(i)} + \varepsilon \left(\frac{(\bar{p}^{(i)} - p) A_e^{(i)} \cos\theta - D^{(i)} \cos\gamma - L^{(i)} \sin\gamma}{m(t)} \right.
$$

$$
\left. + \bar{g}_u^{(i)} - \frac{uv}{r} \right)
$$

$$\dot{r} = v$$

$$\dot{\lambda}_v = q_{vj} + \varepsilon(-\frac{\partial H}{\partial v} - q_{vj}) \qquad ; \dot{\lambda}_u = q_{uj} + \varepsilon(-\frac{\partial H}{\partial u} - q_{uj}) \qquad ; j = 1, \ldots, N$$

$$\dot{\lambda}_r = q_{rj} + \varepsilon(-\frac{\partial H}{\partial r} - q_{rj}) \qquad ; \frac{\partial}{\partial \theta}(\lambda_v \dot{v} + \lambda_u \dot{u} + \lambda_r \dot{r}) = 0 \tag{5.1}$$

where

$$v = V\cos\gamma + W_i \quad ; u = V\sin\gamma + W_k$$

$$H = \lambda_v \left(\frac{(T_{vac}^{(i)} - pA_e^{(i)})\sin\theta - D^{(i)}\sin\gamma + L^{(i)}\cos\gamma}{m(t)} - \frac{\mu_e}{r^2} + \frac{u^2}{r} \right)$$

$$+ \lambda_u \left(\frac{(T_{vac}^{(i)} - pA_e^{(i)})\cos\theta - D^{(i)}\cos\gamma - L^{(i)}\sin\gamma}{m(t)} - \frac{uv}{r} \right) + \lambda_r v \tag{5.2}$$

The terms $\bar{p}^{(i)}$, $\bar{g}_v^{(i)}$, $\bar{g}_u^{(i)}$ are approximations for the average values of the engine nozzle back-pressure and the spherical acceleration components for each flight stage. From previous investigation it is found that including partial terms for these effects improve the approximation, and for the present problem these parameters are chosen as:

$$\bar{p}^{(1)} = p(h_0)/2 \qquad ; \bar{g}_v^{(1)} = \mu_e/r_0^2 - u_0^2/r_0 \qquad ; \bar{g}_u^{(1)} = 0$$

$$\bar{p}^{(2)} = 0 \qquad ; \bar{g}_v^{(2)} = \bar{g}_v^{(1)}/2 \qquad ; \bar{g}_u^{(2)} = 0 \tag{5.3}$$

and they are assumed to be updated continuously in closed loop implementation.

In the following we make use of the analytic portion of the optimality condition in Eq. 5.1 to generate the zero order control, by using the form in Eq. 4.3. This amounts to regarding the dependence of aerodynamic forces on θ as a perturbation of the optimality condition, which results in the celebrated bilinear tangent law

$$\tan\theta_0(t) = \frac{\lambda_{v0j-1} + q_{vj}(t - t_{j-1})}{\lambda_{u0j-1} + q_{uj}(t - t_{j-1})} \tag{5.4}$$

With the above formulation and using the expression in Eq. 5.4 to eliminate the control, the zero order solution ($\varepsilon = 0$) can be expressed as:

$$v_0(t) = v_0(t_{j-1}) + \frac{FD}{k^{(i)}} \left\{ \frac{\varsigma + \Delta}{\sqrt{1+\Delta^2}} \sinh^{-1}(\tan(\varphi+\eta)) - \sinh^{-1}(\tan\varphi) \right\} \Big|_{\varphi(t_{j-1})}^{\varphi(t)}$$

$$-(t-t_{j-1})\overline{g}_v^{(i)} \qquad ; t \in [t_{j-1}, t_j]$$

$$u_0(t) = u_0(t_{j-1}) + \frac{FE}{k^{(i)}} \left\{ \frac{1+\Delta\xi}{\sqrt{1+\Delta^2}} \sinh^{-1}(\tan(\varphi+\eta)) - \xi\sinh^{-1}(\tan\varphi) \right\} \Big|_{\varphi(t_{j-1})}^{\varphi(t)}$$

$$-(t-t_{j-1})\overline{g}_u^{(i)}$$

$$r_0(t) = r_0(t_{j-1}) - \frac{FDC}{k^{(i)}A} \left\{ (\Delta - \tan\varphi)[\frac{\varsigma+\Delta}{\sqrt{1+\Delta^2}}\sinh^{-1}(\tan(\varphi+\eta)) - \sinh^{-1}(\tan\varphi)] \right.$$

$$\left. \sec\varphi - \varsigma\sinh^{-1}(\tan\varphi) \right\} \Big|_{\varphi(t_{j-1})}^{\varphi(t)} + [v_0(t_{j-1}) - \overline{g}_v^{(i)}\frac{t-t_{j-1}}{2}](t-t_{j-1}) - G(t_{j-1})$$

$$\lambda_{v0}(t) = \lambda_{v0j-1} + q_{vj}(t-t_{j-1})$$

$$\lambda_{u0}(t) = \lambda_{u0j-1} + q_{uj}(t-t_{j-1})$$

$$\lambda_{r0}(t) = \lambda_{r0j-1} + q_{rj}(t-t_{j-1}) \qquad\qquad (5.5)$$

where

$$A = \sqrt{q_{vj}^2 + q_{uj}^2} \qquad ; B = (c_v q_{vj} + c_u q_{uj})/A \qquad ; C = \sqrt{c_v^2 + c_u^2 - B^2}$$

$$D = q_{vj}/A \qquad ; E = (c_u A - q_{uj}B)/(AC) \qquad ; F = T_{vac}^{(i)} - \overline{p}^{(i)}A_e^{(i)}$$

$$c_v = \lambda_{v0j-1} - q_{vj}t_{j-1} \ ; c_u = \lambda_{u0j-1} - q_{uj}t_{j-1} \qquad ; c_m = m^{(i)} + k^{(i)}t_{j-1}$$

$$\varphi(t) = \tan^{-1}(\frac{At+B}{C}) \ ; \eta = \begin{cases} \tan^{-1}(1/\Delta) & , \Delta \geq 0 \\ \pi + \tan^{-1}(1/\Delta) & , \Delta < 0 \end{cases}$$

$$\Delta = \frac{c_m A + k^{(i)}B}{k^{(i)}C} \qquad ; \xi = \frac{q_{uj}C}{c_u A - q_{uj}B} \qquad ; \varsigma = \frac{c_v A - q_{vj}B}{q_{vj}C}$$

$$G(t_{j-1}) = \frac{FD}{k^{(i)}} \left\{ \frac{\varsigma+\Delta}{\sqrt{1+\Delta^2}}\sinh^{-1}(\tan(\varphi+\eta)) - \sinh^{-1}(\tan\varphi) \right\} \Big|_{\varphi(t_{j-1})} \qquad (5.6)$$

The above expressions constitute a set of nonlinear interpolating functions and the zero order solution is now expressed in terms of the unknown costate nodal values. To evaluate
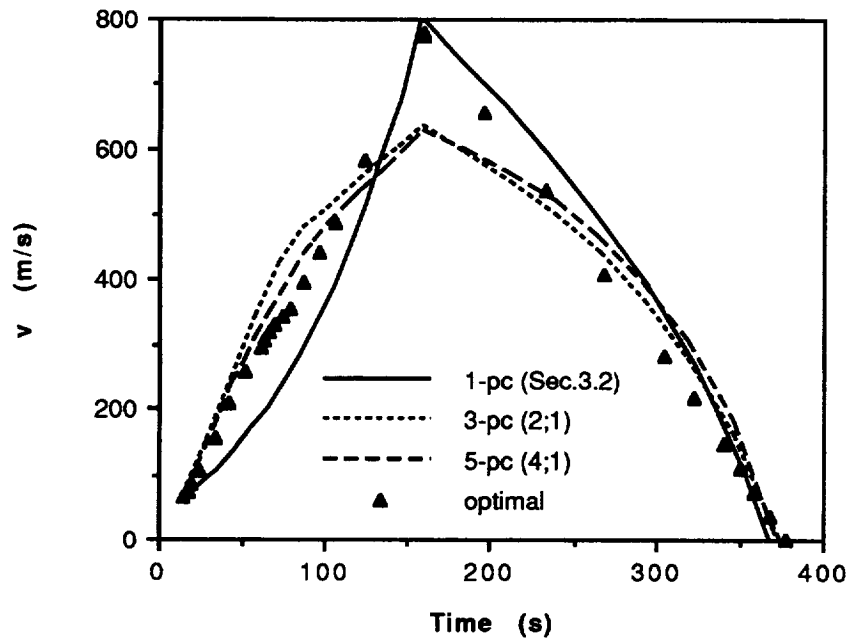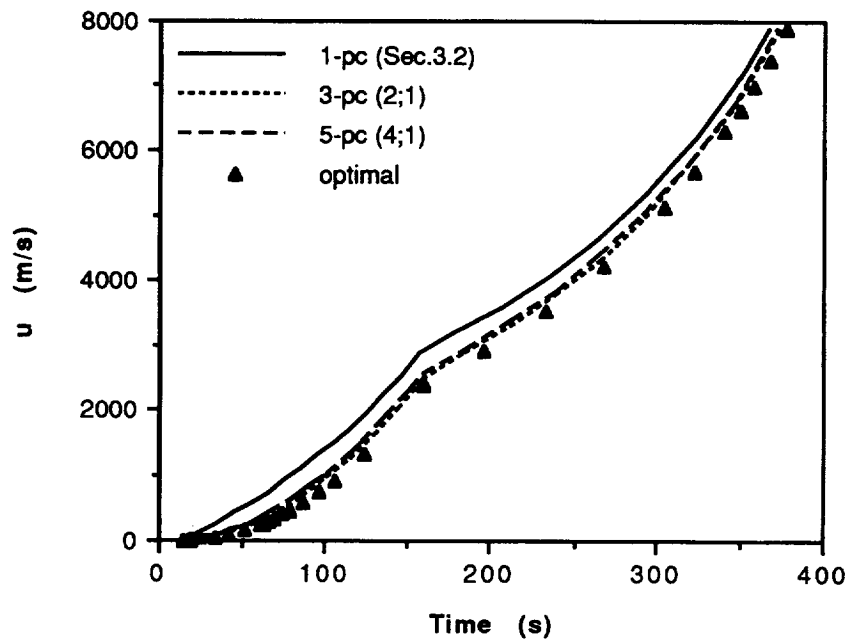
Figure 5.1. Open Loop v Profiles for Various N.

Figure 5.2. Open Loop u Profiles for Various N.

68

these values, the collocation constraints on the costate derivatives in Eq. 4.1 are enforced:

$$q_{vj} = \frac{\lambda_{v0j} - \lambda_{v0j-1}}{t_j - t_{j-1}} = -\frac{\partial H}{\partial v}\Big|_{t=(t_j+t_{j-1})/2;\ \lambda_{v0}=(\lambda_{v0j}+\lambda_{v0j-1})/2;}$$
$$\lambda_{u0}=(\lambda_{u0j}+\lambda_{u0j-1})/2;\ \lambda_{r0}=(\lambda_{r0j}+\lambda_{r0j-1})/2$$

$$q_{uj} = \frac{\lambda_{u0j} - \lambda_{u0j-1}}{t_j - t_{j-1}} = -\frac{\partial H}{\partial u}\Big|_{t=(t_j+t_{j-1})/2;\ \ldots\ ;\ \lambda_{r0}=(\lambda_{r0j}+\lambda_{r0j-1})/2}$$

$$q_{rj} = \frac{\lambda_{r0j} - \lambda_{r0j-1}}{t_j - t_{j-1}} = -\frac{\partial H}{\partial r}\Big|_{t=(t_j+t_{j-1})/2;\ \ldots\ ;\ \lambda_{r0}=(\lambda_{r0j}+\lambda_{r0j-1})/2} \tag{5.7}$$

Since more control activity is expected inside the atmosphere, a denser segmentation is used for the first stage flight, whereas a 1-piece segment is sufficient for the subsequent more nearly exoatmospheric second stage flight. The total number of unknowns to be solved in the zero order problem are 3N+4. Open loop solutions in a stationary atmosphere for several increasing values of N are given in Figs. 5.1 to 5.6. The segmentation is N-1 elements for the first stage flight and one element for the second stage flight. Zero order results using only the regular perturbation approach as given in Sec. 3.2 are also included for comparison. Significant improvements are observed in the costate profiles with the hybrid approach because part of the aerodynamic effects are now accounted for in the zero order formulation. In particular, note from Figs. 5.4 - 5.6 that the zero order solution of Sec. 3.2 amounts to ignoring aerodynamic effects and invoking a flat, non rotating Earth approximation. This results in λ_u and λ_r being constant and λ_v being linear in time (see Figs. 5.4 - 5.6), which from Eq. 5.4 gives the linear tangent steering law. This largely accounts for the failure of the regular perturbation method when aerodynamic effects are included.
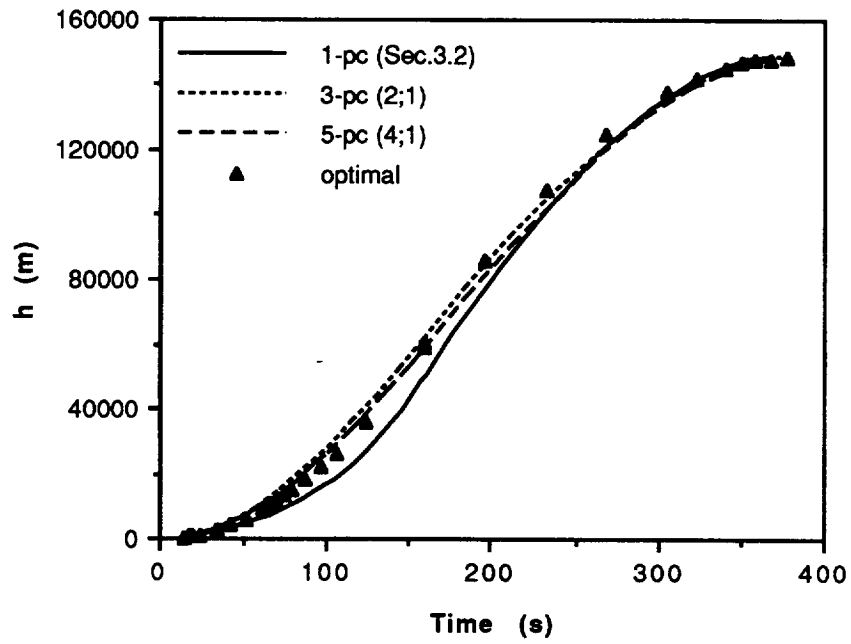
Figure 5.3. Open Loop h Profiles for Various N.
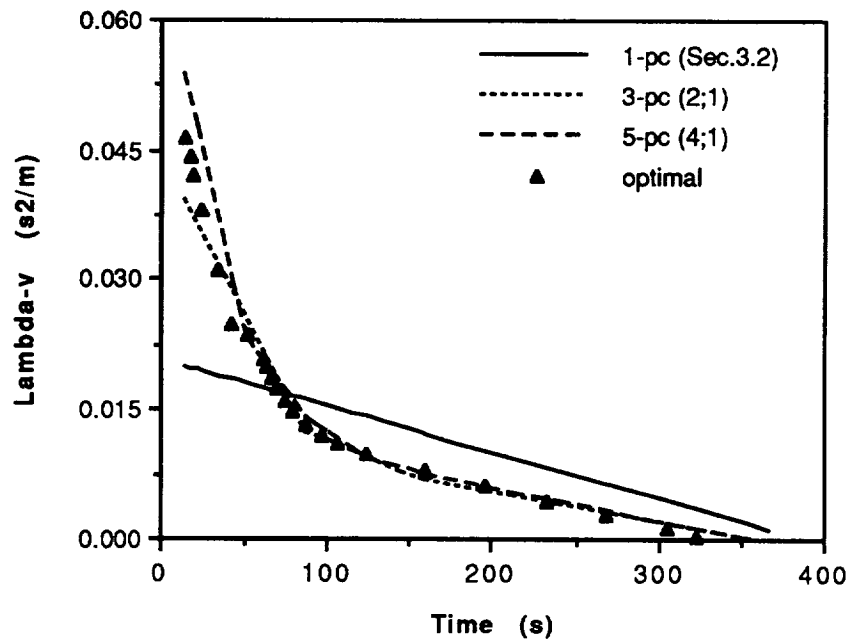
Figure 5.4. Open Loop λ_v Profiles for Various N.

70

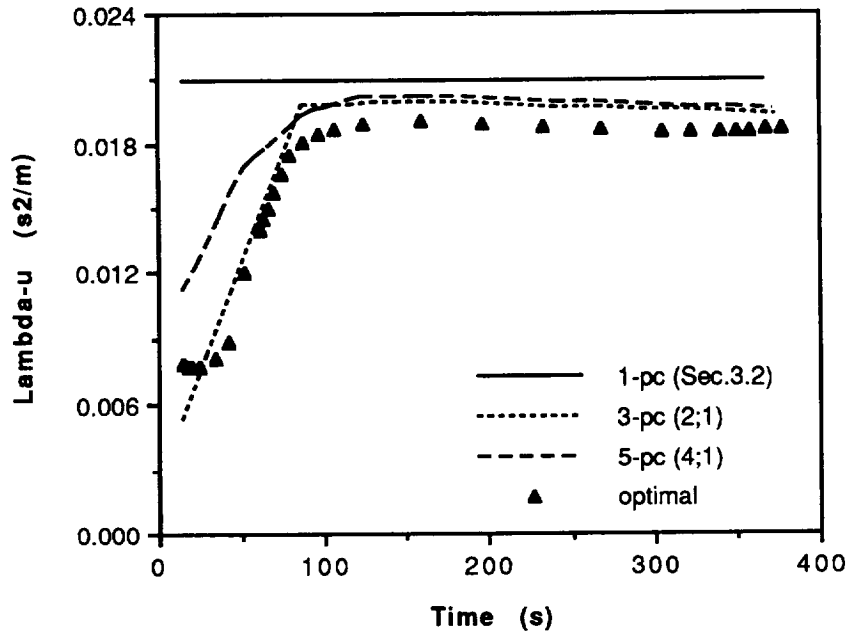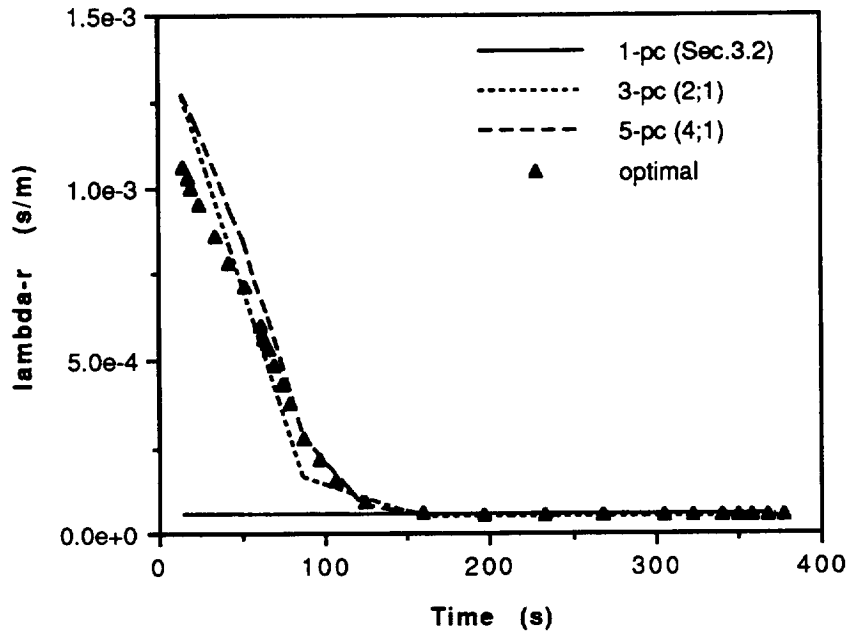Figure 5.5. Open Loop λ_u Profiles for Various N.

Figure 5.6. Open Loop λ_r Profiles for Various N.

5.2 First Order Solution

In this case, the linear differential equations satisfied by the first order terms have the following form:

$$\frac{d}{dt}\begin{bmatrix} v_1 \\ u_1 \\ r_1 \\ \lambda_{v1} \\ \lambda_{u1} \\ \lambda_{r1} \end{bmatrix} = \begin{bmatrix} 0 & 0 & 0 & a_{14j} & a_{15j} & 0 \\ 0 & 0 & 0 & a_{15j} & a_{25j} & 0 \\ 1 & 0 & 0 & 0 & 0 & 0 \\ \dfrac{\partial q_{vj}}{\partial v} & \dfrac{\partial q_{vj}}{\partial u} & \dfrac{\partial q_{vj}}{\partial r} & \dfrac{\partial q_{vj}}{\partial \lambda_v}+f_1\dfrac{\partial q_{vj}}{\partial \theta} & \dfrac{\partial q_{vj}}{\partial \lambda_u}+f_2\dfrac{\partial q_{vj}}{\partial \theta} & -1 \\ \dfrac{\partial q_{uj}}{\partial v} & \dfrac{\partial q_{uj}}{\partial u} & \dfrac{\partial q_{uj}}{\partial r} & \dfrac{\partial q_{uj}}{\partial \lambda_v}+f_1\dfrac{\partial q_{uj}}{\partial \theta} & \dfrac{\partial q_{uj}}{\partial \lambda_u}+f_2\dfrac{\partial q_{uj}}{\partial \theta} & 0 \\ \dfrac{\partial q_{rj}}{\partial v} & \dfrac{\partial q_{rj}}{\partial u} & \dfrac{\partial q_{rj}}{\partial r} & \dfrac{\partial q_{rj}}{\partial \lambda_v}+f_1\dfrac{\partial q_{rj}}{\partial \theta} & \dfrac{\partial q_{rj}}{\partial \lambda_u}+f_2\dfrac{\partial q_{rj}}{\partial \theta} & 0 \end{bmatrix}\begin{bmatrix} v_1 \\ u_1 \\ r_1 \\ \lambda_{v1} \\ \lambda_{u1} \\ \lambda_{r1} \end{bmatrix}$$

$$+\frac{T_1}{T_0}\begin{bmatrix} c_{1j}(t) \\ c_{2j}(t) \\ v_0(t) \\ q_{vj} \\ q_{uj} \\ q_{rj} \end{bmatrix} + \begin{bmatrix} p_{1j}(t) \\ p_{2j}(t) \\ 0 \\ p_{4j}(t) \\ p_{5j}(t) \\ p_{6j}(t) \end{bmatrix} \quad ; t \in [t_{j-1}, t_j] \tag{5.8}$$

Complete expressions are given in Appendix D. As explained earlier, the first stage flight time is fixed, $T = t_f - t_s$, and T_0 represents the zero order second stage open flight time. Therefore, $T_1 = 0$ for the dynamics describing $t \le t_s$, and the second term in Eq. 5.8 is dropped for the elements corresponding to this time interval.

Experience has shown that higher order perturbation corrections are not sensitive to using an exact state transition matrix. This behavior is analogous to the practice of using an approximate Jacobian to solve nonlinear algebraic equations. So we introduced the following approximation to simplify the analysis. The 3 x 5 lower left corner block of the system matrix in Eq. 5.8 represents the effects that second order variations of the atmospheric terms have on the costate variables. By neglecting these terms we are able to derive an approximate state transition matrix for the first order system:

$$\Omega_{A_j}^{(i)}(t, t_{j-1}) = \begin{bmatrix} 1 & 0 & 0 & \omega_{14_j}^{(i)} & \omega_{15_j}^{(i)} & \omega_{16_j}^{(i)} \\ 0 & 1 & 0 & \omega_{24_j}^{(i)} & \omega_{25_j}^{(i)} & \omega_{26_j}^{(i)} \\ t-t_{j-1} & 0 & 1 & \omega_{34_j}^{(i)} & \omega_{35_j}^{(i)} & \omega_{36_j}^{(i)} \\ 0 & 0 & 0 & 1 & 0 & t_{j-1}-t \\ 0 & 0 & 0 & 0 & 1 & 0 \\ 0 & 0 & 0 & 0 & 0 & 1 \end{bmatrix} \quad ; t \in [t_{j-1}, t_j] \tag{5.9}$$

72

Appendix D details the ω terms in Eq. 5.9. The lower right hand block in Eq. 5.9 accounts for spherical Earth effects on the costate solution, neglected in the zero order solution. As will be shown in the numerical results section, this is an important correction for the exoatmospheric phase of flight. By successively applying Eq. 4.6 of N times, the perturbations at t_N for a first order system with piecewise representation are now given by

$$
\begin{bmatrix} x_1(t_N) \\ \lambda_1(t_N) \end{bmatrix} = \Omega^{(2)}_{A_N}(t_N,t_{N-1})\Omega^{(1)}_{A_{N-1}}(t_{N-1},t_{N-2}) \cdots \Omega^{(1)}_{A_1}(t_1,t_0)\begin{bmatrix} x_1(t_0) \\ \lambda_1(t_0) \end{bmatrix} +
$$

$$
\int_{t_{N-1}}^{t_N} \Omega^{(2)}_{A_N}(t_N,\tau)\{ \frac{T_1}{T_0}\begin{bmatrix} C^{(2)}_{1_N}(\tau) \\ C^{(2)}_{2_N}(\tau) \end{bmatrix} + \begin{bmatrix} P^{(2)}_{1_N}(\tau) \\ P^{(2)}_{2_N}(\tau) \end{bmatrix}\}d\tau + \sum_{j=1}^{j=N-1} \Omega^{(2)}_{A_N}(t_N,t_{N-1}) \cdots
$$

$$
\cdots \Omega^{(1)}_{A_{j+1}}(t_{j+1},t_j)\int_{t_{j-1}}^{t_j}\Omega^{(1)}_{A_j}(t_j,\tau)\begin{bmatrix} P^{(1)}_{1_j}(\tau) \\ P^{(1)}_{2_j}(\tau) \end{bmatrix}d\tau \qquad (5.10)
$$

5.3 Numerical Results

Figures 5.7 to 5.10 show the closed loop results for the state variables expressed in the wind frame coordinates. The control is updated at every second and is held constant within each update interval. The total number of elements used in this case is N = 8. Note in Fig. 5.10 that jumps in angle of attack occur at about M = 1.3 and M = 2.3. These are due to the shadowing effects of the booster which causes the control solution to first follow a higher α profile (to reduce drag) followed by a lower profile to correct the trajectory. There is another third small jump at the staging time due to the discontinuous dynamics. This figure also shows a major difference between the zero order and first order solution for α during the end of the second stage flight, which is due to the absence of the spherical Earth corrections in the zero order solution. Even though a large difference exists between the two solutions, the trajectory and the performance index stay very close, and imply that the optimal result is insensitive to control variations.
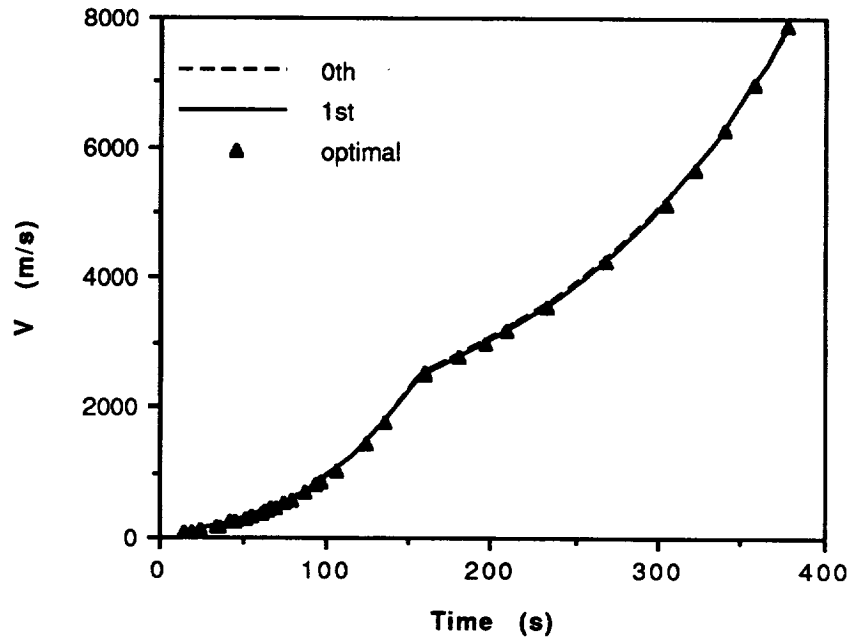
Figure 5.7. Closed Loop Velocity Profile for N=8.
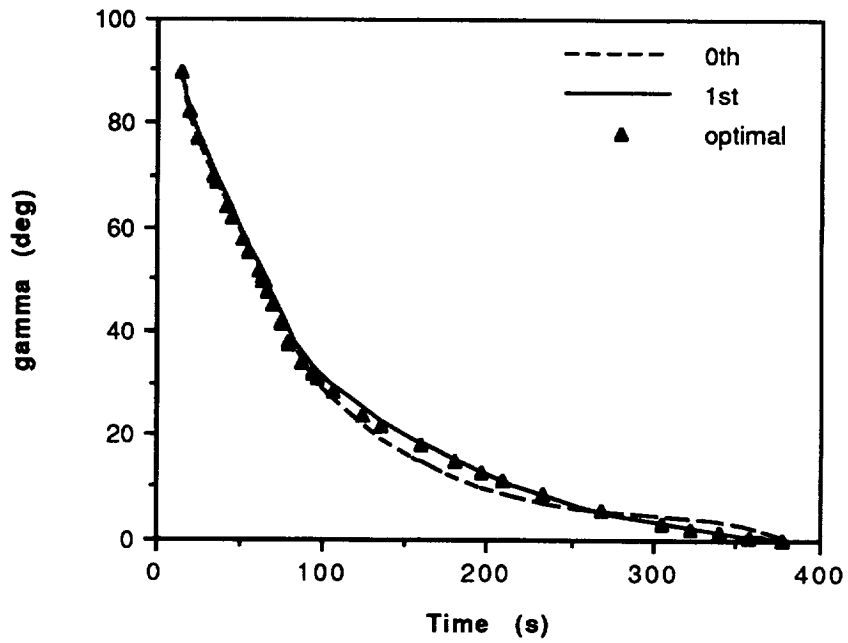
Figure 5.8. Closed Loop Flight-path Angle Profile for N=8.
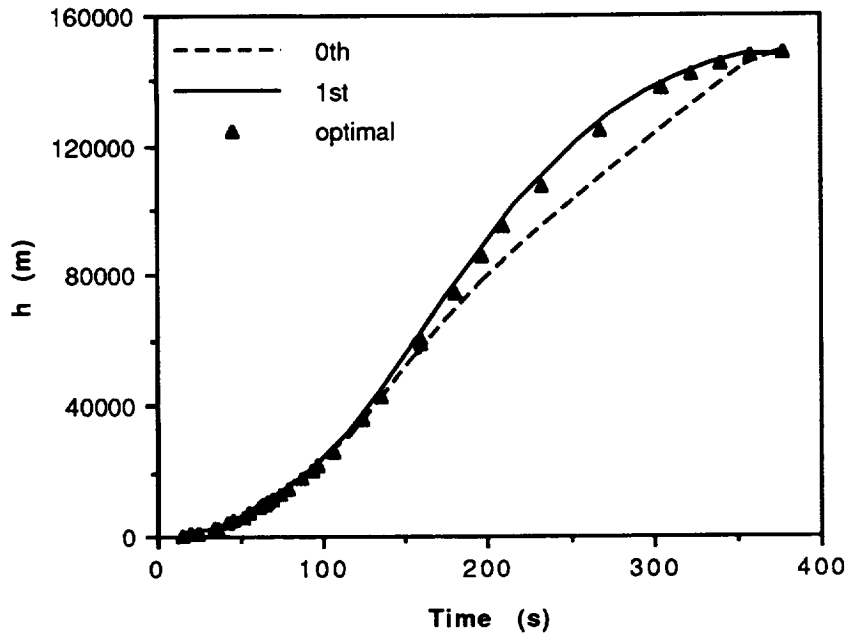
Figure 5.9. Closed Loop Altitude Profile for N=8.
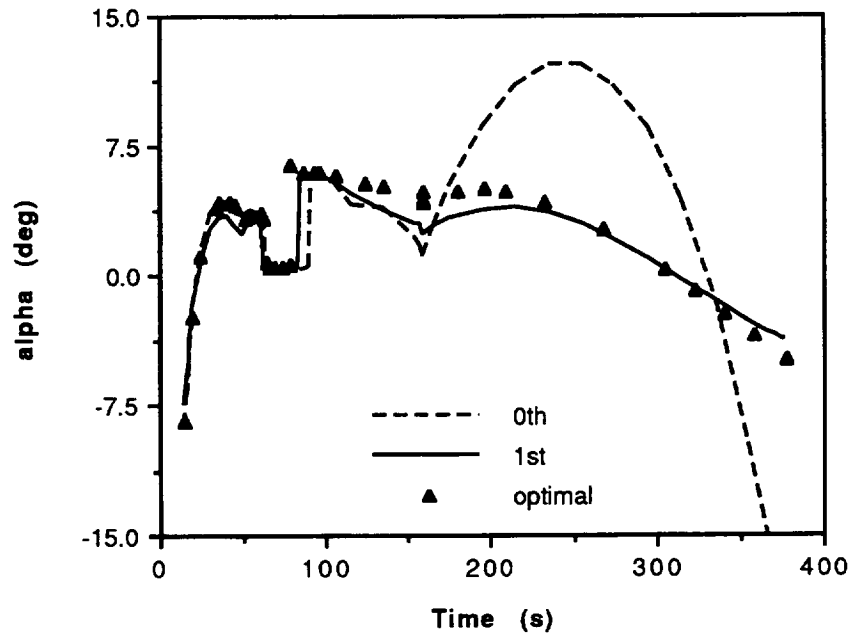
Figure 5.10. Closed Loop Angle of Attack Profile for N=8.

Next, we include the effects of non-stationary atmosphere on the solution. The wind profile used is the interpolated mean winter profile for Kennedy Space Center, shown in Fig. 2.11, and this profile is accounted for in the guidance solution. From earlier investigation it is learned that the performance is not sensitive to control variations, there-
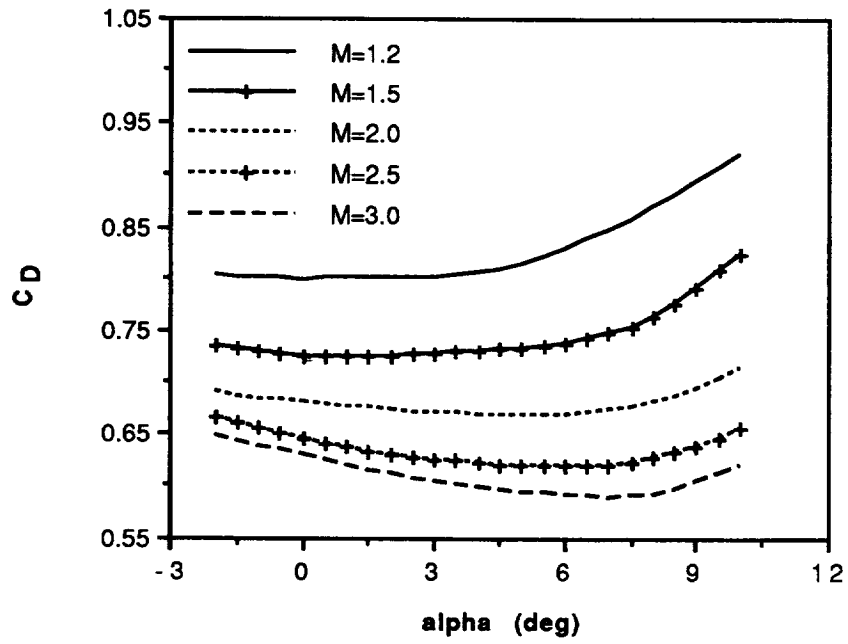
Figure 5.11. Convexized First Stage C_D Profile.
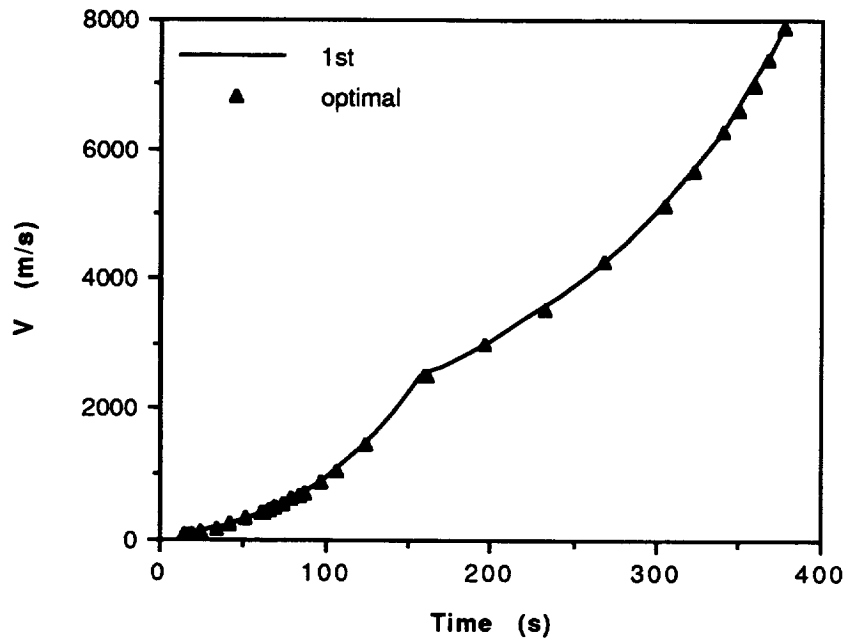
Figure 5.12. Closed Loop Velocity Profile Under Wind
and αq Constraint.

fore attempt is not made to incorporate the control constraint in the analysis. Instead a hard bound on the control is enforced in the simulation, but not in the guidance derivation. The bounds in this case are

$$-167580\,\mathrm{deg\,Nm^{-2}} \le \alpha q \le 167580\,\mathrm{deg\,Nm^{-2}} \tag{5.11}$$

They represent the dynamic loading limits on the vehicle. In addition, the first stage C_D profile was convexized, as shown in Fig. 5.11. This is done to eliminate the objectionable jumps in control that are observed in Fig. 5.10, which have negligible effect on the performance. The results of the closed loop simulation for the unconstrained case are depicted in Figs. 5.12 and 5.15, which show excellent agreement between the first order guided solution and the optimal solution. Fig. 5.16 illustrates the effect of the αq constraint, which is active only over a minor portion of the trajectory. The performance results for this case summarized in Table 5.1.

Table 5.1. Performance Comparison for ALS Vehicle Guidance.

	optimal	1st-order	0th-order
$h(t_f)$	148160m	148160.0m	148160.0m
$\gamma(t_f)$	0°	0.000°	-0.001°
$V(t_f)$	$7858.2\mathrm{ms^{-1}}$	$7858.20\mathrm{ms^{-1}}$	$7858.14\mathrm{ms^{-1}}$
t_f	377.372s	377.382s	378.397s
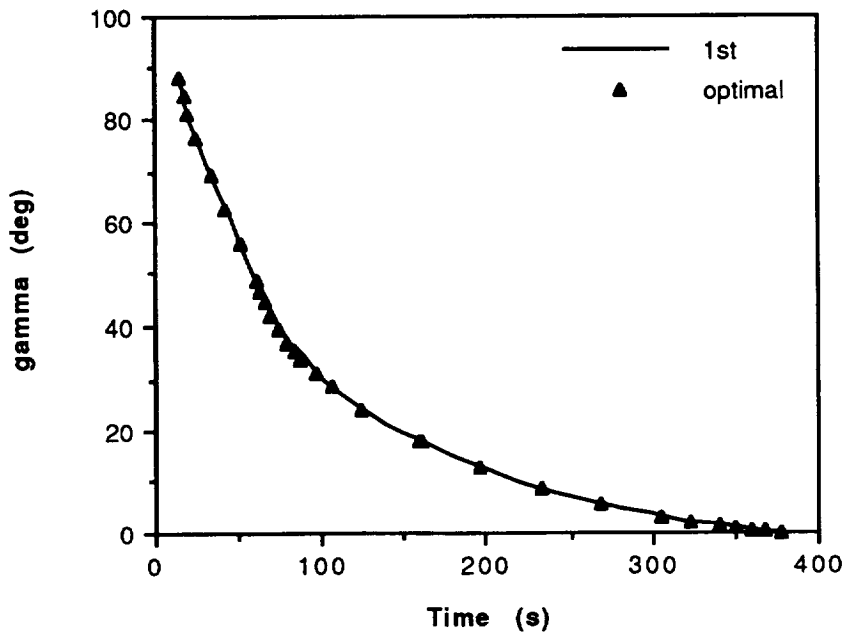
Figure 5.13. Closed Loop Flight-path Angle Profile Under
Wind and αq Constraint.
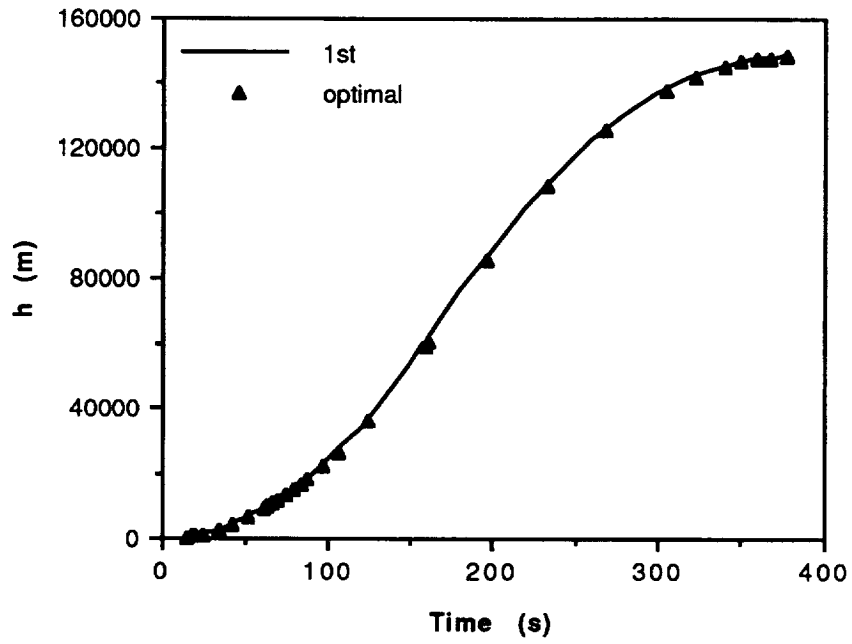
Figure 5.14. Closed Loop Altitude Profile Under Wind
and αq Constraint.
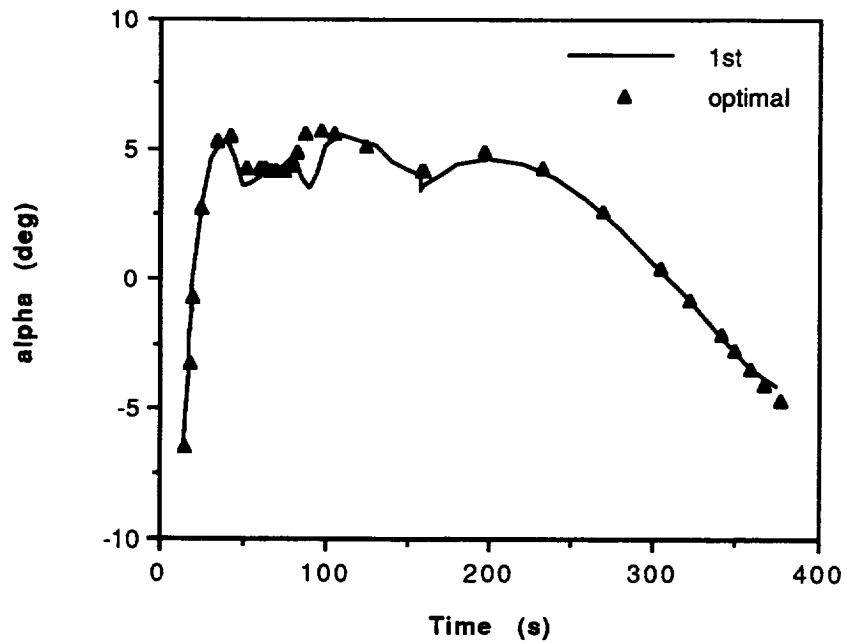
Figure 5.15. Closed Loop Angle of Attack Profile Under
Wind and αq Constraint.

78
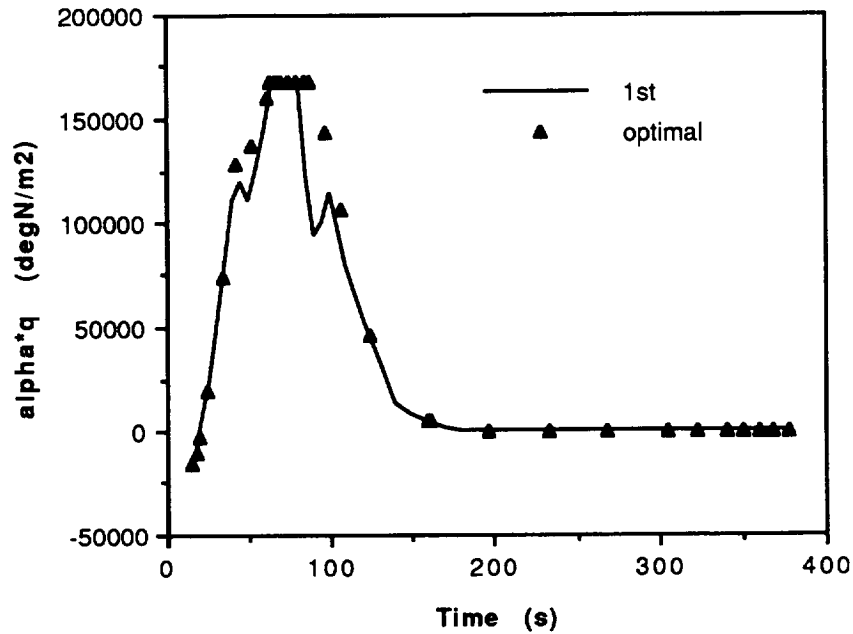
Figure 5.16. Closed Loop αq Profile Under Wind
and αq Constraint.

In this example, the aerodynamic forces have a major effect in the middle portion of the first stage ascent. This is illustrated in Fig. 3.20 which shows the ratios of the lift and drag forces to the thrust components. This explains why the regular perturbation analysis in Sec. 3.2 is not able to correct for the effect of aerodynamic forces in the first order analysis. These forces are simply too large to be treated as perturbation effects, and consequently the calculated first order correction diverged. Use of the collocation method in forming a zero order solution largely accounts for the aerodynamic effect through the mid-element constraints in Eq. 5.7.

5.4 Remarks on the Numerical Results

The results show a high level of fidelity and justify the approximation we have introduced to obtain the state transition matrix in Eq. 5.9. In particular, the first order solution shows significant improvement by correcting for the spherical Earth effects, as illustrated in Fig. 5.10. In this case the zero order solution fails to anticipate the sharp change in the radial acceleration as the orbital condition is approached, even using a continuously updated guess of $\bar{g}_v$. This results in an excessive pull-up of the vehicle during the initial portion of the second stage flight, and is later forced to correct with a large negative α to meet the terminal conditions. However, both zero and first order results give extremely good orbit injection accuracy without requiring a high rate of control update.
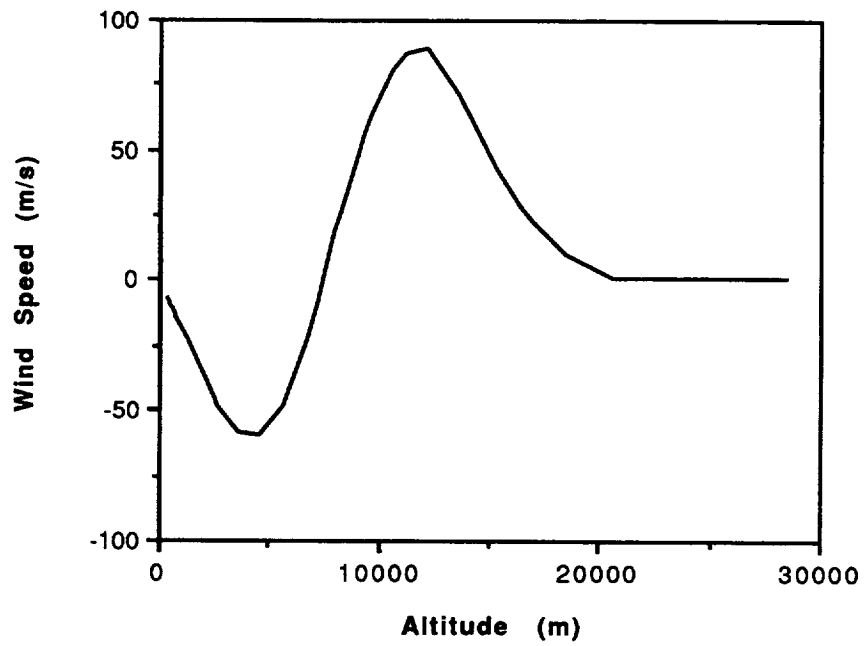
Figure 5.17. A Hypothetical Wind Shear Profile.
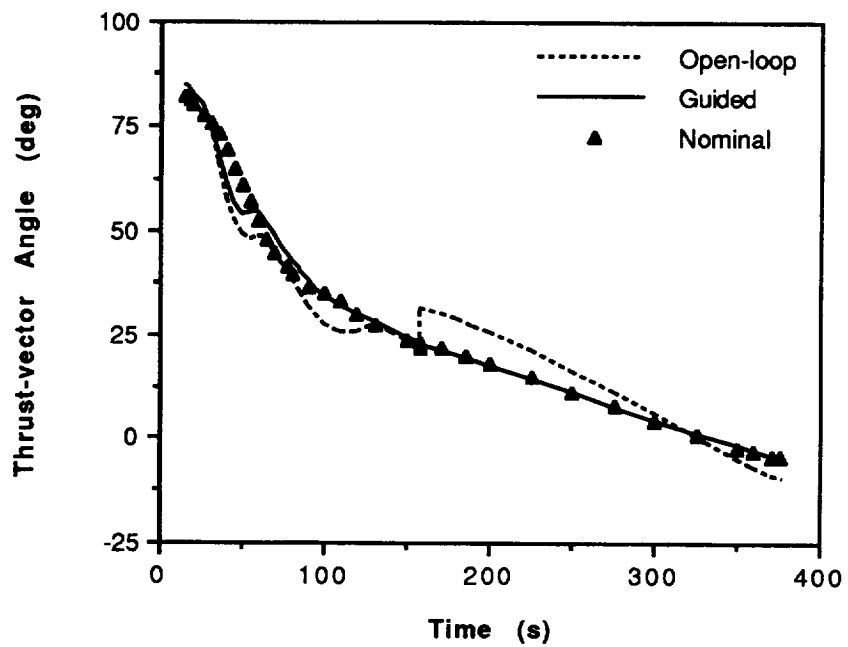
Figure 5.18. Comparison of the Thrust Vector Angle Profiles
under Wind Shear.

The computations for the cases presented here are done on a SPARCstation 1. The CPU time needed for a control update ranges from 0.65s for an 8-element case to less than 0.15s for a 1-element solution during the second stage flight. The Newton's method with Broyden's update of the Jacobian [11] is used in the zero order collocation evaluation and the solution converges typically in 4 iterations. It is apparent from the numerical results that the first order correction is needed mainly to correct for spherical Earth effects which are dominant only in the second stage of flight. Therefore a significant additional savings in computation time would have resulted had we computed this correction only for that phase.

## 5.5 Wind Shear Investigation

To assess the effectiveness of the hybrid approach against wind shear, we show a typical scenario. First, an open loop trajectory using piecewise linear thrust vector angle program for the first stage flight, followed by the closed loop hybrid approach guidance for the second stage flight is simulated with a hypothetical wind shear (cf. Fig. 5.17). The open loop part of the guidance is derived from a linear interpolation of the previous results, which is based on the nominal mean wind profile. Second, a guided trajectory using closed loop guidance for both the first and second stage flight is simulated. This guided solution is assumed to have detected the wind shear, and is therefore included in the calculation. To assure structural integrity, both cases are incorporated with the αq constraints. The first case represents the approach for present launch vehicle operation, ie. an open loop guidance for the endoatmospheric flight using pre-flight atmospheric conditions, and compensated by a closed loop guidance for the exoatmospheric flight. The second case represents the proposed approach for ALS, ie. real-time near optimal guidance. Figs. 5.18 - 5.20 compare the 'Open loop' and the 'Guided' solutions. A point of interest, the 'Nominal' solution with the same linear piecewise control program flying under the nominal wind condition is also included. The 'Open-loop' solution gives poorer performance (cf. Table 5.2). The final time to orbit is 1.13s longer (equivalent to a loss of 4550lbs in payload) than the guided solution, and is also worse than the guided solution

Table 5.2. Performance Comparison under Wind Shear.

	Guided (1st)	Guided (0th)	Open loop
$h(t_f)$	148160.0m	148160.0m	148160.0m
$\gamma(t_f)$	0.000°	-0.000°	0.000°
$V(t_f)$	7858.20ms^{-1}	7858.18ms^{-1}	7858.20ms^{-1}
$-J = t_f$	377.287s	378.243s	378.413s

using only a zero order solution. If the magnitude of the wind shear is further increased by 22%, then open-loop guidance will result in a catastrophic failure unless the αq limit is exceeded.
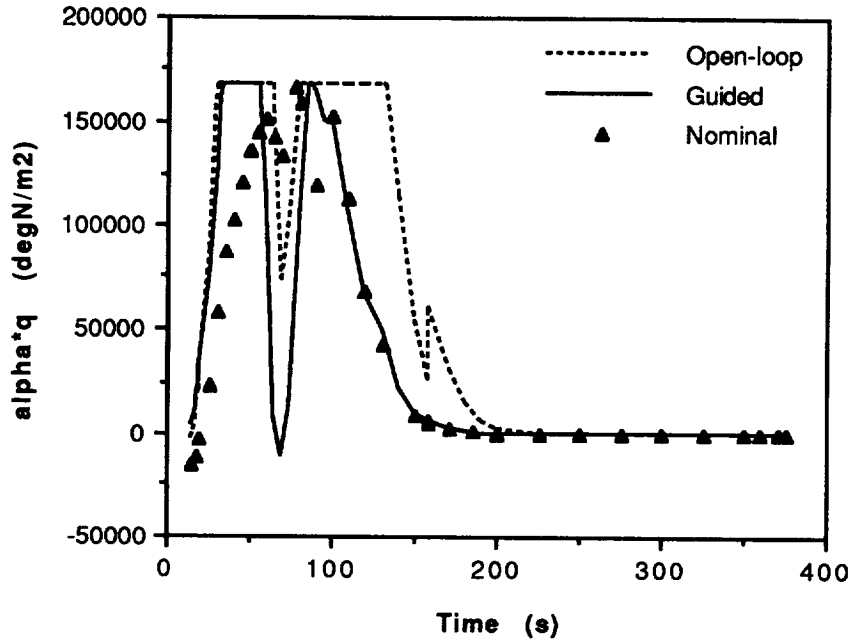

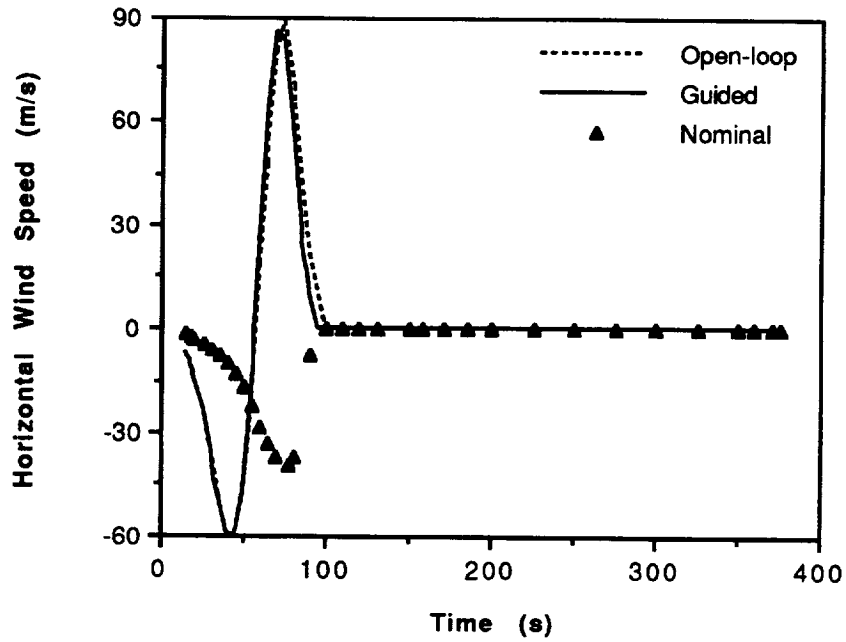Figure 5.19. Comparison of the αq Profiles under Wind Shear.

Figure 5.20. Experienced Horizontal Wind Speed for the 3 Different Simulations.

SECTION VI

CONCLUSIONS AND RECOMMENDATIONS

6.1 Conclusions

The fundamental problem in treating launch vehicle dynamics by singular perturbation methods relates to the inherent large value of longitudinal load factor. As a result, the zero order reduced solution gives a very poor approximation. A manifold solution was also attempted to account for flight path angle dynamics, but this method also fails due to the fact that the dynamics are not separable in the same manner throughout the ascent profile. Regular perturbation analysis gives a better solution in the absence of aerodynamic forces. However, the approach cannot handle guidance for the atmospheric flight phase, which is the main issue of this research. The neglected aerodynamic forces in the zero order solution are simply to large to be considered as a perturbation effect.

A new hybrid approach for the solution of nonlinear problems in optimal control has been developed for this application. This approach is hybrid because it combines the desirable features of numerical and analytical methods. The numerical method of collocation allows a simple formulation for solving a wide variety of optimization problems. The disadvantage of requiring a large number of approximation elements and solving a large dimension set of algebraic equations are compensated for by the analytical approach of regular perturbation. The regular perturbation approach provides higher order correction over the collocation solution without increasing the number of approximation elements. It can also be used to identify intelligent interpolating functions for the collocation solution, which results in a further substantial reduction in the number of finite elements needed for a given level of solution accuracy. These attractive features promise an enhanced real time capability in the solution of optimal control problems, which has been demonstrated in the launch vehicle guidance application. The main results on this problem are that a bilinear tangent steering law can be employed in all flight phases, including the atmospheric phase, and that the collocation solution can be obtained using a small number of elements.

6.2 Recommendations for Future Work

Many important issues remain for future research, and the following recommendations are made in increasing order of complexity:

Identifying More Intelligent Interpolating Functions - Though the zero order solution is capable of handling partial aerodynamic effects, spherical Earth effects were not directly

incormorpated in the analysis. This leads to a poor representation of the zero order solution as the vehicle approaches orbital speed. An investigation should be made to account for this effect in the formulation, and a proposed way to set up the problem is to add a constant perturbation term, similar to the Level 3 formulation in Sec. 4.3.

More Accurate Model - Improvements can be made in the launch vehicle problem by considering a more elaborate dynamic model. The rotating Earth effects and a more complex propulsion model should be considered. It may be necessary to modify the interpolating solution in the collocation approach, depending on the magnitudes of these nonlinearities.

Multi-flight Task Requirements - The hybrid guidance approach can be extended to handle various flight tasks such as deorbit and rendezvous. These requirements will pose terminal constraints on both the downrange and crossrange values, which can be included in a 3-D formulation. Such multi-flight task guidance capability would be very useful to manned vehicles like the Space Shuttle.

Constrained Problem Analysis - For the launch vehicle problem, it is coincidental that the performance is insensitive to control variations, thus allowing the exclusion of the control constraint in the analysis. However, it would be useful to complete the hybrid approach to include analysis of constrained optimization problems. To address the constrained problem requires a guess of the switching structure and a formulation of variable time intervals in which the constraint becomes active.

Launch Vehicles Range Safety Concerns - The range safety issues related to the launch vehicle ascent trajectory occur in the form of state constraints. To avoid potential disaster or to facilitate the retrieval of reusable boosters, the vehicle may be constrained to fly within a narrow corridor of air space. Present methods to handle this type of problem are not efficient and rely purely on numerical means. Future study should include a systematic and simplified formulation that is tractable by analytic methods such as the hybrid approach.

Hybrid Approach with the HJB Expansion - As demonstrated in [14, 37], the regular perturbation analysis can be carried out using the Hamilton-Jacobi-Bellman equation. In this formulation, the perturbation corrections are not represented by a set of linear O. D. E's., and the calculation of the state transition matrix or sensitivity functions are not required. Instead the perturbation corrections are evaluated simply by quadrature. Proposed future research should include a study of the relationships between these two types of formulations (the HJB and the state/costate expansion) and the hybrid approach using the HJB expansion, which promises a much simpler and more efficient evaluation of the perturbation corrections.

84

<u>Manifold Investigation</u> - The failure of the energy approximation analysis indicates that the zero order ($\varepsilon = 0$) reduced solution is far from satisfactory and a higher order approximation is needed. One distinguishing feature of Manifold Theory is the inclusion of ε in the manifold condition [24] which considers the fast variable as a function of the singular perturbation parameter in addition to the slow variable. Although this approach was not successful for this application, due to the varying role of the altitude state, it may be highly useful in other nonlinear optimization problems. A drawback in our analysis is that we had to numerically experiment to determine a solution close to the manifold. This has been accomplished by visual examination of the trajectories in Fig's. 3.5 and 3.6. It would be highly desirable to develop an algebraic test for when the initial condition lies on the manifold solution. An alternative would be to develop an iterative process that converges to the manifold solution.

APPENDIX A

Derivation of Eq. 3.32

We want to show that

$$\frac{T_k}{T_0} \int_{t_o}^{\hat{t}} \Omega_A(\hat{t},\tau) \begin{bmatrix} C_1(\tau) \\ C_1(\tau) \end{bmatrix} d\tau = T_k \frac{t - t_o}{T_0} \begin{bmatrix} \dot{x}_0(\hat{t}) \\ \dot{\lambda}_0(\hat{t}) \end{bmatrix} \tag{A.1}$$

in Eq. 3.32. Let $f_1 = \dot{x}_0(x_0,\lambda_0,\tau)$; $f_2 = \dot{\lambda}_0(x_0,\lambda_0,\tau)$, assuming u being eliminated and recall that

$$C_1 = f_1 + (\tau - t_o)\frac{\partial f_1}{\partial \tau} \qquad ; C_2 = f_2 + (\tau - t_o)\frac{\partial f_2}{\partial \tau} \tag{A.2}$$

The left hand side of (A.1) becomes

$$\frac{T_k}{T_0} \int_{t_o}^{\hat{t}} \Omega_A(\hat{t},\tau) \left\{ \frac{d}{d\tau}\left((\tau - t_o)\begin{bmatrix} f_1 \\ f_2 \end{bmatrix} \right) - (\tau - t_o)\begin{bmatrix} \partial f_1/\partial x_0 & \partial f_1/\partial \lambda_0 \\ \partial f_2/\partial x_0 & \partial f_2/\partial \lambda_0 \end{bmatrix}\begin{bmatrix} f_1 \\ f_2 \end{bmatrix} \right\} d\tau \tag{A.3}$$

Using integration by parts on the first term in (A.3), we have

$$\frac{T_k}{T_0}\left\{ (\tau - t_o)\Omega_A(\hat{t},\tau)\begin{bmatrix} f_1 \\ f_2 \end{bmatrix} \right\} \Big|_{\tau = t_o}^{\tau = \hat{t}} - \frac{T_k}{T_0}\int_{t_o}^{\hat{t}} (\tau - t_o)\left(\frac{d}{d\tau}\Omega_A(\hat{t},\tau) \right)\begin{bmatrix} f_1 \\ f_2 \end{bmatrix} d\tau$$

$$-\frac{T_k}{T_0}\int_{t_o}^{\hat{t}} (\tau - t_o)\Omega_A(\hat{t},\tau)\begin{bmatrix} \partial f_1/\partial x_0 & \partial f_1/\partial \lambda_0 \\ \partial f_2/\partial x_0 & \partial f_2/\partial \lambda_0 \end{bmatrix}\begin{bmatrix} f_1 \\ f_2 \end{bmatrix} d\tau \tag{A.4}$$

Substituting the state transition matrix property

$$\frac{d}{d\tau}\Omega_A(\hat{t},\tau) = -\Omega_A(\hat{t},\tau)\begin{bmatrix} \partial f_1/\partial x_0 & \partial f_1/\partial \lambda_0 \\ \partial f_2/\partial x_0 & \partial f_2/\partial \lambda_0 \end{bmatrix} \tag{A.5}$$

into (A.4), the last two terms cancel and the result is demonstrated. The above state transition matrix is also used to derive Eq. 4.7.

APPENDIX B

State Transition Matrix Expression in Eq. 3.44

The state transition matrix used in the regular perturbation approach in Sec. 3.2 is

$$\Omega_A^{(i)}(t_2,t_1) = \begin{bmatrix} 1 & 0 & 0 & \omega_{14}^{(i)} & \omega_{15}^{(i)} & \omega_{16}^{(i)} \\ 0 & 1 & 0 & \omega_{24}^{(i)} & \omega_{25}^{(i)} & \omega_{26}^{(i)} \\ t_2-t_1 & 0 & 1 & \omega_{34}^{(i)} & \omega_{35}^{(i)} & \omega_{36}^{(i)} \\ 0 & 0 & 0 & 1 & 0 & t_1-t_2 \\ 0 & 0 & 0 & 0 & 1 & 0 \\ 0 & 0 & 0 & 0 & 0 & 1 \end{bmatrix} \tag{B.1}$$

where

$$\omega_{14}^{(i)} = \pi_{14}^{(i)}(t_2) - \pi_{14}^{(i)}(t_1)$$

$$\omega_{15}^{(i)} = \pi_{15}^{(i)}(t_2) - \pi_{15}^{(i)}(t_1)$$

$$\omega_{16}^{(i)} = \pi_{16}^{(i)}(t_2) - \pi_{16}^{(i)}(t_1) + t_1\omega_{14}^{(i)}$$

$$\omega_{24}^{(i)} = \omega_{15}^{(i)}$$

$$\omega_{25}^{(i)} = \pi_{25}^{(i)}(t_2) - \pi_{25}^{(i)}(t_1)$$

$$\omega_{26}^{(i)} = \pi_{26}^{(i)}(t_2) - \pi_{26}^{(i)}(t_1) + t_1\omega_{24}^{(i)}$$

$$\omega_{34}^{(i)} = \pi_{34}^{(i)}(t_2) - \pi_{34}^{(i)}(t_1) - (t_2-t_1)\pi_{14}^{(i)}(t_1)$$

$$\omega_{35}^{(i)} = \pi_{35}^{(i)}(t_2) - \pi_{35}^{(i)}(t_1) - (t_2-t_1)\pi_{15}^{(i)}(t_1)$$

$$\omega_{36}^{(i)} = \pi_{36}^{(i)}(t_2) - \pi_{36}^{(i)}(t_1) - (t_2-t_1)\pi_{16}^{(i)}(t_1) + t_1\omega_{16}^{(i)}$$

$$\pi_{14}^{(i)}(t) = A\left\{ \frac{-\sinh^{-1}[\tan(\theta(t)) - \eta)]}{(\Delta^2+1)^{3/2}} - \frac{\Delta\sin(\theta(t)) + \cos(\theta(t))}{\Delta^2+1} \right\}$$

$$\pi_{15}^{(i)}(t) = A\left\{ \frac{-\Delta\sinh^{-1}[\tan(\theta(t)) - \eta)]}{(\Delta^2+1)^{3/2}} + \frac{\sin(\theta(t)) - \Delta\cos(\theta(t))}{\Delta^2+1} \right\}$$

87

C1-2

$$\pi_{16}^{(i)}(t) = B\left\{\frac{(p+\Delta)\sinh^{-1}[\tan(\theta(t))-\eta)]}{(\Delta^2+1)^{3/2}} + \frac{(p+\Delta)\cos(\theta(t))+(p\Delta-1)\sin(\theta(t))}{\Delta^2+1}\right\}$$

$$A = \frac{T_{vac}^{(i)}}{c_{u0}k^{(i)}} \quad ; \quad B = \frac{A}{q}$$

$$\pi_{25}^{(i)}(t) = A\left\{\frac{-\Delta^2\sinh^{-1}[\tan(\theta(t))-\eta)]}{(\Delta^2+1)^{3/2}} + \frac{\Delta\sin(\theta(t))+\cos(\theta(t))}{\Delta^2+1}\right\}$$

$$\pi_{26}^{(i)}(t) = B\left\{\frac{\Delta(p+\Delta)\sinh^{-1}[\tan(\theta(t))-\eta)]}{(\Delta^2+1)^{3/2}} - \frac{(p+\Delta)\sin(\theta(t))-(p\Delta-1)\cos(\theta(t))}{\Delta^2+1}\right\}$$

$$\pi_{34}^{(i)}(t) = B\left\{\frac{[\Delta+\tan(\theta(t))]\sinh^{-1}[\tan(\theta(t))-\eta)]}{(\Delta^2+1)^{3/2}} + \frac{\Delta\sec(\theta(t))}{\Delta^2+1}\right\}$$

$$\pi_{35}^{(i)}(t) = B\left\{\frac{\Delta[\Delta+\tan(\theta(t))]\sinh^{-1}[\tan(\theta(t))-\eta)]}{(\Delta^2+1)^{3/2}} - \frac{\sec(\theta(t))}{\Delta^2+1}\right\}$$

$$\pi_{36}^{(i)}(t) = \frac{B}{q}\left\{\frac{-(p+\Delta)[\Delta+\tan(\theta(t))]\sinh^{-1}[\tan(\theta(t))-\eta)]}{(\Delta^2+1)^{3/2}} - \frac{(p\Delta-1)\sec(\theta(t))}{\Delta^2+1}\right\}$$

$$(B.2)$$

All the variables are evaluated at the zero order values.

APPENDIX C
State Transition Matrix Expression of Level 1 Formulation in Sec. 4.3

The state transition matrix of Level 1 case for the Duffing's example is

$$\Omega_A(\hat{t},t_0) = \begin{bmatrix} a_{11} & a_{12} & a_{13} & a_{14} \\ a_{21} & a_{11} & -a_{14} & a_{24} \\ -ba_{24} & ba_{23} & a_{11} & -a_{21} \\ -ba_{23} & -ba_{13} & -a_{12} & a_{11} \end{bmatrix} \tag{C.1}$$

For b > 0:

$$\alpha = c - \sqrt{b} \quad ; \; \beta = c + \sqrt{b} \qquad ; \; \bar{t} = \hat{t} - t_0$$

$$a_{11} = \frac{\alpha - c}{\alpha - \beta}\cos(\bar{t}\sqrt{\alpha}) + \frac{c - \beta}{\alpha - \beta}\cos(\bar{t}\sqrt{\beta})$$

$$a_{12} = \frac{\alpha - c}{(\alpha - \beta)\sqrt{\alpha}}\sin(\bar{t}\sqrt{\alpha}) + \frac{c - \beta}{(\alpha - \beta)\sqrt{\beta}}\sin(\bar{t}\sqrt{\beta})$$

$$a_{13} = \frac{-1}{(\alpha - \beta)\sqrt{\alpha}}\sin(\bar{t}\sqrt{\alpha}) + \frac{1}{(\alpha - \beta)\sqrt{\beta}}\sin(\bar{t}\sqrt{\beta})$$

$$a_{14} = \frac{1}{\alpha - \beta}\cos(\bar{t}\sqrt{\alpha}) - \frac{1}{\alpha - \beta}\cos(\bar{t}\sqrt{\beta})$$

$$a_{21} = \frac{c^2 - \alpha c - b}{(\alpha - \beta)\sqrt{\alpha}}\sin(\bar{t}\sqrt{\alpha}) + \frac{b + c\beta - c^2}{(\alpha - \beta)\sqrt{\beta}}\sin(\bar{t}\sqrt{\beta})$$

$$a_{24} = \frac{-\sqrt{\alpha}}{\alpha - \beta}\sin(\bar{t}\sqrt{\alpha}) + \frac{\sqrt{\beta}}{\alpha - \beta}\sin(\bar{t}\sqrt{\beta}) \tag{C.2}$$

For b < 0:

$$\theta = \left(\sqrt{2\sqrt{c^2 - b} - 2c}\right)/2 \qquad ; \; \phi = \sqrt{(c + \sqrt{c^2 - b})/2}$$

$$a_{11} = \cosh(\theta\bar{t})\cos(\phi\bar{t}) + \frac{c + \theta^2 - \phi^2}{2\theta\phi}\sinh(\theta\bar{t})\sin(\phi\bar{t}) \; ; \; a_{14} = \frac{-1}{2\theta\phi}\sinh(\theta\bar{t})\sin(\phi\bar{t})$$

$$a_{12} = \frac{\theta^2 + \phi^2 - c}{2\theta(\theta^2 + \phi^2)}\sinh(\theta\bar{t})\cos(\phi\bar{t}) + \frac{\theta^2 + \phi^2 + c}{2\phi(\theta^2 + \phi^2)}\cosh(\theta\bar{t})\sin(\phi\bar{t})$$

89

$$a_{13} = \frac{-1}{2\theta(\theta^2 + \phi^2)}\sinh(\theta\bar{t})\cos(\phi\bar{t}) + \frac{1}{2\phi(\theta^2 + \phi^2)}\cosh(\theta\bar{t})\sin(\phi\bar{t})$$

$$a_{21} = \frac{c^2 - b - c(\theta^2 + \phi^2)}{2\theta(\theta^2 + \phi^2)}\sinh(\theta\bar{t})\cos(\phi\bar{t}) + \frac{b - c^2 - c(\theta^2 + \phi^2)}{2\phi(\theta^2 + \phi^2)}\cosh(\theta\bar{t})\sin(\phi\bar{t})$$

$$a_{24} = \frac{-1}{2\theta}\sinh(\theta\bar{t})\cos(\phi\bar{t}) - \frac{1}{2\phi}\cosh(\theta\bar{t})\sin(\phi\bar{t}) \qquad (C.3)$$

The state transition matrix has the same structure of that in Level 0 for b = 0.

APPENDIX D
System Matrix and State Transition Matrix Expression
of the First-orderFormulation in Sec. 5.2

The terms defined in Eq. 5.8 have the following expressions:

$$a_{14j} = \frac{T_{vac}^{(i)} - \bar{p}A_e^{(i)}}{m(t)} \left[\frac{\lambda_{u0}^2}{(\lambda_{v0}^2 + \lambda_{u0}^2)^{3/2}} \right]$$

$$a_{15j} = \frac{T_{vac}^{(i)} - \bar{p}A_e^{(i)}}{m(t)} \left[\frac{-\lambda_{v0}\lambda_{u0}}{(\lambda_{v0}^2 + \lambda_{u0}^2)^{3/2}} \right]$$

$$a_{25j} = \frac{T_{vac}^{(i)} - \bar{p}A_e^{(i)}}{m(t)} \left[\frac{\lambda_{v0}^2}{(\lambda_{v0}^2 + \lambda_{u0}^2)^{3/2}} \right]$$

$$f_1 = \frac{-\cos\theta_0}{\lambda_{v0}\sin\theta_0 + \lambda_{u0}\cos\theta_0}$$

$$f_2 = \frac{\sin\theta_0}{\lambda_{v0}\sin\theta_0 + \lambda_{u0}\cos\theta_0}$$

$$c_{1j} = \frac{T_{vac}^{(i)} - \bar{p}A_e^{(i)}}{m(t)} \left[1 + \frac{(t - t_{j-1})k^{(i)}}{m(t)} \right] \frac{\lambda_{v0}}{\sqrt{\lambda_{v0}^2 + \lambda_{u0}^2}} - \bar{g}_v$$

$$c_{2j} = \frac{T_{vac}^{(i)} - \bar{p}A_e^{(i)}}{m(t)} \left[1 + \frac{(t - t_{j-1})k^{(i)}}{m(t)} \right] \frac{\lambda_{u0}}{\sqrt{\lambda_{v0}^2 + \lambda_{u0}^2}} - \bar{g}_u$$

$$p_{1j} = g_1 + \frac{\lambda_{u0}}{\lambda_{v0}^2 + \lambda_{u0}^2} \left\{ \lambda_{v0} \frac{\partial g_1}{\partial\theta_0} + \lambda_{u0} \frac{\partial g_2}{\partial\theta_0} \right\}$$

$$p_{2j} = g_2 - \frac{\lambda_{v0}}{\lambda_{v0}^2 + \lambda_{u0}^2} \left\{ \lambda_{v0} \frac{\partial g_1}{\partial\theta_0} + \lambda_{u0} \frac{\partial g_2}{\partial\theta_0} \right\}$$

$$P_{4j} = -\frac{\partial H}{\partial v} - q_{vj} - \frac{\partial q_{vj}}{\partial\theta} \left\{ \frac{\lambda_{v0}\partial g_1 / \partial\theta_0 + \lambda_{u0}\partial g_2 / \partial\theta_0}{(\lambda_{v0}\sin\theta_0 + \lambda_{u0}\cos\theta_0)(T_{vac}^{(i)} - \bar{p}A_e^{(i)}) / m(t)} \right\}$$

$$P_{5j} = -\frac{\partial H}{\partial u} - q_{uj} - \frac{\partial q_{uj}}{\partial\theta} \left\{ \frac{\lambda_{v0}\partial g_1 / \partial\theta_0 + \lambda_{u0}\partial g_2 / \partial\theta_0}{(\lambda_{v0}\sin\theta_0 + \lambda_{u0}\cos\theta_0)(T_{vac}^{(i)} - \bar{p}A_e^{(i)}) / m(t)} \right\}$$

$$P_{6_j} = -\frac{\partial H}{\partial r} - q_{rj} - \frac{\partial q_{rj}}{\partial \theta} \left\{ \frac{\lambda_{v0}\partial g_1 / \partial \theta_0 + \lambda_{u0}\partial g_2 / \partial \theta_0}{(\lambda_{v0}\sin\theta_0 + \lambda_{u0}\cos\theta_0)(T_{vac}^{(i)} - \bar{p}A_e^{(i)}) / m(t)} \right\}$$

$$\frac{\partial q_{vj}}{\partial \theta} = \left\{ -\frac{\partial^2 H}{\partial\theta\partial v} \right\} \Big|_{t=(t_j+t_{j-1})/2;\, \dots\, ;\, \lambda_{r0}=(\lambda_{r0j}+\lambda_{r0j-1})/2}$$

$$\frac{\partial q_{uj}}{\partial \theta} = \left\{ -\frac{\partial^2 H}{\partial\theta\partial u} \right\} \Big|_{t=(t_j+t_{j-1})/2;\, \dots\, ;\, \lambda_{r0}=(\lambda_{r0j}+\lambda_{r0j-1})/2}$$

$$\frac{\partial q_{rj}}{\partial \theta} = \left\{ -\frac{\partial^2 H}{\partial\theta\partial r} \right\} \Big|_{t=(t_j+t_{j-1})/2;\, \dots\, ;\, \lambda_{r0}=(\lambda_{r0j}+\lambda_{r0j-1})/2} \tag{D.1}$$

where

$$g_1 = \frac{(p-p)A_e^{(i)}\sin\theta_0 - D^{(i)}\sin\gamma_0 + L^{(i)}\cos\gamma_0}{m(t)} + \bar{g}_v - \frac{\mu_e}{r_0} + \frac{u_0^2}{r_0}$$

$$g_2 = \frac{(p-p)A_e^{(i)}\cos\theta_0 - D^{(i)}\cos\gamma_0 - L^{(i)}\sin\gamma_0}{m(t)} + \bar{g}_u - \frac{u_0 v_0}{r_0} \tag{D.2}$$

The remaining partial derivatives $(\partial q_{vj}/\partial v,\ \partial q_{vj}/\partial u,\ \dots)$ are similar to the last three expressions in (F.1).

The approximate state transition matrix in Eq. 5.9 can be obtained by taking the partial derivatives of the zero-order solution in Eq. 5.5 with respect to the initial conditions $\{v_0(t_{j-1}),\ u_0(t_{j-1}),\ r_0(t_{j-1}),\ \lambda_{v0}(t_{j-1}),\ \lambda_{u0}(t_{j-1}),\ \lambda_{r0}(t_{j-1})\}$. So we have:

$$\omega_{14} = \frac{\partial v_0(t)}{\partial\lambda_{v0}(t_{j-1})} = \frac{\partial v_0(t)}{\partial c_v} \qquad ; \omega_{15} = \frac{\partial v_0(t)}{\partial\lambda_{u0}(t_{j-1})} = \frac{\partial v_0(t)}{\partial c_u}$$

$$\omega_{16} = \frac{\partial v_0(t)}{\partial\lambda_{r0}(t_{j-1})} = -\frac{\partial v_0(t)}{\partial q_{vj}} \qquad ; \omega_{24} = \frac{\partial u_0(t)}{\partial\lambda_{v0}(t_{j-1})} = \frac{\partial u_0(t)}{\partial c_v}$$

$$\omega_{25} = \frac{\partial u_0(t)}{\partial\lambda_{u0}(t_{j-1})} = \frac{\partial u_0(t)}{\partial c_u} \qquad ; \omega_{26} = \frac{\partial u_0(t)}{\partial\lambda_{r0}(t_{j-1})} = -\frac{\partial u_0(t)}{\partial q_{vj}}$$

$$\omega_{34} = \frac{\partial r_0(t)}{\partial\lambda_{v0}(t_{j-1})} = \frac{\partial r_0(t)}{\partial c_v} \qquad ; \omega_{35} = \frac{\partial r_0(t)}{\partial\lambda_{u0}(t_{j-1})} = \frac{\partial r_0(t)}{\partial c_u}$$

$$\omega_{36} = \frac{\partial r_0(t)}{\partial\lambda_{r0}(t_{j-1})} = -\frac{\partial r_0(t)}{\partial q_{vj}} \tag{D.3}$$

For example, using the chain rule, ω_{14} is given by

$$\omega_{14} = \frac{\partial v_0}{\partial D}\frac{\partial D}{\partial c_v} + \frac{\partial v_0}{\partial \Delta}\frac{\partial \Delta}{\partial c_v} + \frac{\partial v_0}{\partial \varsigma}\frac{\partial \varsigma}{\partial c_v} + \frac{\partial v_0}{\partial \varphi}\frac{\partial \varphi}{\partial c_v} + \frac{\partial v_0}{\partial \eta}\frac{\partial \eta}{\partial c_v} \qquad (D.4)$$

Symbolic manipulation programs such as *Mathematica, MACSYMA* can be used to obtain the analytic expressions of the above derivatives, and to write the subroutines needed for their computation.

REFERENCES

1. Brusch, R. G., Reed, T. E., "Real-time Launch Vehicle Steering Programme Selection, " *Journal of the British Interplanetary Society*, Vol. 26, 1973, pp. 279 - 290.

2. Chandler, D. C., Smith, I. E., "Development of the Iterative Guidance Mode with its Application to Various Vehicles and Missions, " *Journal of Spacecraft and Rockets*, Vol. 4, 1967, pp. 898 - 903.

3. McHenry, R. L., Brand, T. J., Long, A. D., Cockrell, B. F., Thibodeau, J. R. III, "Space Shuttle Ascent Guidance, Navigation and Control, " *Journal of the Astronautical Sciences*, Vol. XXVII, 1978, pp. 1 - 38.

4. Johnson, I. L., "Optimal Rocket Thrust Profile Shaping using Third-degree Spline Function Interpolation, " AIAA Paper No. 74-823, 1974.

5. Well, K. H., Tandon, S. R., "Rocket Ascent Trajectory Optimization via Recursive Quadratic Programming, " *Journal of the Astronautical Sciences*, Vol. XXX, 1982, pp. 101 - 116.

6. Well, K. H., "Ariane V Ascent Trajectory Optimization with a First-stage Splash Down Constraint, " *Proceedings of Control Application of Nonlinear Programming and Optimization Conference*, 1989.

7. Brusch, R., "Trajectory Optimization for the Atlas/Centaur Launch Vehicle, " *Journal of Spacecraft and Rockets*, Vol. 14, 1977, pp. 550 - 555.

8. Hargraves, C. R., Paris, S. W., "Direct Trajectory Optimization Using Nonlinear Programming and Collocation, " *AIAA Journal of Guidance, Control, and Dynamics*, Vol.10, 1987, pp. 338 - 342.

9. Pamadi, B. N., "Adaptive Guidance for an Aero-assisted Boost Vehicle, " *Proceedings of AIAA Guidance, Navigation & Control Conference*, 1988, pp. 995 - 1005.

10. Oberle, H. J., Grimm, W., "BNDSCO, A Program for Numerical Solution of Optimal Control Problems, " English Translation of DFVLR-Mitt. 85-05, 1985.

11. Broyden, C. G., "A Class of Methods for Solving Nonlinear Simultaneous Equations, " *Mathematics of Computation*, Vol. 19, 1965, pp. 577 - 583.

12. Breakwell, J. V., Rauch, H. E., "Optimum Guidance for a Low Thrust Interplanetary Vehicle, " *AIAA Journal*, Vol. 4, 1966, pp. 693 - 704.

13. Jacobson, R. A., Powers, W. F., "Iterative Explicit Guidance for Low Thrust Spacecraft, " *Journal of Spacecraft and Rockets*, Vol. 11, 1974, pp. 494 - 497.

14. Feeley, T. S., Speyer, J. L., "A Real-time Approximate Optimal Guidance Law for Flight in a Plane, " *Proceedings of American Control Conference*, 1990, pp. 2356 - 2361.

15. Leung, S. K., Calise, A. J., "An Approach to Optimal Guidance of an Advanced Launch Vehicle Concept, " *Proceedings of American Control Conference*, 1990, pp. 1824 - 1828.

16. Hodges, D. H., Calise, A. J., Bless, R. R., Leung, S. K., "A Weak Hamiltonian Finite Element method for Optimal Guidance of an Advanced Launch Vehicle," *Proceedings of American Control Conference*, 1989, pp. 2036 - 2043.

17. Leung, S. K., Calise, A. J., "A Hybrid Approach to Near-optimal Launch Vehicle Guidance, " *Proceedings of AIAA Guidance, Navigation & Control Conference*, to appear, 1992.

18. Hodges, D. H., Bless, R. R., Calise, A. J., Leung, S. K., "Finite Element Method for Optimal Guidance of an Advanced launch Vehicle, " *AIAA Journal of Guidance, Control, and Dynamics*, Vol. 15, No. 3, 1992, pp. 664 - 671.

19. Leung, S. K., Calise, A. J., "A Hybrid Approach to Solution of Optimal Control Problems, " *AIAA Journal of Guidance, Control, and Dynamics*, Vol. 17, No. 5, 1994, pp. 966-974.

20. Leung, S. K., Calise, A. J., "Hybrid Approach to Near-optimal Launch Vehice Guidance, " *AIAA Journal of Guidance, Control, and Dynamics*, Vol. 17, No. 5, 1994, 1994, pp. 881-888.

21. Calise, A. J., Hodges, D. H., Leung, S. K., Bless, R. R., "Optimal Guidance Law Development of an Advanced Launch System - Interim Progress Report," Dec. 88 - May 89, *Georgia Institute of Technology* , 1989.

22. Calise, A. J., Hodges, D. H., Leung, S. K., Bless, R. R., "Optimal Guidance Law Development of an Advanced Launch System - Interim Progress Report," June 89 - Nov. 89, *Georgia Institute of Technology*, 1989.

23. Calise, A. J., Hodges, D. H., Leung, S. K., Bless, R. R., "Optimal Guidance Law Development of an Advanced Launch System - Interim Progress Report," Dec. 89 - June 90, *Georgia Institute of Technology*, 1989.

24. Calise, A. J., Hodges, D. H., Leung, S. K., Bless, R. R., "Optimal Guidance Law Development of an Advanced Launch System - Interim Progress Report," June 90 - Dec. 90, *Georgia Institute of Technology, NASA CR-187652*, 1990.

25. Calise, A. J., Hodges, D. H., Leung, S. K., Bless, R. R., "Optimal Guidance Law Development of an Advanced Launch System - Interim Progress Report," Dec. 90 - Jun. 91, *Georgia Institute of Technology, NASA CR-192189*, 1991.

26. Bless, R. R., , "Time-Domain Finite Elements in Optimal Control With Application to Launch-Vehicle Guidance" NASA CR 4376, May 1991.

27. Marchal, C., "Survey Paper: Chattering Arcs and Chattering Controls, " *Journal of Optimization Theory and Applications*, Vol. 11, 1973, pp. 441 - 468.

28. Press, W. H., Flannery, B. P., Teukolsky, S. A., Vetterling, W. T., *Numerical Recipes, the Art of Scientific Computing*, Cambridge University Press, 1986.

29. Minzer, R. A., et al., "U. S. Standard Atmosphere, 1975 (COESA 1975), " Goddard Space Flight Center, NASA TR-459, 1975.

30. Calise, A. J., Moerder, D. D., "Singular Perturbation Techniques for Real Time Aircraft Trajectory Optimization and Control, " NASA CR-3597, 1992.

31. Ardema, M. D., "Singular Perturbations in Flight Mechanics, " NASA TM X-62, 380, 1977.

32. Kokotovic, P., Khalil, K. H., O'Reilly, J., *Singular Perturbation Methods in Control: Analysis and Design*, Academic Press, 1986.

33. Bryson, A. E., Ho, Y. C., *Applied Optimal Control*, Hemisphere Publishing Corp., 1968.

34. Junkins, J. L., "An Asymptotic Perturbation Method for Non-linear Optimal Control Problems, " *AIAA Journal of Guidance, Control, and Dynamics*, Vol. 9, 1986, pp. 357 - 367.

35. Baldwin, J. F., Williams, J. H. S., "The Use of a Method of Perturbations in the Synthesis of Closed Loop Optimal Control Laws for Nonlinear Systems, " *Automatica*, Vol. 5., 1969, pp. 357 - 367.

36. Prenter, P. M., *Splines and Variational Methods*, Wiley, 1975.

37. Bensoussan A., *Perturbation Methods in Optimal Control*, John Wiley & Sons, 1982.

REPORT DOCUMENTATION PAGE

1. AGENCY USE ONLY (Leave blank)	2. REPORT DATE	3. REPORT TYPE AND DATES COVERED
	April 1995	Contractor Report

4. TITLE AND SUBTITLE

Optimal Guidance Law Development for an Advanced Launch System

5. FUNDING NUMBERS

G NAG1-939

WU 232-01-04-05

6. AUTHOR(S)

Anthony J. Calise and Martin S. K. Leung

7. PERFORMING ORGANIZATION NAME(S) AND ADDRESS(ES)

Georgia Institute of Technology
School of Aerospace Engineering
Atlanta, GA 30332

8. PERFORMING ORGANIZATION REPORT NUMBER

9. SPONSORING / MONITORING AGENCY NAME(S) AND ADDRESS(ES)

National Aeronautics and Space Administration
Langley Research Center
Hampton, VA 23681-0001

10. SPONSORING / MONITORING AGENCY REPORT NUMBER

NASA CR-4667

11. SUPPLEMENTARY NOTES

Langley Technical Monitor: Daniel D. Moerder
Final Report

12a. DISTRIBUTION / AVAILABILITY STATEMENT

Unclassified - Unlimited

Subject Categories 12, 16, 31, 64, and 66

12b. DISTRIBUTION CODE

13. ABSTRACT (Maximum 200 words)

The objective of this research effort was to develop a real-time guidance approach for launch vehicles ascent to orbit injection. Various analytical approaches combined with a variety of model order and model complexity reduction have been investigated. Singular perturbation methods were first attempted and found to be unsatisfactory. The second approach based on regular perturbation analysis was subsequently investigated. It also fails because the aerodynamic effects (ignored in the zero order solution) are too large to be treated as perturbations. Therefore, the study demonstrates that perturbation methods alone (both regular and singular perturbations) are inadequate for use in developing a guidance algorithm for the atmospheric flight phase of a launch vehicle. During a second phase of the research effort, a hybrid analytic/numerical approach was developed and evaluated. The approach combines the numerical methods of collocation and the analytical method of regular perturbations. The concept of choosing intelligent interpolating functions is also introduced. Regular perturbation analysis allows the use of a crude representation for the collocation solution, and intelligent interpolating functions further reduce the number of elements without sacrificing the approximation accuracy. As a result, the combined method forms a powerful tool for solving real-time optimal control problems. Details of the approach are illustrated in a fourth order nonlinear example. The hybrid approach is then applied to the launch vehicle problem. The collocation solution is derived from a bilinear tangent steering law, and results in a guidance solution for the entire flight regime that includes both atmospheric and exoatmospheric flight phases.

14. SUBJECT TERMS

Optimal Guidance, Trajectory Optimization, Perturbation Methods

15. NUMBER OF PAGES

107

16. PRICE CODE

A06

17. SECURITY CLASSIFICATION OF REPORT	18. SECURITY CLASSIFICATION OF THIS PAGE	19. SECURITY CLASSIFICATION OF ABSTRACT	20. LIMITATION OF ABSTRACT
Unclassified	Unclassified		